

**FERROELECTRIC THIN FILMS IN THE $\text{Pb}_5\text{Ge}_3\text{O}_{11}$
AND $\text{Pb}_5\text{Ge}_3\text{O}_{11}$ - $\text{PbZr}_x\text{Ti}_{1-x}\text{O}_3$ SYSTEMS**

by

Steven M. Landin

ARTHUR LAKES LIBRARY
COLORADO SCHOOL OF MINES
GOLDEN, CO 80401

ProQuest Number: 10796661

All rights reserved

INFORMATION TO ALL USERS

The quality of this reproduction is dependent upon the quality of the copy submitted.

In the unlikely event that the author did not send a complete manuscript and there are missing pages, these will be noted. Also, if material had to be removed, a note will indicate the deletion.



ProQuest 10796661

Published by ProQuest LLC (2019). Copyright of the Dissertation is held by the Author.

All rights reserved.

This work is protected against unauthorized copying under Title 17, United States Code
Microform Edition © ProQuest LLC.

ProQuest LLC.
789 East Eisenhower Parkway
P.O. Box 1346
Ann Arbor, MI 48106 – 1346

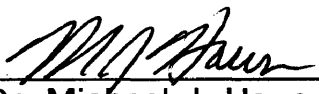
A thesis submitted to the Faculty and the Board of Trustees of the Colorado School of Mines in partial fulfillment of the requirements for the degree of Doctor of Philosophy (Materials Science).

Golden, Colorado

Date MARCH 23, 1996

Signed: 

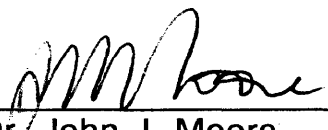
Steven M. Landin

Approved: 

Dr. Michael J. Haun
Thesis Advisor

Golden, Colorado

Date 3/24/96



Dr. John J. Moore
Professor and Director,
Materials Science

Abstract

Research was performed on solution-derived ferroelectric thin films in the $\text{Pb}_5\text{Ge}_3\text{O}_{11}$ and $\text{Pb}_5\text{Ge}_3\text{O}_{11}\text{-PbZr}_x\text{Ti}_{1-x}\text{O}_3$ systems. The overall objective of this research was to develop a better understanding of the relationships between composition, processing methods, crystallization, microstructure and electrical properties for these compositions. Lead germanate, $\text{Pb}_5\text{Ge}_3\text{O}_{11}$, is a uniaxial ferroelectric with a low dielectric constant and relatively high pyroelectric coefficient resulting in excellent pyroelectric performance characteristics. The combination of lead germanate with ferroelectric lead zirconate titanate, $\text{PbZr}_x\text{Ti}_{1-x}\text{O}_3$, offers the potential to optimize thin film properties for specific applications by adjusting the ratios of the two phases.

The results of this research define the time/temperature relationships involved in the phase development, crystallographic orientation and grain growth of solution-derived lead germanate thin films. Thin films of $\text{Pb}_5\text{Ge}_3\text{O}_{11}$ can be reproducibly fabricated with c-axis orientations greater than 98%. The grain size of these films can be adjusted from less than $0.1\mu\text{m}$ to over $10\mu\text{m}$ by precisely controlling the thermal annealing profile. Processing difficulties encountered during the fabrication of $\text{Pb}_5\text{Ge}_3\text{O}_{11}$ and $\text{Pb}_5\text{Ge}_3\text{O}_{11}\text{-PbZr}_x\text{Ti}_{1-x}\text{O}_3$ thin films are described. Potential interpretations and solutions are presented. C-axis oriented $\text{Pb}_5\text{Ge}_3\text{O}_{11}$ thin films with grain sizes greater than 2 to $3\mu\text{m}$ displayed pyroelectric properties without electrical poling. After poling, these films displayed pyroelectric performance characteristics similar to the commercially used single crystal, triglycine sulphate.

TABLE OF CONTENTS

	Page
ABSTRACT	iii
LIST OF FIGURES	vii
LIST OF TABLES	xiv
ACKNOWLEDGMENTS	xv
I. INTRODUCTION	1
1.1 Statement of Problem	1
1.2 Objectives	2
1.3 Scope of the Thesis	3
II. LITERATURE REVIEW	5
2.1 Ferroelectrics - Background and Theory	5
2.1.1 General / Phenomenology	6
2.1.2 Structure / Crystallography	8
2.1.3 Domains	8
2.1.4 Soft Modes	9
2.2 Ferroelectric Thin Films	13
2.2.1 Thickness Effects	14
2.2.2 Surface Effects	16
2.3 Pyroelectric Properties	18

2.4	Lead Germanate	23
2.4.1	Kinetics of $\text{Pb}_5\text{Ge}_3\text{O}_{11}$ Formation	23
2.4.2	$\text{Pb}_5\text{Ge}_3\text{O}_{11}$ Structure and Phase Transition	25
2.4.3	Thermal Expansion	30
2.4.4	Ferroelectric Properties	33
2.4.5	Pyroelectric Properties	35
2.4.6	Thin Films	36
2.4.7	Preferred Orientation	39
2.5	Lead Zirconate Titanate	40
2.5.1	$\text{PbZr}_x\text{Ti}_{1-x}\text{O}_3$ Structure and Phase Transition	40
2.5.2	Electrical Properties	42
2.5.3	Thermal Expansion	42
2.5.4	Thin Film Formation and Orientation	43
2.5.5	Thin Film Electrical Properties	46
2.6	Lead Germanate / Lead Zirconate Titanate	47
III. EXPERIMENTAL PROCEDURE		48
3.1	Solution Processing	48
3.2	Thin Film Fabrication	51
3.3	Characterization	55
3.3.1	Phase Development and Orientation	55
3.3.2	Physical Properties	56
3.3.3	Electrical Properties	56
IV. RESULTS AND DISCUSSION		59
4.1	Phase Development in $\text{Pb}_5\text{Ge}_3\text{O}_{11}$ Thin Films	59
4.1.1	$\text{Pb}_{5.7}\text{Pb}$	59
4.1.2	Metastable $\text{Pb}_5\text{Ge}_3\text{O}_{11}$	59
4.1.3	Stable $\text{Pb}_5\text{Ge}_3\text{O}_{11}$	62
4.1.4	Shifting of (00l) Diffraction Peaks	65
4.1.5	PbO , PbGeO_3 and Pb_3GeO_5	81

4.2	Phase Development in $\text{Pb}_5\text{Ge}_3\text{O}_{11}$ - $\text{PbZr}_x\text{Ti}_{1-x}\text{O}_3$ Thin Films	84
4.3	Microstructure and Preferred Orientation	94
4.3.1	Time / Temperature Relationships	94
4.3.2	Microstructure Optimization	115
4.4	Electrical Properties	122
V.	SUMMARY AND CONCLUSIONS	140
VI.	SUGGESTIONS FOR FUTURE WORK	146
	REFERENCES	149

LIST OF FIGURES

	Page
2.1. A ferroelectric hysteresis loop of polarization versus electric field . . .	7
2.2. The relative directions of applied field, depolarization field and polarization	10
2.3. Plot of energy versus k for a paraelectric phase	12
2.4. A periodic domain structure model	15
2.5. The bending of the conduction and valence bands due to the polarization change at the surface	17
2.6. Idealized apatite, nasonite and lead germanate structures	26
2.7. (A) Spontaneous polarization versus temperature for $\text{Pb}_5\text{Ge}_3\text{O}_{11}$ and (B) P_s^2 versus $T_c - T$	27
2.8. Gyration coefficient of $\text{Pb}_5\text{Ge}_3\text{O}_{11}$ versus temperature	29
2.9. P_s^2 versus $T_c - T$ for the composition $\text{Pb}_5\text{Ge}_2\text{SiO}_{11}$	29
2.10. Thermal expansion of lead germanate	31
2.11. Dielectric constant versus temperature for single crystal $\text{Pb}_5\text{Ge}_3\text{O}_{11}$	34
2.12. Dielectric constant versus temperature for thermally evaporated $\text{Pb}_5\text{Ge}_3\text{O}_{11}$ thin films	37
2.13. Sub-solidus phase diagram of the PbTiO_3 - PbZrO_3 system	41

3.1. Flow chart of experimental procedure	49
3.2. Diagram of the rapid thermal processing system	54
4.1. X-ray diffraction patterns for single layer $Pb_5Ge_3O_{11}$ films annealed for one minute	60
4.2. X-ray diffraction patterns for single layer $Pb_5Ge_3O_{11}$ films annealed at 450°C	61
4.3. X-ray diffraction patterns for the (200) peak for (A) a single layer $Pb_5Ge_3O_{11}$ film annealed at 600°C for 10 seconds and (B) a single layer $Pb_5Ge_3O_{11}$ film annealed at 600°C for 30 seconds	63
4.4. The change in the (200) diffraction peak position with annealing time	64
4.5. X-ray diffraction patterns for single layer $Pb_5Ge_3O_{11}$ films annealed at 600°C	66
4.6. The (006) diffraction peak for a single layer $Pb_5Ge_3O_{11}$ film annealed at 450°C for 10 seconds	67
4.7. X-ray diffraction patterns for the (A) (003) and (B) (006) peaks for a single layer $Pb_5Ge_3O_{11}$ film annealed at 450°C for 60 seconds	68
4.8. X-ray diffraction patterns for the (A) (003) and (B) (006) peaks for a single layer $Pb_5Ge_3O_{11}$ film annealed at 450°C for 120 seconds	70
4.9. The splitting and shifting of the (006) diffraction peak position with annealing time for single layer $Pb_5Ge_3O_{11}$ films annealed at 450°C	71

4.10. X-ray diffraction patterns for the (A) (003) and (B) (006) peaks for a single layer $\text{Pb}_5\text{Ge}_3\text{O}_{11}$ film annealed at 700°C for 30 seconds	72
4.11. The change in the (003) diffraction peak position with annealing time for single layer $\text{Pb}_5\text{Ge}_3\text{O}_{11}$ films	73
4.12. The change in the (006) diffraction peak position with annealing time for single layer $\text{Pb}_5\text{Ge}_3\text{O}_{11}$ films	74
4.13. The variation of lattice parameters with composition for $\text{Pb}_3\text{Ge}_{2-x}\text{Si}_x\text{O}_7$	79
4.14. X-ray diffraction patterns for single layer $\text{Pb}_5\text{Ge}_3\text{O}_{11}$ films annealed at 700°C	82
4.15. X-ray diffraction patterns for single layer $\text{Pb}_5\text{Ge}_3\text{O}_{11}$ films annealed at 450°C	83
4.16. X-ray diffraction patterns for four layer films of varying composition, annealed at 500°C for 60 seconds after each layer and 700°C for 10 minutes after the final layer	85
4.17. X-ray diffraction patterns for single layer $4\text{Pb}_5\text{Ge}_3\text{O}_{11}\text{-PbZr}_{0.5}\text{Ti}_{0.5}\text{O}_3$ films annealed at 600°C	87
4.18. X-ray diffraction patterns for single layer $4\text{Pb}_5\text{Ge}_3\text{O}_{11}\text{-PbZr}_{0.5}\text{Ti}_{0.5}\text{O}_3$ films annealed at 700°C	88
4.19. X-ray diffraction patterns for single layer $\text{Pb}_5\text{Ge}_3\text{O}_{11}\text{-}4\text{PbZr}_{0.5}\text{Ti}_{0.5}\text{O}_3$ films annealed at 700°C	89
4.20. X-ray diffraction patterns for $4\text{Pb}_5\text{Ge}_3\text{O}_{11}\text{-PbZr}_{0.5}\text{Ti}_{0.5}\text{O}_3$ films and the corresponding fitted curves in the region of the PG(006). (A) A single layer film annealed at 600°C for 30 seconds. (B) A single layer film annealed at 600°C for 60 seconds	91

4.21. X-ray diffraction patterns for $4\text{Pb}_5\text{Ge}_3\text{O}_{11}$ - $\text{PbZr}_{0.5}\text{Ti}_{0.5}\text{O}_3$ films and the corresponding fitted curves in the region of the PG(006). (A) A single layer film annealed at 600°C for 120 seconds. (B) A single layer film annealed at 600°C for 300 seconds	92
4.22. X-ray diffraction patterns comparing c-axis oriented to non-oriented $\text{Pb}_5\text{Ge}_3\text{O}_{11}$ microstructures	95
4.23. X-ray diffraction patterns for single layer $\text{Pb}_5\text{Ge}_3\text{O}_{11}$ films annealed for one minute	96
4.24. X-ray diffraction patterns for four layer $\text{Pb}_5\text{Ge}_3\text{O}_{11}$ films. (A) 500°C for one minute after each layer, 500°C for ten minutes after the final layer. (B) 500°C for one minute after each layer, 700°C for ten minutes after the final layer. (C) 700°C for one minute after each layer, 700°C for ten minutes after the final layer	98
4.25. AFM micrograph of the surface of a two layer $\text{Pb}_5\text{Ge}_3\text{O}_{11}$ film annealed at 350°C for one minute after each layer and 700°C for ten minutes after the final layer	99
4.26. AFM micrograph of the surface of a 15-layer $\text{Pb}_5\text{Ge}_3\text{O}_{11}$ film annealed at 450°C for one minute after each layer and 700°C for 20 minutes after the final layer	100
4.27. AFM micrograph of the surface of a 15-layer $\text{Pb}_5\text{Ge}_3\text{O}_{11}$ film annealed at 450°C for one minute after each layer and 700°C for 30 minutes after the final layer	101
4.28. Optical micrograph of a 15-layer $\text{Pb}_5\text{Ge}_3\text{O}_{11}$ film annealed at 450°C for one minute after each layer and 700°C for 30 minutes after the final layer (1000X)	102
4.29. AFM micrograph of the surface of a 12-layer $\text{Pb}_5\text{Ge}_3\text{O}_{11}$ film annealed at 450°C for one minute after each layer and 730°C for 3 minutes after the final layer	104

4.30. AFM micrograph of the surface of a 12-layer $\text{Pb}_5\text{Ge}_3\text{O}_{11}$ film annealed at 450°C for one minute after each layer and 730°C for 4 minutes after the final layer	105
4.31. AFM micrograph of the surface of a 12-layer $\text{Pb}_5\text{Ge}_3\text{O}_{11}$ film annealed at 450°C for one minute after each layer and 730°C for 6 minutes after the final layer	106
4.32. Optical micrographs of four layer $\text{Pb}_5\text{Ge}_3\text{O}_{11}$ films annealed at 450°C for one minute after each layer and (A) 730°C for 4 minutes after the final layer (1000X) (B) 730°C for 6 minutes after the final layer (1000X)	107
4.33. X-ray diffraction patterns for 12-layer $\text{Pb}_5\text{Ge}_3\text{O}_{11}$ films annealed at 450°C for one minute after each layer and (A) 730°C for 4 minutes after the final layer (B) 730°C for 6 minutes after the final layer	108
4.34. Optical micrographs of four layer $\text{Pb}_5\text{Ge}_3\text{O}_{11}$ films annealed at 350°C for one minute after each layer and (A) 730°C for 10 minutes after the final layer (1000X) (B) 730°C for 20 minutes after the final layer (1000X)	109
4.35. Optical micrographs of two layer $\text{Pb}_5\text{Ge}_3\text{O}_{11}$ films annealed at 450°C for one minute after each layer and (A) 760°C for 10 seconds after the final layer (1000X) (B) 760°C for 5 minutes after the final layer (500X)	110
4.36. Optical micrographs of two layer $\text{Pb}_5\text{Ge}_3\text{O}_{11}$ films annealed at 450°C for one minute after each layer and 760°C for one minute after the final layer (1000X)	111
4.37. Optical micrographs of two layer $\text{Pb}_5\text{Ge}_3\text{O}_{11}$ films annealed at 450°C for one minute after each layer and (A) 760°C for 2 minutes after the final layer (125X) (B) 760°C for 3 minutes after the final layer (1000X)	113

4.38. X-ray diffraction pattern for a two layer $\text{Pb}_5\text{Ge}_3\text{O}_{11}$ film annealed at 450°C for one minute after each layer and 760°C for two minutes after the final layer	114
4.39. AFM micrograph of a two layer PbTiO_3 film annealed at 350°C for one minute after each layer and 700°C for 10 minutes after the final layer	116
4.40. AFM micrograph of a film consisting of two layers of $\text{Pb}_5\text{Ge}_3\text{O}_{11}$ annealed at 350°C for one minute after each layer and 700°C for ten minutes after the final layer. This $\text{Pb}_5\text{Ge}_3\text{O}_{11}$ film was deposited on a two layer PbTiO_3 film with identical processing conditions.	117
4.41. Schematic diagram of the proposed "open" microstructure that develops in $\text{Pb}_5\text{Ge}_3\text{O}_{11}$ films annealed to develop a large grain size	118
4.42. $\text{Pb}_5\text{Ge}_3\text{O}_{11}$ film configurations for microstructural optimization . . .	119
4.43. Optical micrograph of a 12-layer $\text{Pb}_5\text{Ge}_3\text{O}_{11}$ film annealed at 450°C for one minute after each layer, then 730°C for 5 minutes and 760°C for one minute after the final layer (1000X)	120
4.44. Dielectric data for an 8-layer $\text{Pb}_5\text{Ge}_3\text{O}_{11}$ film annealed at 450°C for one minute after each layer and 450°C for 10 minutes after the final layer. (A) Dielectric constant versus temperature. (B) Dielectric loss versus temperature	123
4.45. Dielectric data for an 8-layer $\text{Pb}_5\text{Ge}_3\text{O}_{11}$ film annealed at 500°C for one minute after each layer and 500°C for 10 minutes after the final layer. (A) Dielectric constant versus temperature. (B) Dielectric loss versus temperature	124
4.46. Dielectric data for an 8-layer $\text{Pb}_5\text{Ge}_3\text{O}_{11}$ film annealed at 700°C for one minute after each layer and 700°C for 10 minutes after the final layer. (A) Dielectric constant versus temperature. (B) Dielectric loss versus temperature	125

4.47. A ferroelectric hysteresis loop for a 12-layer $\text{Pb}_5\text{Ge}_3\text{O}_{11}$ film annealed at 700°C for one minute after each layer and 700°C for 10 minutes after the final layer	128
4.48. Pyroelectric current and pyroelectric coefficient versus temperature for a 10-layer $\text{Pb}_5\text{Ge}_3\text{O}_{11}$ film annealed at 700°C for one minute after each layer and 700°C for 10 minutes after the final layer. Poling conditions were 15KV/cm	129
4.49. Pyroelectric current and pyroelectric coefficient versus temperature for a $\text{Pb}_5\text{Ge}_3\text{O}_{11}$ film with the configuration diagramed in Figure 4.42B. Electrical poling was not performed on this sample	132
4.50. Pyroelectric current and pyroelectric coefficient versus temperature for a $\text{Pb}_5\text{Ge}_3\text{O}_{11}$ film with the configuration diagramed in Figure 4.42D. Electrical poling was not performed on this sample	133
4.51. Pyroelectric current and pyroelectric coefficient versus temperature for a $\text{Pb}_5\text{Ge}_3\text{O}_{11}$ film with the configuration diagramed in Figure 4.42D. Poling conditions were 10KV/cm	134
4.52. Pyroelectric current and pyroelectric coefficient versus temperature up to temperatures above the ferroelectric to paraelectric transition for the $\text{Pb}_5\text{Ge}_3\text{O}_{11}$ film described in Figure 4.51	136
4.53. Dielectric constant and dissipation factor versus temperature for a $\text{Pb}_5\text{Ge}_3\text{O}_{11}$ film with the configuration described in Figure 4.51	138

LIST OF TABLES

	Page
1. Properties related to pyroelectric performance for selected single crystal pyroelectric materials	21
2. Pyroelectric figures of merit for selected single crystal pyroelectric materials	22
3. Thermal expansion coefficients of $\text{Pb}_5\text{Ge}_3\text{O}_{11}$	32
4. Comparison of molar composition to weight percent and volume percent for compositions investigated	51
5. Lead germanate film thicknesses as a function of annealing conditions and number of layers	52
6. Approximate surface grain size for $\text{Pb}_5\text{Ge}_3\text{O}_{11}$ thin films as a function of annealing time and temperature	97
7. Pyroelectric data for a 10-layer $\text{Pb}_5\text{Ge}_3\text{O}_{11}$ film annealed at 700°C for one minute after each layer and 700°C for 10 minutes after the final layer	130
8. Pyroelectric coefficients for a lead germanate film before and after electrical poling	135

ACKNOWLEDGMENTS

I would like to take this opportunity to express my sincere gratitude to everyone who assisted in the completion of this work. The following persons deserve a special mention and thanks for their contributions.

My sincere thanks go to Dr. Michael Haun, my advisor, for his guidance, technical support and patience throughout the course of this work.

Many thanks to my colleagues, Ivan Cornejo and Marc Ritland for their encouragement, technical support, and the constant exchange of ideas.

A big thanks to Chris Reed and Schuller International, Inc. for their expertise and assistance with atomic force microscopy.

Thanks go to Alice Jensen and Scott Pawelka for their constant help with all of the odds and ends.

As always, I owe a lot of thanks to my parents for their continued love and encouragement.

A special thanks goes to all of my rock climbing partners for supplying a crucial balance in my everyday life and a proper perspective during the stressful moments.

And finally, I would like to thank the Office of Naval Research and the National Science Foundation for providing the funding that supported this research.

I. Introduction

1.1. Statement of Problem

The purpose of this research was to develop an understanding of the processing/property relationships for solution-derived ferroelectric thin films in the $\text{Pb}_5\text{Ge}_3\text{O}_{11}$ and $\text{Pb}_5\text{Ge}_3\text{O}_{11}\text{-PbZr}_x\text{Ti}_{1-x}\text{O}_3$ systems. Ferroelectric thin films combine the unique electrical properties of ferroelectrics with the useful geometric possibilities of thin film devices. The wide range of device possibilities include nonvolatile memory, pyroelectric detectors, capacitors, SAW substrates and electro-optic devices. Many of the current obstacles involved with this rapidly expanding technology concern the control of material composition and crystallization resulting in the desired performance criteria. The challenge is to optimize material properties for particular applications in combination with reproducible processing conditions.

$\text{Pb}_5\text{Ge}_3\text{O}_{11}$ (PG) is a ferroelectric material that offers unique device possibilities in the microelectronics industry. Lead germanate is a particularly promising candidate material for polycrystalline pyroelectric detector applications due to its low processing temperatures, 180° domains, good pyroelectric properties, and easy alignment of its polar direction perpendicular to the substrate in polycrystalline films. A polycrystalline pyroelectric detector element that has performance characteristics similar to the currently utilized single crystal detector elements would serve as a very significant expansion of possible pyroelectric device applications. Previous investigations on lead germanate thin films indicate the potential of this material, however they also describe many processing difficulties or were

vague in regards to extremely significant issues related to the specific definition of processing parameters.

The mixed ferroelectric system, $\text{Pb}_5\text{Ge}_3\text{O}_{11}$ - $\text{PbZr}_x\text{Ti}_{1-x}\text{O}_3$ offers a potentially unique combination of ferroelectric properties and processing conditions. Due to its excellent electrical properties, $\text{PbZr}_x\text{Ti}_{1-x}\text{O}_3$ (PZT) is the most widely used polycrystalline piezoelectric material. The combination of lead germanate and PZT offers the potential of optimizing device properties by adjusting the ratio of these two components. It is envisioned that a high PG / low PZT ratio may provide optimized pyroelectric properties while a low PG / high PZT ratio may optimize piezoelectric properties and processing conditions. The compatibility of lead germanate and PZT as a mixed ferroelectric system has not been extensively investigated.

This research represents the first work to investigate thin films in the $\text{Pb}_5\text{Ge}_3\text{O}_{11}$ - $\text{PbZr}_x\text{Ti}_{1-x}\text{O}_3$ system and one of the first to investigate $\text{Pb}_5\text{Ge}_3\text{O}_{11}$ thin films fabricated by solution processing. It is also one of the first to investigate thin films that crystallize into multiple ferroelectric phases.

1.2. Objectives

The objectives of this research include:

- Fabricate thin ferroelectric films of $\text{Pb}_5\text{Ge}_3\text{O}_{11}$ and $\text{Pb}_5\text{Ge}_3\text{O}_{11}$ - $\text{PbZr}_x\text{Ti}_{1-x}\text{O}_3$ compositions on silicon substrates.
- Examine the compatibility of $\text{Pb}_5\text{Ge}_3\text{O}_{11}$ and $\text{PbZr}_x\text{Ti}_{1-x}\text{O}_3$ as a mixed ferroelectric system.
- Study the kinetics of phase formation in both the $\text{Pb}_5\text{Ge}_3\text{O}_{11}$ and $\text{Pb}_5\text{Ge}_3\text{O}_{11}$ - $\text{PbZr}_x\text{Ti}_{1-x}\text{O}_3$ thin film systems and relate them to

processing time and temperature.

- Establish relationships between structural changes and processing time and temperature for both systems.
- Establish relationships between the orientation of $\text{Pb}_5\text{Ge}_3\text{O}_{11}$ and $\text{PbZr}_x\text{Ti}_{1-x}\text{O}_3$ with the processing time, temperature, and film composition.
- Establish relationships between the grain size of lead germanate with processing time and temperature.
- Optimize the lead germanate thin film microstructural characteristics for pyroelectric applications.
- Examine the potential electrical properties derived from thin films of $\text{Pb}_5\text{Ge}_3\text{O}_{11}$ and $\text{Pb}_5\text{Ge}_3\text{O}_{11}$ - $\text{PbZr}_x\text{Ti}_{1-x}\text{O}_3$.

1.3. Scope of the Thesis

The thesis begins with a literature review which provides general background information on ferroelectric materials, pyroelectric properties and ferroelectric thin films. More detailed information is provided regarding lead germanate and lead zirconate titanate.

The experimental procedure states the materials and methods used for both the processing and characterization of the thin films.

The results and discussion section contains the findings of the film characterization and the proposed interpretation of those results. Results on phase development, crystallographic orientation, microstructure and electrical properties are reported.

The summary and conclusions section provides a summary of the results for this research as well as how these results impact the scientific

understanding of lead germanate and its potential for commercial applications in pyroelectric device applications.

The final section discusses future work in regards to ferroelectric thin films in these systems that would merit further research.

II. Literature Review

2.1. Ferroelectrics - Background and Theory

Ferroelectrics exhibit a spontaneous polarization that is reversible with the application of an electric field. Ferroelectrics were given their name due to the fact that their features are, in many ways, analogous to those of ferromagnetism. These materials have become increasingly important in recent years as new applications and more in-depth theories regarding their properties are being found.

Ferroelectrics were first discovered in 1920 when Joseph Valasek found that the polarization of Rochelle salt, $\text{NaKC}_4\text{H}_4\text{O}_6 \cdot 4\text{H}_2\text{O}$, could be reversed with an external electric field [1]. Interest in the discovery did not quickly spread due to the difficulty of reproducibly making the salt with the correct composition. There was a belief that this was one of nature's "great accidents".

The first series of ferroelectric crystals was produced from 1935 to 1938 [2]. These crystals were phosphates and arsenates. An example of these is KH_2PO_4 . These crystals, with a much simpler structure than Rochelle salt, allowed a much more accurate theoretical understanding of the ferroelectric phenomena. Slater gave the first basic model for ferroelectricity in 1941 in relationship to these compounds [3]. He assumed that there was an ordering of hydrogen atoms that occurred during the transition from the nonpolar phase to the polar phase.

The next breakthrough wasn't made until 1945 when ferroelectricity was discovered in barium titanate [2]. At the time, BaTiO_3 was being

investigated as a dielectric replacement for mica. Of major significance was the fact that barium titanate was even easier to manufacture and investigate due to its stability and simple structure - five atoms per unit cell. The composition of barium titanate of course meant that Slater's theory on the ordering of hydrogen atoms and their required presence had to be rejected as a model for ferroelectricity. BaTiO_3 has a perovskite structure and many other ferroelectrics were subsequently discovered which shared this same structure.

Significant advancement in the understanding of ferroelectrics was made in 1960 when Cochran contributed the displacive lattice instability found in ferroelectrics to the ionic motions of the atoms or lattice modes [4]. This work essentially began the modern understanding of ferroelectric behavior.

2.1.1. General / Phenomenology

Ferroelectrics are characterized by two or more orientational states in the absence of an electric field. These states can be shifted, one to another, by the application of an electric field. Ferroelectrics undergo a structural phase transition where a higher symmetry phase transforms to a lower symmetry phase with a spontaneous polarization. This polarization is defined as electric dipole moment per unit volume. A plot of polarization versus electric field results in a hysteresis loop for ferroelectrics (Fig. 2.1). If an electric field, $E > E_c$, is applied there is a net polarization in the material. E_c is defined as the coercive field and corresponds to the field at which switching from one polarization state to another takes place. If the electric field is then removed, $E = 0$ the material retains a remnant polarization, P_r . If

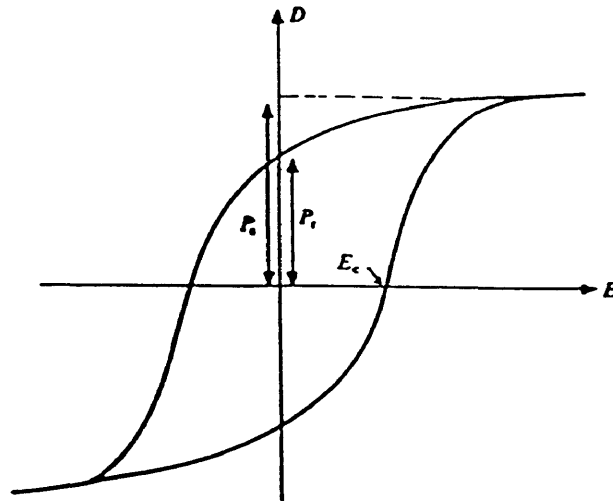


Figure 2.1. A ferroelectric hysteresis loop of polarization versus electric field [2].

an electric field, $E < -E_c$, is now applied, there is a net polarization in the opposite direction and removal of the electric field will result in a remnant polarization, $-P_r$. This application of a reversed electric field has caused the polarization to rotate in the opposite direction. The area of the hysteresis is equivalent to the energy required to reorient the polarization. At low temperatures the coercive field is large and the polarization configuration is "frozen" in. At increasingly elevated temperatures, the coercive field is reduced until the hysteresis behavior is eliminated and the material obeys the linear Curie-Weiss Law [5]. The material is now paraelectric. The temperature of this occurrence is the transition temperature (T_c).

2.1.2. Structure / Crystallography

Of the 32 crystal classes, 11 have a center of symmetry and therefore have no polar properties. Of the remaining 21 non-centric classes, 20 exhibit an electrical polarity when subjected to stress. This is a linear effect and is termed piezoelectricity. Ten of these 20 piezoelectric classes have a unique polar axis and therefore possess a spontaneous polarization. These are the pyroelectric classes. Ferroelectrics are a subgroup of pyroelectrics. The ferroelectrics are characterized by two or more orientational states in the absence of an electric field. These states can be shifted, one to another, by the application of an electric field [2].

2.1.3. Domains

Since at least two directions are equivalent in a ferroelectric material, different regions within the same crystal may polarize in different directions as a means to minimize the depolarization energy. This minimization of energy is in terms of both mechanical and electrical energy. A volume of uniform polarization defines a domain. In uniaxial ferroelectrics there are only two polar directions, related by 180° . Adjacent domains in a uniaxial ferroelectric have polarizations in the opposite direction. If the entire crystal is polarized in the same direction, that crystal would be regarded as single domain. Multiaxial ferroelectrics can develop domains related by orientations other than 180° depending on symmetry. The boundary separating domains is called a domain wall which also has an energy associated with it. The overall polarization of a crystal is dependent on the difference between opposing polarization volumes. This is determined through a minimization of

the total energy, that is, the depolarization energy and the domain wall energy [2]. Domain motion (reorientation) is dependent on such factors as temperature, strain, crystal size, etc.

2.1.4. Soft Modes

The concept of soft modes of lattice vibrations can be used to help explain how a material can make the phase transition from a higher to lower symmetry. A soft mode can basically be defined as a transverse optical mode of lattice vibration whose frequency tends towards zero as the temperature approaches some critical temperature. The soft modes of a crystal have a strong effect on the crystal properties such as permittivity, piezoelectricity and the elastic constants.

The movement of atoms to positions other than their equilibrium positions is through normal vibrational modes. The reduction in frequency of the soft mode causes a reduction in the restoring force exerted on the displaced atoms. Those displaced atoms are then "frozen" in place. If only some atoms are moved relative to the others, a phase transition takes place. Ferroelectrics undergo a ferrodistorive structural phase transition where these soft modes are centered in the Brillouin zone in the reduced zone reciprocal lattice. If the mode condensation occurs in a location other than the center, the structural transition is termed antiferrodistorive. This most often occurs at the zone boundary [2].

In order to understand how the transverse optical frequency can be reduced you must consider the effect of the electric field. If you consider a local field problem, E_{loc} is equal to the applied field, E_0 , plus a contribution proportional to the size of the induced dipole moments. This contribution is

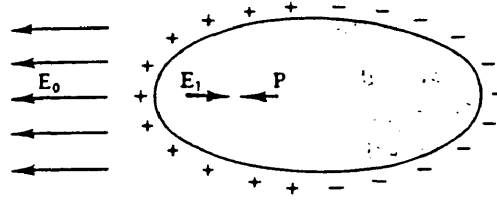


Figure 2.2. Relative directions of applied field (E_0), depolarization field (E_1) and polarization [6].

termed the depolarization field (E_1). This depolarization field from the induced dipole moments can be dependent on the position within the cell. The depolarization field tends to oppose the applied field [6] (Fig. 2.2) and reduces the restoring force on the displaced ions and the oscillation frequency of the ions. For the principal axes of an ellipsoid, the components of this field would be,

$$E_{1x} = -\frac{N_x P_x}{\epsilon_0} ; E_{1y} = -\frac{N_y P_y}{\epsilon_0} ; E_{1z} = -\frac{N_z P_z}{\epsilon_0}$$

where N_x , N_y and N_z are the depolarization factors whose sum equals one. ϵ_0 is the permittivity of free space. So, for a spherical volume,

$$E_{LOC} = E_0 - \frac{P}{3\epsilon_0}$$

Without these mechanisms the transverse optical frequency can be described as:

$$\omega_0^2 = \frac{\alpha}{\mu}$$

where α is the force constant and μ is the reduced mass,

$$\mu = \frac{m_+ m_-}{m_+ + m_-}$$

The tendency for the depolarization field to reduce the applied field will therefore reduce the optical mode frequency. For a cubic lattice this reduced frequency is described as [2],

$$\omega_0^2 = \frac{\alpha}{\mu} - \frac{\frac{4\pi}{3} \frac{Q^2}{V_p}}{1 - \frac{4\pi}{3} \frac{(a_+ + a_-)}{V_p}}$$

where: Q = Effective Charge

a_{\pm} = Atomic Polarizabilities

V_p = Volume of the Primitive Unit Cell

So it can be seen that the resulting frequency will be reduced from the original magnitude.

The Lyddane-Sachs-Teller Relation is the classic correlation between the increase in dielectric constant and the decrease in soft mode frequency observed at the transition temperature.

$$\frac{\omega_{LO}^2}{\omega_{TO}^2} = \frac{\epsilon}{\epsilon_{\infty}}$$

This equation relates the clamped, static dielectric constant, ϵ and the high

frequency ($\omega \gg \omega_{\text{lattice}}$) dielectric constant, ϵ_{∞} to the longitudinal and transverse optical modes, ω_{LO} and ω_{TO} . The dielectric constant at high frequency is due to contributions from the electrical polarization only. Keep in mind that the dielectric constant is related to the material's ability to polarize. The dielectric constant of the material will increase towards infinity as ω_{TO}^2 goes to zero. A phase transition will then occur to form a more stable structure. So, as a basic summary to this discussion, the electrostatic dipole forces tend to reduce the transverse optical frequency, but do not

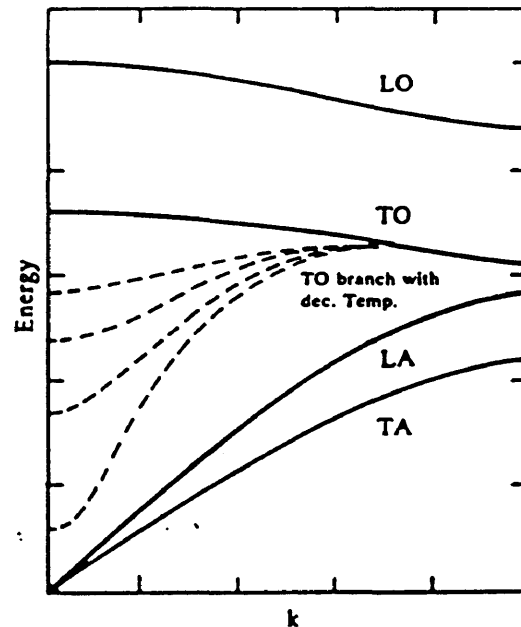


Figure 2.3. Plot of energy versus k for a paraelectric phase. The dashed lines represent the reduction in the energy of the transverse optical branch as the transition temperature is approached [7].

have a significant effect on the longitudinal optical frequency (Fig. 2.3).

Raman scattering is a very useful characterization technique to study soft mode behavior and was in fact one of the first techniques used to describe this occurrence. In Raman scattering, the phonons involved in optical processes are studied. Other techniques that can be used to study soft modes include neutron scattering, infra-red spectroscopy and x-ray scattering. One advantage of neutron scattering is its capability to measure both the wavelength and time dependence of dynamic correlations. Dispersion relations can be measured over the entire Brillouin Zone[10].

2.2. Ferroelectric Thin Films

Ferroelectric thin films have been the focus of increasingly intensive research activity in recent years. The potential applications include optical shutters and modulators, surface acoustic wave devices, field effect transistors, IR sensors and nonvolatile memories [8]. Development of these films has used such fabrication methods as radio frequency sputtering, chemical vapor deposition, ion beam deposition, electron beam evaporation and sol-gel methods. Most of the difficulties in developing these materials have been associated with the technology involved and the actual property relations and interactions. As is usually the case, the technology involved has advanced much faster than the scientific understanding. Ferroelectric films don't often show properties similar to those of bulk crystalline materials [9]. For example, thin film ferroelectrics generally do not show a sharp peak in permittivity at the transformation temperature. One reason for this is the high tensile stresses associated with the thin layer. Quite simply, we just

don't understand enough about the relationships between processing methods and the material properties of the thin films.

2.2.1. Thickness Effects

The thickness of the ferroelectric has a very strong effect on the electrical properties that is not well understood. The relationships between thickness and properties such as spontaneous polarization actually serve to define optimum processing "windows".

The depolarization energy (W_E) for a simple periodic domain structure (Fig. 2.4) can be described as [2],

$$W_E = \frac{\epsilon^* \cdot d \cdot P_0^2 \cdot V}{t}$$

Where: d = Domain Width

t = Crystal Thickness

P_0 = Polarization at the center of the domain

V = Crystal Volume

ϵ^* = Constant dependent on the dielectric constants

The domain wall energy (W_w) can be described as,

$$W_w = \frac{\sigma}{d} \cdot V$$

where σ is the energy per unit area of the domain wall. A minimization of ($W_E + W_w$) results in the equilibrium value of the domain width,

$$d = \left[\frac{\sigma \cdot t}{\epsilon^* \cdot P_0^2} \right]^{\frac{1}{2}}$$

If the crystal thickness decreases to where the domain width is approximately equal to the domain wall thickness, the depolarization energy can no longer be minimized and the material will cease to exhibit ferroelectric properties [2]. So, at this critical thickness, the spontaneous polarization goes to zero. This thickness for single crystal barium titanate is estimated at 200Å however for thin film barium titanate, change in P_s versus d is observed at 400Å [9]. So, finite size effects must be considered in determining a lower thickness limit that still exhibits the desired properties of the bulk material.

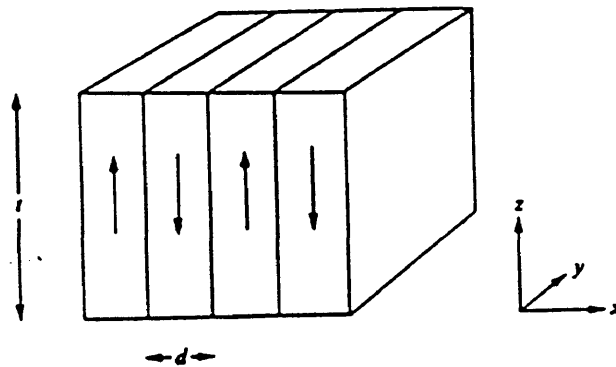


Figure 2.4. A periodic domain structure model [2].

2.2.2. Surface Effects

At the surface of a material there is effectively a reduction from three dimensions to two dimensions. Material properties can be significantly altered at a free surface. In a bulk material, these surface effects are not generally significant, however with thin films, the entire sample may be characteristic of a surface. The domain wall velocity at the surface may be expressed as,

$$v = v_{\infty} \exp\left(\frac{-\delta}{E}\right)$$

Where: $\delta = \delta_0(1 + d_0/d)$

δ = Activation field for domain wall movement

d_0 = Surface Layer Thickness

d = Sample Thickness

So, at the surface, domain wall mobility will decrease which will then lead to an increase in the depolarization energy [2].

The use of metal electrodes on ferroelectrics also results in surface effects. Above the transition temperature, the ferroelectric - metallic junction would behave as a Schottky Barrier Junction with a potential(V):

$$V = \frac{2kT}{e} \ln\left[\frac{z}{z_0} + 1\right]$$

Where: $z_0 = (2\epsilon\epsilon_0kT / N_0e^2)^{1/2}$

N_0 = Surface concentration of carriers

The term, z_0 is the thickness of the surface layer where the field drops to one half its value at the surface. The polarization can have a large effect on the free-carrier density and the surface fields. Below the transition temperature, in the ferroelectric region, the charge density at the surface must neutralize the depolarization fields in the bulk. The theory is that this compensating charge is located at the surface [2]. The field produced by this surface charge will penetrate to a significant depth and affects the electrical transport phenomena. This field causes a bending of the energy bands at the surface (Fig. 2.5).

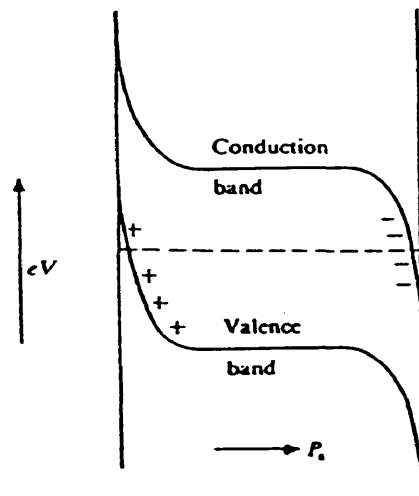


Figure 2.5. The bending of the conduction and valence bands due to the polarization change at the surface[2].

2.3. Pyroelectric Properties

Pyroelectric materials exhibit a spontaneous polarization and form permanent dipoles in the structure. Ferroelectric materials are a subgroup of pyroelectrics with the added characteristic of a spontaneous polarization that is reversible with the application of an electric field.

The polarization of pyroelectric materials changes with a change in temperature. The total dielectric displacement (\vec{D}) for a polar material can be expressed as:

$$\vec{D} = \epsilon \vec{E} + \vec{P}_s$$

Where: ϵ = relative permittivity
 \vec{E} = applied field
 \vec{P}_s = spontaneous polarization

At a constant field, the partial derivative with respect to temperature is:

$$\frac{\partial \vec{D}}{\partial T} = \frac{\partial \vec{P}_s}{\partial T} + \vec{E} \frac{\partial \epsilon}{\partial T}$$

The pyroelectric coefficient (\vec{p}) is given as:

$$\frac{\partial \vec{P}_s}{\partial T} = \vec{p}$$

The pyroelectric coefficient is in fact a vector, \vec{p} , however device geometries allow it to be described as a scalar and will be denoted as (p) in subsequent equations. Units for the pyroelectric coefficient are C/cm²°C or C/m²°C.

The pyroelectric current (I_p) can be described by:

$$I_p = pA \frac{\partial T}{\partial t}$$

Where: A = surface area of electrode

Response can only be obtained from a time varying flux (ie. for a constant source of heat flux, either the heat source or the detector must be moving, or the source flux must be "chopped" as a means of modulation).

The possible device applications for pyroelectric materials are extensive. Several examples include, intruder alarms, fire alarms, thermal imaging (vidicon), and laser detection. In the case of an intruder alarm, a human body emits maximum power at a wavelength of approximately $9.5\mu\text{m}$. Pyroelectric materials that absorb strongly in this region of wavelength can be chosen and filters can be used to reduce the detection of radiation from other sources [11].

The actual performance of a pyroelectric material is dependent on a number of other material properties as well as device design and operating parameters. Material properties affecting performance include, dielectric constant (K), density (ρ), specific heat per unit mass (C), thermal diffusivity (D) and the dissipation factor ($\tan \delta$). Halliyal et al.[12] describe a number of "pyroelectric figures of merit", (F), that relate a material's pyroelectric performance:

$F_2 = p/\rho C$	Current Mode (current to a low impedance amplifier). This configuration is uncommon.
$F_3 = p/\rho CK$	Voltage Mode (voltage to a high impedance amplifier).
$F_4 = p/\rho CKD$	Thermal Imaging (unreticulated vidicons).

$$F_5 = p/\rho CK^{1/2} \tan \delta^{1/2} \quad \text{Voltage Mode (the pyroelectric element is the limiting factor for detector sensitivity).}$$

The most commonly cited pyroelectric figure of merit is for the voltage mode relating the pyroelectric coefficient to the dielectric constant (relative permittivity) (K) and the specific heat per unit volume ($C\rho = C' \text{ J/cm}^3\text{°C}$) according to the relation, $F_3 = p/KC'$. F_3 is termed the pyroelectric voltage responsivity figure of merit. Inclusion of the dissipation factor as in F_5 probably results in a more realistic indication of material performance. In the case of samples with a thin film geometry, the specific heat would be inappropriate and is not included. The units for the pyroelectric voltage responsivity figure of merit (F_3) are generally expressed as $\text{A}\cdot\text{cm}/\text{W}$ or $\text{C}\cdot\text{cm}/\text{J}$, both being equivalent. For thin film geometries where the specific heat is removed from the expression, the dielectric permittivity rather than the dielectric constant (relative permittivity) is used in the calculations resulting in units of $\text{V}/\text{cm}\text{°C}$. This pyroelectric voltage responsivity figure of merit for thin film geometries will be referred to as F_v .

The properties for several single crystal pyroelectric materials are given in Table 1. The resulting figures of merit (F_2 - F_5) are listed in Table 2. Triglycine sulphate (TGS) and modifications of TGS show superior performance in large area infra-red detection. TGS, however, has a number of disadvantages associated with its use. TGS is hygroscopic, mechanically weak, dissociates above 100°C , and has a very low transition temperature of 49°C [11]. Materials such as $\text{Pb}_5\text{Ge}_3\text{O}_{11}$ (PG) offer an attractive alternative to TGS. PG offers nearly equal pyroelectric performance for certain applications combined with a greatly increased tolerance to environmental conditions, ie. temperature and moisture.

Table 1. Properties related to pyroelectric performance for selected single crystal pyroelectric materials [13].

Material	p (10^{-4} C/m ² K)	K	$\tan\delta$	C' (10^6 J/m ³ K)	D (10^{-7} m ² /s)	T_c (°C)
Triglycine Fluoberyllate (TGFB) at 60°C	7.0	50	0.028	2.5	2.7	73
Deuterated Triglycine Sulphate (DTGS) at 40°C	5.4	43	0.020	2.4	2.9	61
Triglycine Sulphate (TGS) at 35°C	6.0	55	0.025	2.6	2.8	49
LiTaO ₃ (LT)	2.3	54	0.006	3.2	13.0	618
Sr _{0.5} Ba _{0.5} Nb ₂ O ₆ (SBN)	6.5	380	0.003	2.1	-	121
Pb ₅ Ge ₃ O ₁₁ (PG)	1.1	45	0.001	2.0	3.0	177
Pb _{4.7} Ba _{0.3} Ge ₃ O ₁₁ (PBG)	3.1	81	0.005	2.0	3.0	70

Table 2. Pyroelectric figures of merit for selected single crystal pyroelectric materials [13].

Material	F_2 (10^{-10} Cm/J)	F_3 (10^{-12} Cm/J)	F_4 (10^{-5} C/mW)	F_6 (10^{-10} Cm/J)
Triglycine Fluoberyllate (TGFB) at 60°C	2.80	5.60	2.07	2.37
Deuterated Triglycine Sulphate (DTGS) at 40°C	2.25	5.23	1.80	2.43
Triglycine Sulphate (TGS) at 35°C	2.32	4.23	1.51	1.98
LiTaO ₃ (LT)	0.72	1.33	0.10	1.26
Sr _{0.6} Ba _{0.6} Nb ₂ O ₆ (SBN)	3.10	0.81	-	2.90
Pb ₆ Ge ₃ O ₁₁ (PG)	0.55	1.22	0.41	2.59
Pb _{4.7} Ba _{0.3} Ge ₃ O ₁₁ (PBG)	1.55	1.91	0.64	2.44

2.4. Lead Germanate

Speranskaya [14] first reported the congruently melting compound, $\text{Pb}_5\text{Ge}_3\text{O}_{11}$ in a study of the phase diagram for the GeO_2 - PbO system. Ferroelectricity in $\text{Pb}_5\text{Ge}_3\text{O}_{11}$ was discovered by Iwasaki et al.[15] and Nanamatsu et al.[16]. Lead germanate is a uniaxial ferroelectric with a spontaneous polarization aligned with the c-axis. $\text{Pb}_5\text{Ge}_3\text{O}_{11}$ has a second order phase transition [17] from a ferroelectric trigonal phase to a paraelectric hexagonal phase at approximately 177°C [15,16,18]. Ferroelectric $\text{Pb}_5\text{Ge}_3\text{O}_{11}$ is also optically active [19,20]. The reversal of the spontaneous polarization causes an enantiomorphic transformation resulting in a reversal in the sign of the optical rotatory power [19]. This handedness of the optical activity makes lead germanate potentially useful for electro-optic devices.

2.4.1. Kinetics of $\text{Pb}_5\text{Ge}_3\text{O}_{11}$ Formation

The kinetics of $\text{Pb}_5\text{Ge}_3\text{O}_{11}$ formation have been studied primarily through the crystallization of lead germanate glass. $\text{Pb}_5\text{Ge}_3\text{O}_{11}$ is easily formed as a glass by quenching from the melt. Ge^{4+} is a glass network former, similar to Si^{4+} . Glass et al.[21] found that the density of $\text{Pb}_5\text{Ge}_3\text{O}_{11}$ glass is within 3% of the crystalline phase. This indicates that the packing density of the GeO_4 tetrahedra is very similar in the vitreous and crystalline phases.

The formation of metastable lead germanate prior to the crystallization of stable $\text{Pb}_5\text{Ge}_3\text{O}_{11}$ from the vitreous state has been reported by several researchers. Hasegawa et al.[22] reported a metastable phase with a

$\text{Pb}_3\text{Ge}_2\text{O}_7$ composition and a hexagonal structure (Ref. JCPDS 27-1188). This phase was described as transforming to stable $\text{Pb}_5\text{Ge}_3\text{O}_{11}$ at 489°C . The hexagonal lattice parameters were, $a = 10.16\text{\AA}$ and $c = 19.37\text{\AA}$. Nassau et al.[23] described a metastable phase with a nearly identical x-ray diffraction pattern to that given by Hasegawa et al.[22]. This phase crystallized from roller quenched glass at 370°C and transformed to stable $\text{Pb}_5\text{Ge}_3\text{O}_{11}$ at 490°C . The metastable phase had a grain size from 100\AA to several microns at 450°C . After one minute at 520°C , all of the metastable phase was transformed with crystallite sizes of only $\sim 30\text{nm}$. It was therefore proposed that nucleation occurred within the metastable crystals and that the composition must be $\text{Pb}_5\text{Ge}_3\text{O}_{11}$ since $\text{Pb}_3\text{Ge}_2\text{O}_7$ would require PbO from a glassy phase to diffuse back into the crystals for transformation to occur. The rapid transformation would rule out that diffusion process. The hexagonal lattice parameters reported by Nassau et al.[23] for the metastable phase were, $a = 10.19\text{\AA}$ and $c = 19.34\text{\AA}$ (Ref. JCPDS 33-751). Otto has reported a metastable hexagonal $\text{Pb}_5\text{Ge}_3\text{O}_{11}$ phase with different lattice parameters (Ref. JCPDS 34-51). This phase was reported to form with lattice parameters, $a = 10.18\text{\AA}$ and $c = 29.01\text{\AA}$. This has a similar a-axis dimension however the c-axis parameter is 50% longer.

As previously discussed, for lead germanate crystallized from glass, the metastable phase transforms to the stable $\text{Pb}_5\text{Ge}_3\text{O}_{11}$ at approximately 490°C with crystallite sizes less than $0.1\mu\text{m}$. Malevanaya et al.[24] observed that for recrystallized lead germanate glass, grain size varied only slightly with temperature between 500 and 600°C . This temperature region is characterized by a rapid nucleation rate with grain sizes from 0.3 to $0.4\mu\text{m}$. Above approximately 650°C , rapid grain growth was observed. At 720°C , grain sizes ranged from 10 to $40\mu\text{m}$ [24]. Rapid grain growth in the

region of 0.85 to 0.95 T_{melt} is typical due to enhanced diffusion at these elevated temperatures.

2.4.2. $\text{Pb}_5\text{Ge}_3\text{O}_{11}$ Structure and Phase Transition

The lead germanate structure consists of interleaving layers of tetrahedral GeO_4 groups and double tetrahedral Ge_2O_7 groups in equal numbers and perpendicular to the c-axis [25,26]. This structure can be described as a combination of the apatite and nasonite structures (Fig.2.6). There are three formula units per unit cell.

The ferroelectric phase has a trigonal $P3$ symmetry [19,27]. Iwasaki et al.[18] reported the room temperature ferroelectric lattice constants to be $a = 10.251\text{\AA}$ and $c = 10.685\text{\AA}$ with a calculated density of 7.326 g/cm^3 . Newnham et al.[27] reported $a = 10.190\text{\AA}$ and $c = 10.624\text{\AA}$ while Hasegawa et al.[22] reported $a = 10.23\text{\AA}$ and $c = 10.54\text{\AA}$.

The paraelectric phase has a hexagonal $P\bar{6}$ symmetry. The lattice constants at 200°C are reported to be $a = 10.26\text{\AA}$ and $c = 10.69\text{\AA}$ [28]. The ferroelectric-paraelectric transition is reported to involve a -0.0323% change in the cell volume which corresponds to $-0.309\text{ \AA}^3/\text{unit cell}$. This value was determined by studying the pressure induced phase transition of lead germanate [29].

Iwata [30] described the paraelectric/ferroelectric phase transition as being a reorientation of the germanate groups. An oxygen ion in the GeO_4 oscillates with a large amplitude (0.34\AA) in the c-direction above the transition temperature. This oxygen assumes its ferroelectric position at the transition which causes the GeO_4 to incline and the Ge_2O_7 to twist.

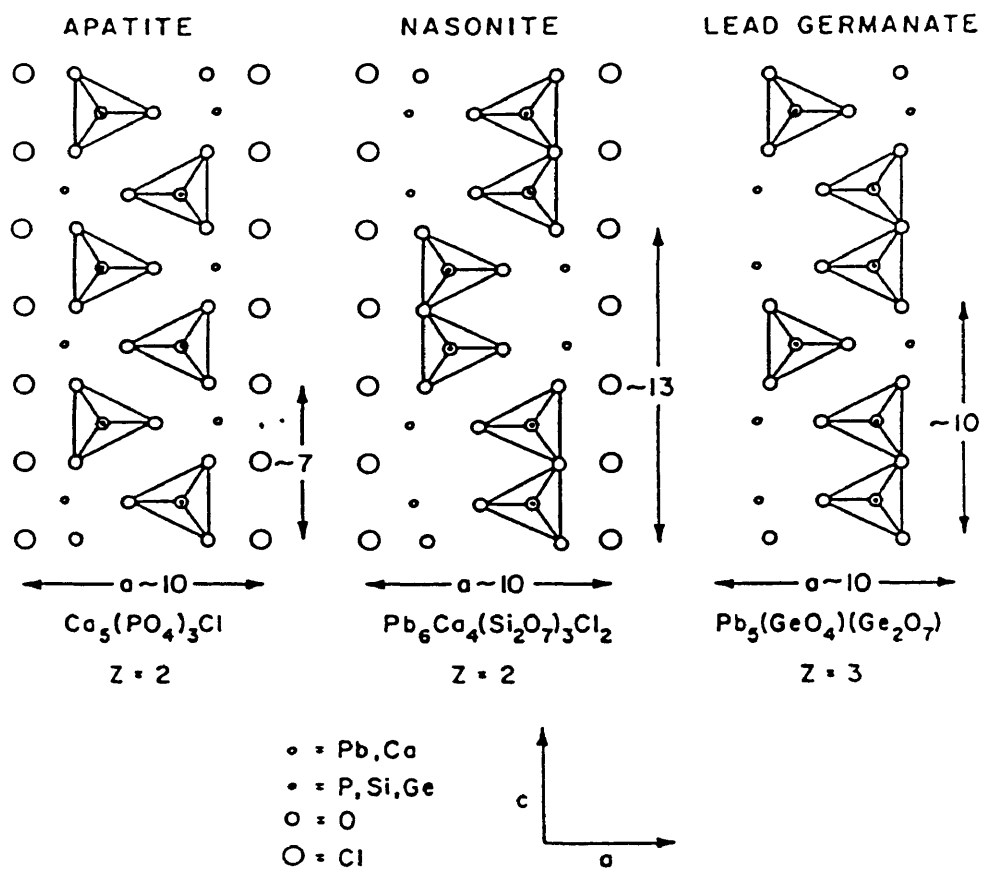


Figure 2.6. Idealized apatite, nasonite and lead germanate structures [27].

Neighboring lead atoms then displace resulting in the ferroelectric polar structure. The oxygen atom acts as a "trigger" for the transition. Its displacive type phase transition is described by the instability of the soft TO vibrational mode.

There has been some debate over the possibility of a phase change in the region of 140°C. Iwasaki et al.[18] showed that the data of P_s^2 versus $(T_c - T)$ exhibits a sharp change in slope at approximately 150°C (Fig.2.7A,B). Gavrilov et al.[31] utilized Mossbauer diffraction and angular correlations of annihilation γ -rays to investigate the phase transition of $Pb_5Ge_3O_{11}$. They concluded based on their results that at the transition temperature, only atoms in the Ge_2O_7 shift to their ferroelectric positions. This alone was

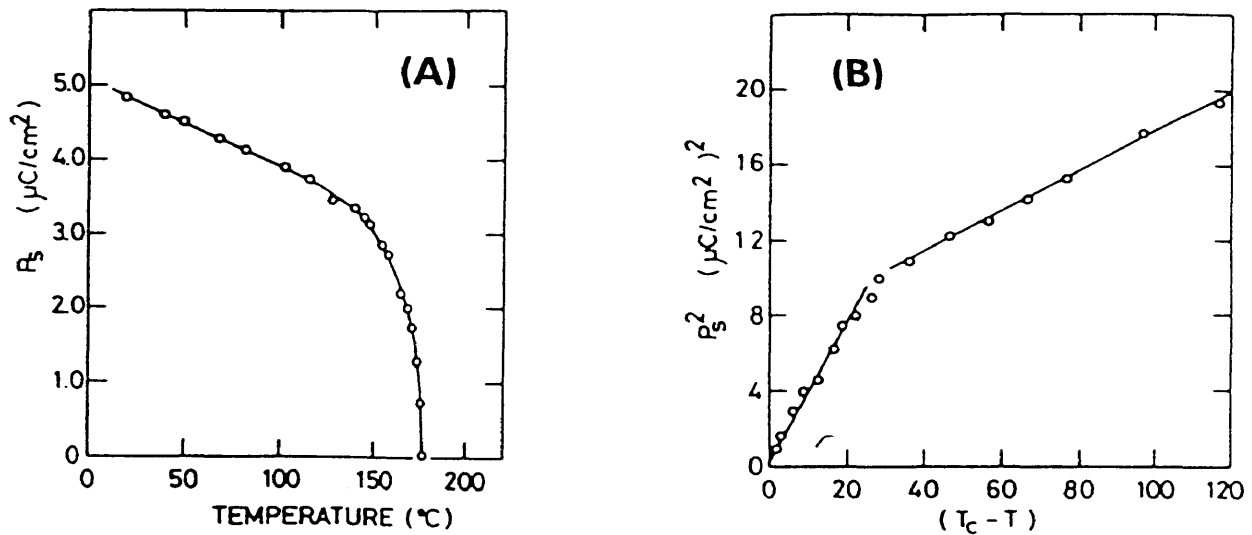


Figure 2.7. (A) Spontaneous polarization (P_s) versus temperature for $Pb_5Ge_3O_{11}$ and (B) P_s^2 versus $T_c - T$ [18].

stated to cause the $P\bar{6}$ to P3 symmetry change. At $\sim 136^\circ\text{C}$, the relaxation motions of GeO_4 and associated Pb^{2+} ions become frozen into the ferroelectric positions. This is due to the motion of the oxygen ion as described by Iwata [30]. From point charge calculations, $P_{\text{s}(\text{GeO}_4)} = -1.78\mu\text{C}/\text{cm}^2$, $P_{\text{s}(\text{Ge}_2\text{O}_7)} = 2.37\mu\text{C}/\text{cm}^2$ and $P_{\text{s}(\Sigma\text{Pb})} = 1.08\mu\text{C}/\text{cm}^2$. The total spontaneous polarization is then calculated to be $1.67\mu\text{C}/\text{cm}^2$ [31]. The addition of the contributions to P_{s} from the GeO_4 and Pb results in a reduction of the net P_{s} by $-0.70\mu\text{C}/\text{cm}^2$. Gavrilov et al.[31] proposed that this explained the anomaly in the slope of the P_{s}^2 versus $(T_{\text{c}}-T)$ data given by Iwasaki et al.[18] (Fig.2.7A,B). The large discrepancy between the predicted value of P_{s} from point charge calculations and the experimental value of $4.8\mu\text{C}/\text{cm}^2$ [18] is most probably due to neglecting the electronic contribution from the lead atoms [30].

The optical rotary properties do not seem to be affected by this low temperature anomaly. Iwasaki et al.[18] gave data of the gyration coefficient, $(g)_{33}$ versus temperature which does not show the anomaly exhibited by the P_{s} (Fig.2.8). This would seem to indicate that the phase change at 177°C is solely responsible for the optical activity of the crystal. This could be further supported by the data given by Iwasaki et al.[18] for silicon additions to lead germanate in the ratio of $\text{Pb}_5(\text{Ge}_2\text{O}_7)(\text{SiO}_4)$. In this case, the silicon addition is sufficient to replace the GeO_4 single tetrahedrals in the structure with SiO_4 . The phase transition shows a linear decrease with silicon additions. The P_{s}^2 versus $(T_{\text{c}}-T)$ data is linear with no anomaly (Fig.2.9). In fact the slope is very similar to that of $\text{Pb}_5\text{Ge}_3\text{O}_{11}$ below 140°C . The optical activity is suppressed slightly, however is still present. If silicon does substitute preferentially in the GeO_4 tetrahedra, these observations

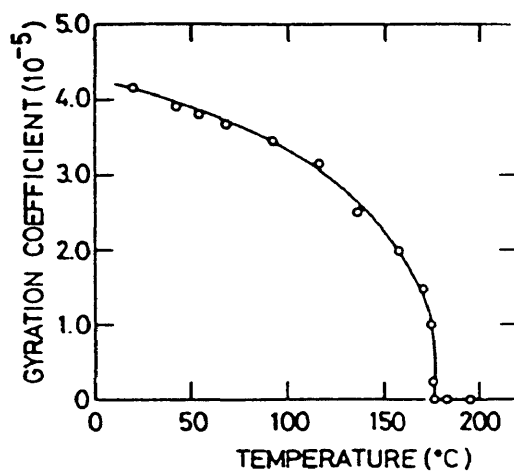


Figure 2.8. Gyration coefficient of $\text{Pb}_5\text{Ge}_3\text{O}_{11}$ versus temperature [18].

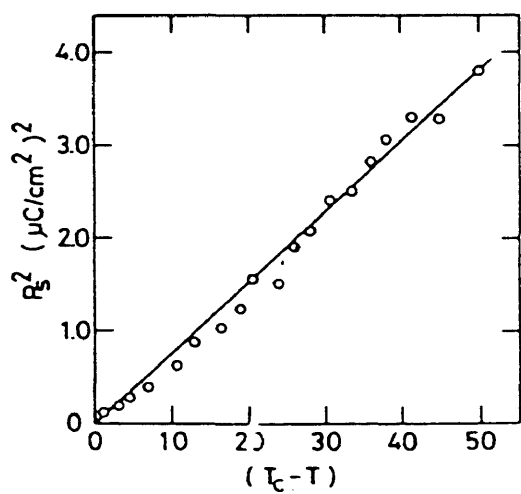


Figure 2.9. P_g^2 versus $T_c - T$ for the composition $\text{Pb}_5\text{Ge}_2\text{SiO}_{11}$ [18].

would tend to confirm that Ge_2O_7 groups are in fact responsible for the optical activity and the transition at 177°C . However, it is not clear that the substitution involves only the GeO_4 tetrahedra. Bush and Venevtsev [32] have reported that for a silicon substitution of up to 39%, the solid solution has the form:



where $(y+z)/3 = x$ in the formula, $\text{Pb}_5(\text{Ge}_{1-x}\text{Si}_x)_3\text{O}_{11}$

The possibility of a high temperature phase transition has also been reported due to an anomaly in both the thermal expansion and the dielectric constant [33,34,35]. This transition was found to occur between approximately 300° and 320°C and is described as occurring with no change in the hexagonal symmetry [34].

2.4.3. Thermal Expansion

Iwasaki et al.[18] reported linear thermal expansion coefficients of $\alpha_a = 7.75 \times 10^{-6}/^\circ\text{C}$ and $\alpha_c = 7.79 \times 10^{-6}/^\circ\text{C}$ for the ferroelectric phase and $\alpha_a = 13.8 \times 10^{-6}/^\circ\text{C}$ and $\alpha_c = 13.4 \times 10^{-6}/^\circ\text{C}$ for the paraelectric phase. Their data also showed an anomaly in the thermal expansion in the region of the phase transition. From 150° to 180°C , the expansion was very low in both the a-axis and c-axis directions (Fig.2.10). Malinowski et al.[34] found the thermal expansion coefficients to be $\alpha_a \approx 9.7 \times 10^{-6}/^\circ\text{C}$ and $\alpha_c \approx 6.0 \times 10^{-6}/^\circ\text{C}$ for the ferroelectric phase. In the paraelectric phase, the a-axis expansion ranged from $\alpha_a \approx 10 \times 10^{-6}/^\circ\text{C}$ at 200°C to $15.5 \times 10^{-6}/^\circ\text{C}$ at 297°C . The c-axis parameters ranged from $\alpha_c \approx 12.9 \times 10^{-6}/^\circ\text{C}$ at 200°C to $18 \times 10^{-6}/^\circ\text{C}$ at 297°C (Table 3). Mainowski et al.[34] also reported that an additional phase

change occurred at approximately 298°C which also resulted in a change of the thermal expansion coefficients. This high temperature paraelectric phase was described as being only a slight distortion of the low temperature paraelectric phase and still maintaining the same hexagonal symmetry.

In comparison to the thermal expansion coefficients of lead germanate, the thermal expansion of silicon (ie., substrates for thin films) is approximately $3 \times 10^{-6}/^{\circ}\text{C}$.

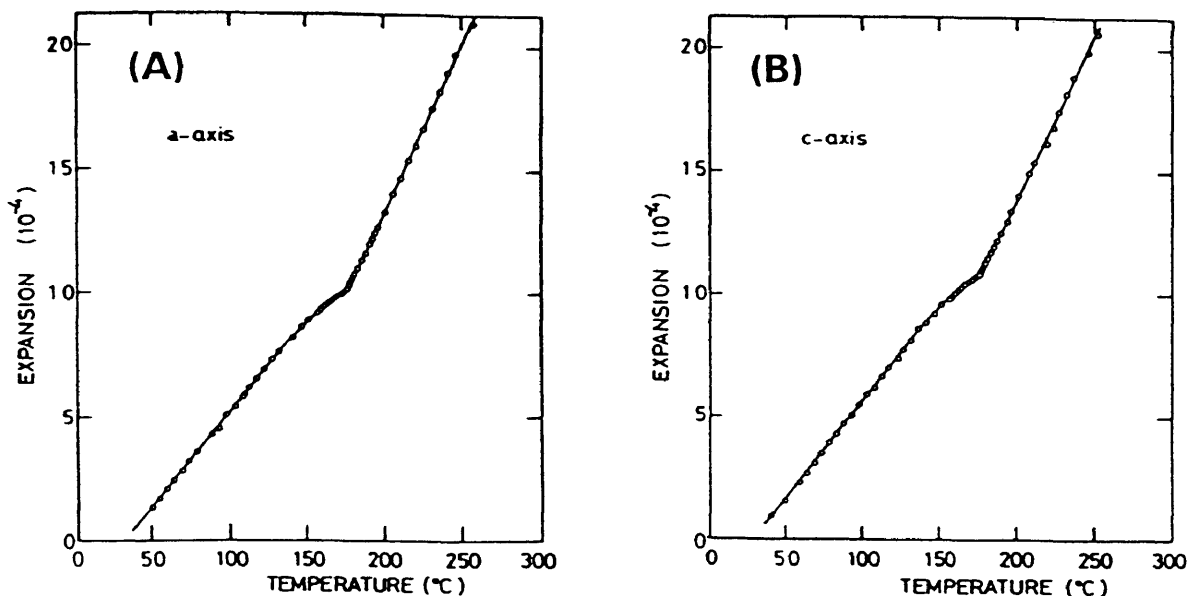


Figure 2.10. Thermal expansion (Δ/l_0) of lead germanate. (A) Along the a-axis. (B) Along the c-axis [18].

Table 3. Thermal expansion coefficients of $\text{Pb}_5\text{Ge}_3\text{O}_{11}$ [34].

Temperature (°C)	X-ray Diffraction Ref.[32]		Dilatometric Ref.[18]	
	α_a ($10^{-6}/^\circ\text{C}$)	α_c ($10^{-6}/^\circ\text{C}$)	α_a ($10^{-6}/^\circ\text{C}$)	α_c ($10^{-6}/^\circ\text{C}$)
Ferroelectric				
76 to 140	9.72	8.2	7.75	7.79
140 to 148	9.73	6.2		
148 to 160	9.71	5.6		
160 to 164	9.68	5.1		
164 to 168	9.57	5.0		
Paraelectric I				
170 to 176	9.56	11.8	13.8	13.4
176 to 200	10.00	12.9		
200 to 244	13.50	12.9		
244 to 260	13.60	13.6		
260 to 276	14.00	14.0		
276 to 292	14.20	15.2		
292 to 294	15.10	16.8		
294 to 296	15.50	20.6		
296 to 297.2	15.50	17.9		
Paraelectric II				
297.2 to 298	15.70	2.3		
298 to 299.2	15.00	4.6		
299.2 to 300	14.30	9.3		
300 to 304		14.5		
304 to 312		13.8		
312 to 332		13.8		

2.4.4. Ferroelectric Properties

Iwasaki et al.[18] gave a saturation polarization at room temperature of approximately $4.8\mu\text{C}/\text{cm}^2$ (Fig.2.7) and a coercive field of 16KV/cm for single crystal $\text{Pb}_5\text{Ge}_3\text{O}_{11}$. The room temperature dielectric constant along the c-axis was found to be 41, while along the a-axis the dielectric constant was 22 (Fig.2.11). The dielectric constant showed a peak at the transition temperature with a value of approximately 3000 for single crystals.

The dielectric constant of lead germanate has been found to be dependent on both grain size and sample thickness. Mansingh et al.[36] studied polycrystalline lead germanate samples with grain sizes ranging from 40 to $300\mu\text{m}$ and found that the dielectric constant is lowered with a reduction in grain size at all measurement frequencies. They attribute this reduction to the formation of a nonferroelectric grain boundary layer of low dielectric constant and conductivity. Mansingh et al.[37] found that the dielectric constant of single crystal lead germanate samples decreased with decreasing sample thickness at all measurement frequencies. They assumed that there was a formation of a homogenous surface layer of low dielectric constant. This was believed to be due to the barrier potential at the metal-insulator junction.

The dielectric properties of lead germanate have also been shown to be very sensitive to pressure [29,38,39,40]. Gesi and Ozawa [38] reported that the transition temperature and the dielectric constant decreased with increasing hydrostatic pressure. The width of the dielectric peak increased with increasing pressure. Gebhardt and Müller-Lierheim [39] reported that the soft mode frequency (ω_i) is not affected by applied uniaxial stress

however hydrostatic pressure does lower ω_f with a corresponding $-11 \pm 2^\circ\text{C}/\text{Kbar}$ dependence of the transition temperature. Kirk et al.[29] gave a pressure dependency for the transition temperature of $-15.5^\circ\text{C}/\text{kbar}$. This compares to $-5.5^\circ\text{C}/\text{kbar}$ for barium titanate.

The grain size of lead germanate also has a large impact on the ferroelectric properties. Glass et al.[21] found normal ferroelectric behavior only when the grain size was greater than approximately 1 micron. Grain sizes on the order of 10nm were determined to be too small to stabilize ferroelectric order. In their study of $\text{Pb}_5\text{Ge}_3\text{O}_{11}$ recrystallized from glass,

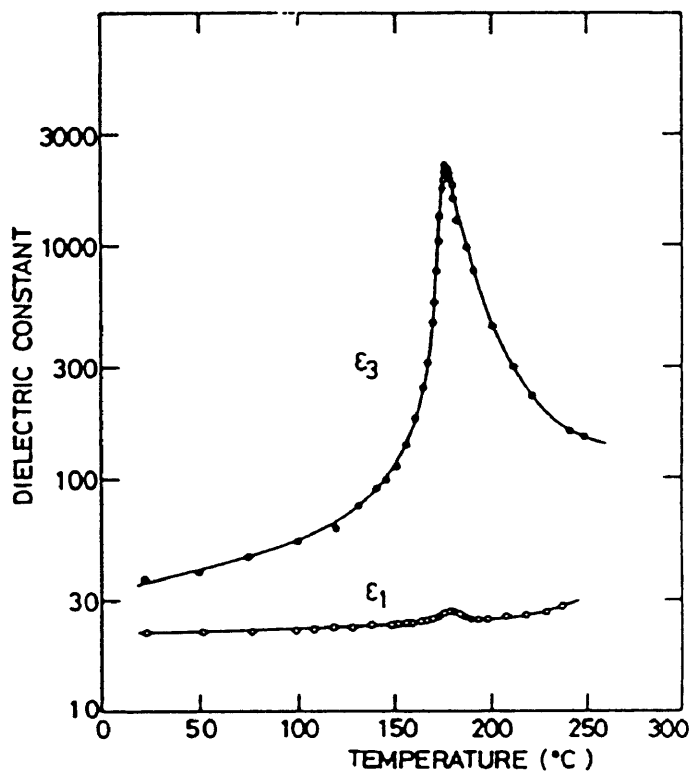


Figure 2.11. Dielectric constant versus temperature for single crystal $\text{Pb}_5\text{Ge}_3\text{O}_{11}$ along the a-axis and the c-axis [18].

results show that as annealing times and temperatures are reduced, the dielectric transition becomes more diffuse. For a sample annealed at 520°C for one minute, no dielectric peak was found at the transition and the sample could not be poled. Malevanaya et al.[27] also confirmed the effect of grain size in $\text{Pb}_5\text{Ge}_3\text{O}_{11}$. They determined that internal stress played the dominant role with an increase in stress with decreasing grain size. Lead germanate has only 180° domains and therefore shows no stress relaxation due to 90° domains as in perovskites. By x-ray diffraction, stress was determined to be ~1kbar for a sample with a grain size of 0.3 μm . This corresponded to a transition temperature of ~145°C.

2.4.5. Pyroelectric Properties

Lead germanate has received considerable interest in its possible pyroelectric applications. It presents several advantages over detector materials such as triglycine sulphate (TGS) such as stability, both in terms of temperature and chemical reactivity. Jones et al.[41] first reported the pyroelectric properties of both single crystal and polycrystalline lead germanate. Single crystal values for the pyroelectric coefficient were $0.95 \times 10^{-8} \text{C/cm}^2\text{°C}$ along the c-axis. For polycrystalline samples with a grain size of 15-20 μm , the pyroelectric coefficient was $0.5 \times 10^{-8} \text{C/cm}^2\text{°C}$. Other researchers have reported single crystal values of up to $12 \times 10^{-9} \text{C/cm}^2\text{°C}$ [42,43] along the c-axis. This pyroelectric coefficient (p) is relatively low in comparison to some other pyroelectric materials.

The actual performance of a pyroelectric material, however, is also dependent on other material properties. These material properties include dielectric constant, specific heat per unit volume, thermal diffusivity, and

dissipation factor. Various pyroelectric figures of merit are used to relate these properties to the pyroelectric performance (Section 2.3). The most commonly cited pyroelectric figure of merit is for the voltage mode and is termed the pyroelectric voltage responsivity figure of merit, F_3 . F_3 is used to describe bulk materials and has units of $A \cdot cm/W$ or $C \cdot cm/J$, both being equivalent. In the case of thin films, the pyroelectric voltage figure of merit will be designated by F_v with units of $V/cm^{\circ}C$ (Section 2.3).

The low relative permittivity of lead germanate ($\epsilon_r \approx 40$) results in high voltage responsivity. Takahashi [42] reported $F_3 \approx 0.96 \times 10^{-10} A \cdot cm/W$ for single crystal and $F_3 \approx 0.65 \times 10^{-10} A \cdot cm/W$ for polycrystalline lead germanate samples. Luff et al. [44] reported a maximum figure of merit (F_3) of $1.04 \times 10^{-10} A \cdot cm/W$ for polycrystalline lead germanate samples. These values compare to $F_3 \approx 0.24 \times 10^{-10} A \cdot cm/W$ for polycrystalline $PbZr_{0.7}Ti_{0.3}O_3$.

Substitutions of barium for lead and silicon for germanium show potential for improving the pyroelectric performance. Single crystals with a composition of $Pb_{4.7}Ba_{0.3}Ge_3O_{11}$ were found to have a pyroelectric coefficient of $32 \times 10^{-9} C/cm^2^{\circ}C$ combined with an increase in DC resistivity [43]. Thick films in this system were found to have a pyroelectric coefficient of $5.1 \times 10^{-9} C/cm^2^{\circ}C$ [45]. Single crystals of $Pb_5Ge_2SiO_{11}$ have been reported with pyroelectric coefficients of up to $30 \times 10^{-9} C/cm^2^{\circ}C$ [43] while polycrystalline samples in this system had values from 10 - $20 \times 10^{-9} C/cm^2^{\circ}C$ [46].

2.4.6. Thin Films

Thin films of lead germanate have been fabricated through a variety of methods including; vacuum condensation [47], sputtering [48-53], thermal

evaporation [54], flash evaporation [55,56], laser ablation [57,58] and sol gel [59,60,61].

Tomashpol'skii and Pentegova [47] first reported the fabrication of lead germanate thin films in 1973 through the use of vacuum condensation. They report a spontaneous polarization of $2.8\mu\text{C}/\text{cm}^2$ which is roughly 1/2 the single crystal value. Other researchers have reported polarization values ranging between 2.1 and $3.3\mu\text{C}/\text{cm}^2$.

The dielectric properties of lead germanate thin films are generally greatly reduced from those of single crystals. Figure 2.12 shows the dielectric constant versus temperature for thermally evaporated thin films of lead germanate. The room temperature dielectric constant of $\text{Pb}_5\text{Ge}_3\text{O}_{11}$ thin

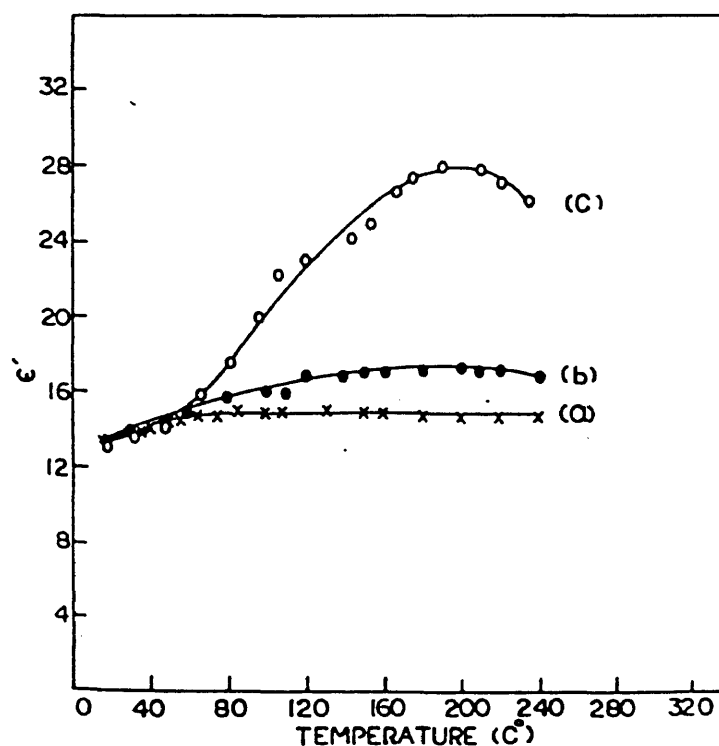


Figure 2.12. Dielectric constant versus temperature for thermally evaporated $\text{Pb}_5\text{Ge}_3\text{O}_{11}$ thin films of thickness: (A) $0.8\mu\text{m}$, (B) $1.0\mu\text{m}$ and (C) $1.8\mu\text{m}$ [54].

films is generally in the range of 15 to 20 with maximum dielectric constant values in the range of 30 to 100 at the transition temperature. The transition is also observed to be much broader than in the case of single crystal lead germanate. Schmitt et al.[50] observed that a decrease in grain size dramatically increased the breadth of the transition, while reducing the maximum peak in the dielectric constant. They indicated that a grain size of $\geq 2\mu\text{m}$ and a thickness greater than $1\mu\text{m}$ was required to obtain ferroelectric hysteresis loops. Mansingh and Krupanidhi [54] also report that films greater than $1.2\mu\text{m}$ in thickness were required to get good ferroelectric behavior. An exception to the reports on ferroelectric properties of the thin films is the work of Lee and Dey in 1992 [59]. They describe "crack free" films formed by sol gel processing, 1600\AA thick with good hysteresis loops, a remnant polarization of $3.3\mu\text{C}/\text{cm}^2$ and a spontaneous polarization of $3.7\mu\text{C}/\text{cm}^2$. Their processing technique consisted of placing the films directly on a hot plate at 450°C for one minute between each layer. The films were four layers thick with a 15 minute, 450°C hot plate annealing after the final layer. The substrate material was (111)Pt/Ti/SiO₂/Si.

Researchers using the deposition techniques of sputtering [53] and thermal evaporation [54,55] have reported a need for oxygen annealing to obtain the correct Pb₅Ge₃O₁₁ stoichiometry. Mansingh and Krupanidhi [54,55] found that annealing for six hours in an oxygen atmosphere resulted in a decrease of the conductivity by three orders of magnitude. They theorized that non-stoichiometry may cause a structural change, however they did not report any structural parameters. Maiwa et al.[53] saw a decrease of 0.30\AA in the c-axis parameter for lead germanate films formed by sputtering. Films showing this decrease exhibited no peak in the dielectric constant. Following a post deposition annealing in oxygen, the

films were found to regain the correct c-axis dimension and also showed a dielectric peak.

Thin films of $\text{Pb}_5\text{Ge}_3\text{O}_{11}$ and $\text{Pb}_5\text{Ge}_{3-x}\text{Si}_x\text{O}_{11}$ have received interest for their possible application as pyroelectric detectors. Schmitt et al.[52] have reported $\text{Pb}_5\text{Ge}_3\text{O}_{11}$ films modified with 20% Si and 1% Nd to have a pyroelectric figure of merit (F_v) of 6800V/cm°C. This value is comparable to that of TGS (7100V/cm°C).

2.4.7. Preferred Orientation

$\text{Pb}_5\text{Ge}_3\text{O}_{11}$ and $\text{Pb}_5\text{Ge}_{3-x}\text{Si}_x\text{O}_{11}$ have been found to exhibit preferred orientation of the c-axis in samples prepared by glass recrystallization, screen printing, and a variety of thin film deposition techniques. This orientation effect is especially significant since the c-axis is the direction of the polarization in lead germanate.

For $\text{Pb}_5\text{Ge}_3\text{O}_{11}$ samples formed as a glass with polished surfaces prior to recrystallization at 675-695°C for four hours, c-axis orientations up to 80% were observed [62,63]. This degree of c-axis orientation was found to contribute a nearly 100% increase in the spontaneous polarization and approximately a 35% increase in the pyroelectric activity.

Takahashi et al.[42,46,64] have shown c-axis orientations of up to 39% for samples prepared by screen printing. Cornejo et al.[65] prepared lead germanate thick films by screen printing on Al_2O_3 substrates with orientations of up to 60% in the c-axis.

Thin films of lead germanate have shown the most significant orientational effects. Virtually all research related to lead germanate thin films has reported c-axis orientation after an annealing step. Lee and Dey

[59] showed virtually 100% c-axis orientation for thin films prepared by spin coating and annealing at 450°C. Landin and Haun [61] have also reported orientations of greater than 98% for films prepared by spin coating.

2.5. Lead Zirconate Titanate

Of the current ferroelectric thin film materials under investigation, $\text{PbZr}_x\text{Ti}_{1-x}\text{O}_3$ (PZT) is particularly promising as a candidate material for many applications such as ferroelectric random access memories, SAW substrates and infrared detectors [66]. PZT is also the most widely used polycrystalline piezoelectric material.

2.5.1. $\text{PbZr}_x\text{Ti}_{1-x}\text{O}_3$ Structure and Phase Transition

Lead zirconate titanate is a ferroelectric material with the perovskite structure. This pseudocubic ABO_3 has either a tetragonal or rhombohedral structure below the Curie temperature. The tetragonal structure results from an elongation of the c-axis while the rhombohedral is due to a distortion along the body diagonal.

PbTiO_3 has a tetragonal structure ($P4mm$) in its ferroelectric state below the transition temperature of approximately 492°C, and a paraelectric cubic structure ($Pm3m$) above that temperature. Lead titanate shows a very large tetragonal distortion. At its phase transition, this c/a distortion is approximately 1.018 [67]. After cooling to room temperature, this distortion increases to approximately 1.064 [67]. Due to the distortion of the structure, pure lead titanate fractures extensively on cooling through the transition temperature.

PbZrO_3 has an orthorhombic structure and is antiferroelectric. The substitution of Zr^{4+} for Ti^{4+} has the effect of reducing the tetragonal distortion of the pure lead titanate. At a composition of approximately $\text{PbZr}_{0.52}\text{Ti}_{0.48}\text{O}_3$, a morphotropic phase boundary is found which separates the ferroelectric tetragonal phase (at higher PbTiO_3 compositions) from the ferroelectric rhombohedral phase (at lower PbTiO_3 compositions) (Fig.2.13). This phase boundary has been determined to have a width that is dependent on both firing time and temperature [68]. The boundary simply represents the composition with equal tetragonal and rhombohedral phase content.

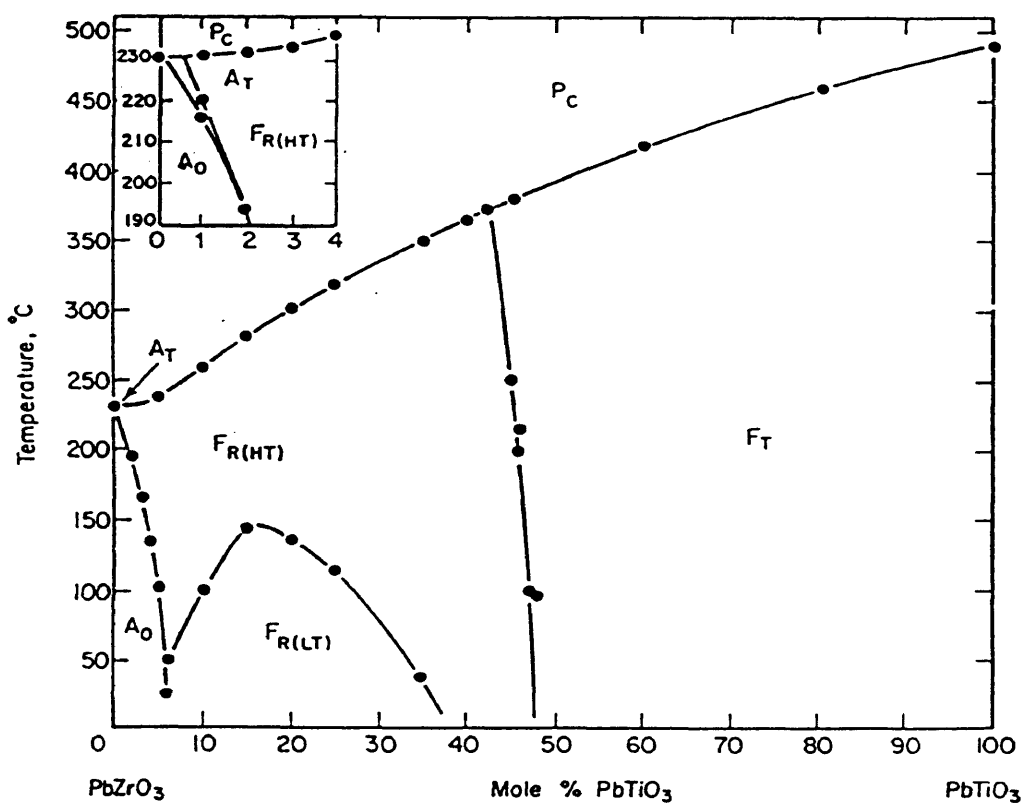


Figure 2.13. Sub-solidus phase diagram of the PbTiO_3 - PbZrO_3 System [67].

Most electromechanical properties are maximized near this composition. The primary reason for the optimized properties is the coexistence of both the tetragonal and rhombohedral structures. Polarization in a tetragonal material occurs along the [001] crystallographic directions, therefore there are six possible directions. In the rhombohedral structure, polarization occurs along the [111] resulting in eight possible directions. With both structures present, a total of 14 crystallographic directions are possible for the electrical polarization. In a polycrystalline sample, this results in better dipole alignment and therefore enhanced properties. The actual ferroelectric-paraelectric phase transition in PZT is dependent on composition. A 52/48 composition has its Curie temperature at approximately 386°C [67].

2.5.2. Electrical Properties

Single crystal PbTiO_3 has a room temperature dielectric constant in the range of 150 and is expected to have a spontaneous polarization of approximately $81\mu\text{C}/\text{cm}^2$ based solely on its structure [67]. Lead titanate in bulk form has a pyroelectric coefficient on the order of $10 \times 10^{-8}\text{C}/\text{cm}^2\text{C}$. Polycrystalline $\text{PbZr}_x\text{Ti}_{1-x}\text{O}_3$ shows a maximum polarization of approximately $47\mu\text{C}/\text{cm}^2$ for a composition of $\text{PbZr}_{0.56}\text{Ti}_{0.44}\text{O}_3$. The dielectric constant of PZT ranges from 700 to 1500 at room temperature. The pyroelectric coefficient for PZT in bulk form is approximately $3.5\text{-}17 \times 10^{-8}\text{C}/\text{cm}^2\text{C}$ [69].

2.5.3. Thermal Expansion

Pure PbTiO_3 displays a volume expansion upon cooling through the transition temperature due to the large tetragonal distortion. PbZrO_3 on the

other hand has a volume contraction upon cooling through the transition temperature. The combined result for PZT is a very slight volumetric expansion when cooling through the transition temperature.

Polycrystalline $\text{PbZr}_x\text{Ti}_{1-x}\text{O}_3$ shows a low thermal expansion coefficient, $\sim 1.5\text{-}2 \times 10^{-6}/^\circ\text{C}$ below the transition temperature. Above the transition temperature, the thermal expansion coefficient is approximately $9 \times 10^{-6}/^\circ\text{C}$.

2.5.4. Thin Film Formation and Orientation

Thin films based on PbTiO_3 and $\text{PbZr}_x\text{Ti}_{1-x}\text{O}_3$ are being studied extensively for applications in the microelectronics industry. Formation methods have included a wide variety of physical and chemical deposition techniques. The primary substrate material under consideration has been platinized silicon due to its compatibility with current IC technology. Lead titanate thin films are particularly attractive for the application of pyroelectric detectors. This is due to their large pyroelectric constant and low dielectric constant resulting in a high figure of merit for voltage responsivity. This is particularly optimized for films with a c-axis orientation.

Typical annealing temperatures for PZT thin films range from 600 to 750°C. Initially, a nanocrystalline matrix of pyrochlore is observed to form [70,71]. The pyrochlore structure is cubic and not ferroelectric. This is followed by the nucleation and growth of the perovskite phase. The perovskite phase has been found to grow with a rosette structure. These rosettes grow radially within the confines of the film and are single crystal in nature [70,71,72]. Growth is limited by the proximity of neighboring rosettes but typical diameters are observed to range from 0.5 μm to as large as 20 μm . Tuttle et al.[71] felt that the perovskite rosettes crystallized at

platinum "hillocks" or crystallites protruding from the electrode when the annealing temperature was between 500°C and 550°C. At approximately 650°C, they speculated that homogeneous nucleation of the perovskite phase occurred within the pyrochlore matrix.

The orientation of PbTiO_3 and $\text{PbZr}_x\text{Ti}_{1-x}\text{O}_3$ thin films can have a significant impact on the electrical properties. Lead zirconate titanate thin films on (111)Pt/Ti/SiO₂/Si substrates have been observed to orient in either the (100), (111) or random directions. Researchers using (100)Pt/(100)MgO substrates have obtained the (001) orientation for both lead titanate and PZT.

The (111) orientation of PZT on (111)Pt/Si has been attributed to either lattice matching of the PZT(111) to the Pt(111) or the matching of the PZT(111) to the (111) of the Pt_{5.7}Pb transient intermetallic phase. Chen and Chen [73] have reported that a transient intermetallic phase, Pt_{5.7}Pb, forms initially on Pt(111)/Ti/SiO₂/Si substrates upon the heating of amorphous PZT films formed by sol gel. They attributed this formation to the reduction of Pb⁺² during pyrolysis. Their study characterized films placed directly into a preheated tube furnace with no prior pyrolysis.

Brooks et al.[74] reported that oxygen content in the films was one of the most important parameters in controlling the orientation of solution derived PZT films crystallized by rapid thermal annealing. After pyrolysis between temperatures of 350 and 450°C, their films had the same microstructures and phases, amorphous with some small ordered regions of ~5nm. For films pyrolyzed at 350°C followed by rapid thermal annealing at 600°C, (111) columnar perovskite with some isolated pyrochlore present as a nanocrystalline phase was observed. The pyrochlore phase was reported to be of the type, Pb₂Ti₂O₆ (JCPDS 26-142). This is not a lead deficient

pyrochlore but rather a metastable variant which rapidly transforms to perovskite. Zirconium is believed to substitute freely for titanium giving a Zr/Ti ratio similar to the starting composition. For films pyrolyzed at 420°C followed by rapid thermal annealing at 600°C, (100) oriented perovskite was observed to form, with some pyrochlore present even after 300 seconds. The difference in pyrolysis temperatures resulted in different PZT orientations. These researchers believed that pyrolysis at 420°C or higher contributed to some of the lead ions increasing their valence state to Pb^{4+} , resulting in the formation of a more stable $Pb_2(Zr,Ti)_2O_{7-x}$ pyrochlore phase. This resulted in a slower pyrochlore to perovskite transformation for those films. Annealing in an oxygen-rich atmosphere tended to favor the (100) orientation. It was proposed that the stability of the pyrochlore phase influences the transformation kinetics and therefore the nucleation and growth leading to the final microstructure.

Random orientation of PZT films was achieved by Brooks et al.[74] by implementing prehydrolysis of the precursor solution followed by incomplete pyrolysis prior to rapid thermal annealing.

Rapid thermal processing is being used extensively in the processing of PZT thin films. It has been found that heating the films at a rate greater than 50°C/minute substantially improves the ferroelectric properties [75]. It is believed that rapid heating rates promote the evolution of gaseous species during pyrolysis prior to the densification of the amorphous film network. This would tend to reduce defects within the film.

2.5.5. Thin Film Electrical Properties

The electrical properties of PbTiO_3 and $\text{PbZr}_x\text{Ti}_{1-x}\text{O}_3$ thin films are closely related to their crystallographic orientation. Typically, PbTiO_3 thin films have a dielectric constant in the range of 200 and a pyroelectric coefficient of approximately $1.0\text{-}2.0 \times 10^{-8} \text{C/cm}^2\text{C}$ [69,76]. Bell et al.[77] reported lead titanate thin films with a dielectric constant of 259 and pyroelectric coefficient of $1.31 \times 10^{-8} \text{C/cm}^2\text{C}$. This results in a pyroelectric voltage responsivity figure of merit equivalent to $576 \text{ V/cm}^{\circ}\text{C}$.

Polycrystalline thin films with an increased orientation along a polar crystallographic direction will show significantly increased pyroelectric properties. Lead titanate films with a highly c-axis oriented microstructure have been fabricated using rf-magnetron sputtering [78]. These films were modified with a 0.10 lanthanum substitution for lead and were reported to have pyroelectric coefficients of $5.3 \times 10^{-8} \text{C/cm}^2\text{C}$ and a dielectric constant of 200. This very high pyroelectric coefficient was obtained without electrical poling. The corresponding pyroelectric voltage responsivity figure of merit would be approximately $3000 \text{ V/cm}^{\circ}\text{C}$.

Lead zirconate titanate thin films typically have dielectric constants in the range of 600-1000, remnant polarizations of approximately $24 \mu\text{C/cm}^2$, and pyroelectric coefficients on the order of $1 \times 10^{-8} \text{C/cm}^2\text{C}$ for compositions near the morphotropic phase boundary [69,79,80,81]. Tuttle et al.[82] observed a remnant polarization of $60.9 \mu\text{C/cm}^2$ for 40/60 PZT films with an 83% volume fraction of (00l) orientation. These highly c-axis oriented films were calculated to have a pyroelectric voltage responsivity figure of merit double that of a randomly oriented film, however this voltage responsivity is still very low compared to lead titanate or lead germanate.

2.6. Lead Germanate - Lead Zirconate Titanate

Eysel et al.[83] first proposed the idea of using lead germanate as a ferroelectric "cement" due to its low melting temperature. The actual combination of $\text{Pb}_5\text{Ge}_3\text{O}_{11}$ with either PbTiO_3 or $\text{PbZr}_{1-x}\text{Ti}_x\text{O}_3$ has only been studied to a limited extent. Schulze and Biggers [84] used lead germanate as a grain boundary phase to stabilize the polarization in PZT. They report that multiple phases did form with a very low solubility of Ge^{4+} into the PZT structure. However, their findings also show that $\text{Pb}_5\text{Ge}_3\text{O}_{11}$ tended to dissolve PbO from the PZT resulting in the formation of Pb_3GeO_5 at processing temperatures of between 800 and 1300°C.

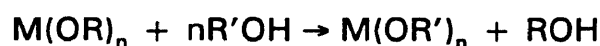
Other research on these diphasic ferroelectric systems has focused on glass-ceramics [65,85,86,87] and thick films [87,88,89]. Cornejo [87] found that while the degree of orientation for $\text{Pb}_5\text{Ge}_3\text{O}_{11}$ thick films was decreased with additions of PbTiO_3 or $\text{PbZr}_{1-x}\text{Ti}_x\text{O}_3$, the electrical properties were enhanced.

III. Experimental Procedure

3.1 Solution Processing

Precursors for the sol gel processing consisted of metal-organic compounds, including a metal salt, lead(II) acetate trihydrate $[\text{Pb}(\text{C}_2\text{H}_3\text{O}_2) \cdot 3\text{H}_2\text{O}]$,^a and metal alkoxides. The metal alkoxides consist of a metal or metalloid atom bonded to one or more alkyl groups through an intermediate oxygen and have the general form, $\text{M}(\text{OR})_n$. Alkoxides used included, germanium ethoxide $[\text{Ge}(\text{OC}_2\text{H}_5)_4]$,^b titanium isopropoxide $[\text{Ti}(\text{OC}_3\text{H}_7)_4]$,^a and zirconium n-propoxide $[\text{Zr}(\text{OC}_3\text{H}_7)_4]$.^a The solvent used in the process was 2-methoxyethanol $[\text{C}_3\text{H}_8\text{O}_2]$.^a One difficulty usually encountered in the use of alkoxide solutions is the ease with which the solutions undergo an irreversible hydrolysis. The low relative humidity of the research location contributed significantly to minimizing this problem.

The processing followed successive stages of reflux and distillation as outlined in Figure 3.1. This promoted an exchange of alkyls between the alkoxides and the solvent according to the general equation:



Initially, the lead acetate was dissolved in 2-methoxyethanol with a ratio in excess of 8:1 solvent. The solution was refluxed for one hour after which distillation was conducted until the temperature reached the boiling point of

^a Aldrich, Milwaukee, WI

^b Gelest, Inc., Tullytown, PA

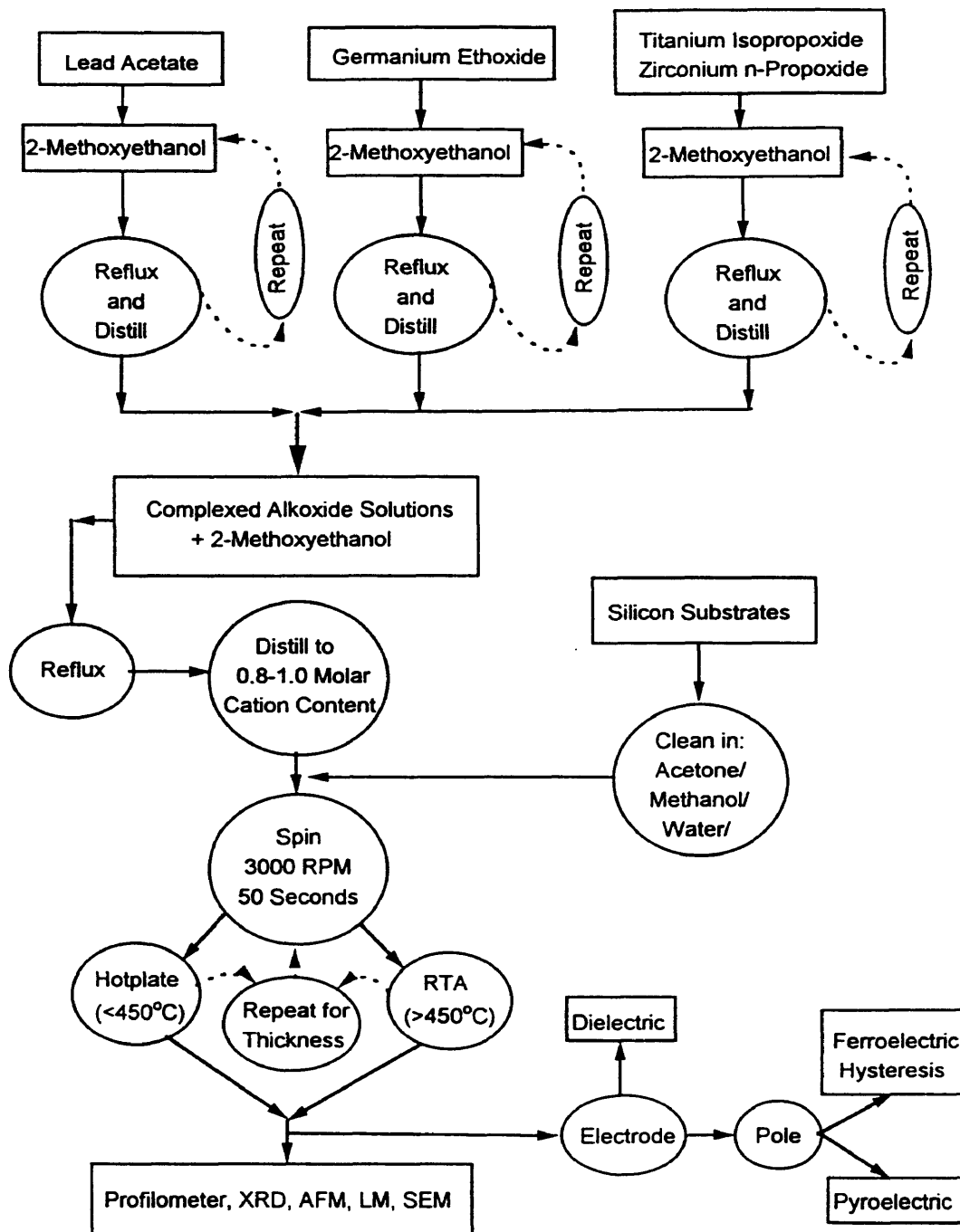
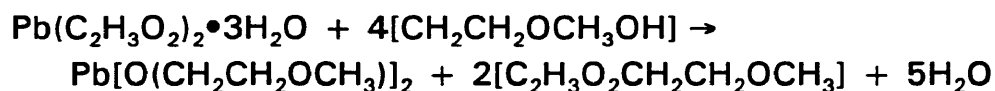
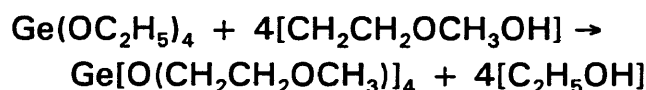


Figure 3.1. Flow chart of the experimental procedure.

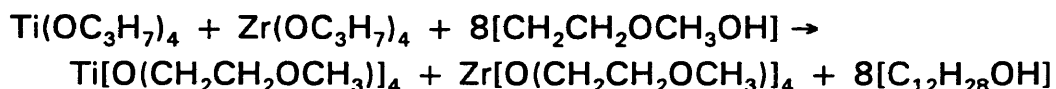
the 2-methoxyethanol solvent ($\sim 121^\circ\text{C}$ in Golden, CO). These steps were repeated in order to assure the elimination of the reaction bi-products. The lead acetate exchange reaction followed:



The bi-products of this reaction are methoxyethyl acetate and water. Similar steps were performed for solutions of germanium and for titanium/zirconium. These exchange reactions followed:



and



Following these exchange reactions, all metal cations carried the same organic ligand, $[\text{O}(\text{CH}_2\text{CH}_2\text{OCH}_3)]_n$.

The complexed precursor solutions were then combined in the presence of excess 2-methoxyethanol, refluxed, and distilled to a final composition of between 0.8 and 1.0 molar for the total cation content. No pre-hydrolysis was performed on the solutions prior to the spin coating procedure. Compositions studied and their corresponding weight and volume ratios are given in Table 4.

Table 4. Comparison of molar composition to weight percent and volume percent for compositions investigated.

Molar Composition	Weight Percent		Volume Percent	
	Pb ₅ Ge ₃ O ₁₁	PbZr _½ Ti _½ O ₃	Pb ₅ Ge ₃ O ₁₁	PbZr _½ Ti _½ O ₃
Pb ₅ Ge ₃ O ₁₁	100	0	100	0
4Pb ₅ Ge ₃ O ₁₁ -PbZr _½ Ti _½ O ₃	95	5	95	5
Pb ₅ Ge ₃ O ₁₁ -PbZr _½ Ti _½ O ₃	83	17	84	16
Pb ₅ Ge ₃ O ₁₁ -4PbZr _½ Ti _½ O ₃	54	46	56	44
PbZr _½ Ti _½ O ₃	0	100	0	100

3.2 Thin Film Fabrication

Spin coating^a was utilized for the formation of the thin films. Substrates were (100) oriented silicon with a titanium buffer layer and a (111) oriented platinum electrode.^b This layered configuration can be thought of as (111)Pt/Ti/SiO₂/Si. Prior to spinning, the substrates were cleaned by ultrasound in successive stages of acetone, methanol and distilled water. Substrates were kept under water until used, at which time they were dried by briefly applying to a hotplate. The precursor solutions were filtered to 0.2 microns immediately prior to the spin procedure. Individual layers were formed by spinning at 3000 RPM for 50 seconds.

^a Specialty Coating Systems, Inc., Indianapolis, IN, Model P6204

^b Ramtron Corp., Colorado Springs, CO

Table 5. Lead germanate film thicknesses as a function of annealing conditions and number of layers.

Annealing Conditions	Single Layer Films	Four Layer Films
As Deposited	≈ 2100Å	≈ 8500Å
150°C, 60 sec/layer	≈ 1900Å	≈ 7750Å
250°C, 60 sec/layer	≈ 1300Å	≈ 5100Å
350°C, 60 sec/layer	≈ 1250Å	≈ 4800Å
450°C, 60 sec/layer	≈ 1250Å	≈ 5000Å

Deposition was immediately followed by an annealing step. Increased thicknesses were obtained by successive spin/anneal steps (Table 5).

The annealing stage was performed in two different manners. For temperatures of up to 450°C, samples were placed directly on a preheated hotplate resulting in an almost instant increase to the annealing temperature. For temperatures above 450°C, a rapid thermal annealing procedure was used. The heating and cooling rates for this method were adjusted to 33°C/sec (2000°C/min).

The rapid thermal processing (RTP) was performed using a custom designed gradient furnace/drive system (Fig.3.2). The gradient tube furnace was constructed by winding Kanthal A-1 wire (B&S 16)^a onto a mullite tube^b with an outside diameter of 2.5in. The tube length was a total of 30 in., however the windings were spaced out over only 17 inches of the tube.

^a National Element, Troy, MI

^b Coors Ceramics, Golden, CO

The gradient was achieved by variations in the number of windings per inch. The maximum hot zone was positioned at 19-23 in. from the furnace entrance. The design utilized a 220 volt power supply. The total resistance of the furnace element was 27 ohms with a maximum power of approximately 2000 watts and a current of 8.6 amps. Temperature control within the furnace was achieved through a custom built furnace controller which allowed the equilibration of the furnace to a constant profile. The furnace itself exhibited a high degree of thermal stability over time.

The sample annealing temperature, heating rate and annealing time were controlled through the implementation of an external drive system which adjusted the sample's position in the furnace gradient. This allowed virtually any temperature (furnace maximum = 1180°C) to be achieved at equivalent heating rates up to 5000°C/min. The pusher system consisted of a stepper motor/driver/indexer^a which operated a 36in. rail table^b with optical limits and home. A mullite pushrod mounted on the rail table facilitated sample insertion into the furnace. The samples were supported on platinum foil with a 0.003in. fine gauged thermocouple positioned directly beneath the foil. The thin diameter of the thermocouple served to help minimize the signal response time. The thermocouple signal was monitored by a programmable thermocouple meter and could be read directly or sent via RS-232 serial communications to the controlling computer.

^a Parker Hannifin Corp., Daedal Div., Harrison City, PA, Part No. SX57-83

^b Parker Hannifin Corp., Daedal Div., Harrison City, PA, Part No. 506361S-LHO

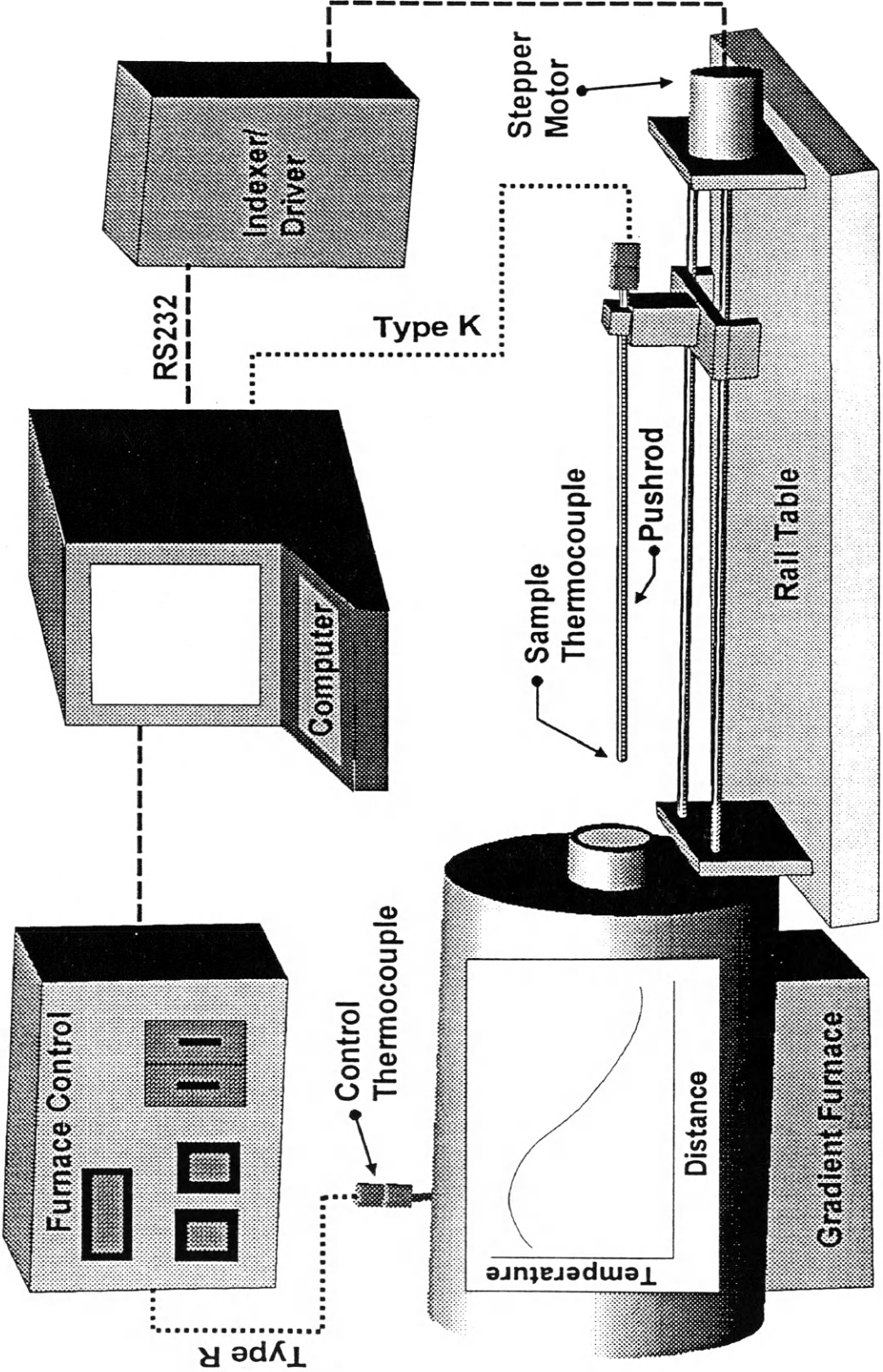


Figure 3.2. Schematic diagram of the rapid thermal processing system.

3.3 Characterization

3.3.1 Phase Development and Orientation

Phase development in the $\text{Pb}_5\text{Ge}_3\text{O}_{11}$ and $\text{PbZr}_x\text{Ti}_{1-x}\text{O}_3\text{-Pb}_5\text{Ge}_3\text{O}_{11}$ systems was performed by x-ray diffractometry^a. Cu-K α radiation and a scan rate of $1.20^\circ 2\theta/\text{min}$ were used. The degree of c-axis orientation of $\text{Pb}_5\text{Ge}_3\text{O}_{11}$ was determined using the method outlined by Lotgerling [90]. A quality factor, F is used to describe the degree of orientation according to,

$$F = \frac{(P' - P_o)}{(1 - P_o)}$$

$$\textit{Where: } P = \frac{\textit{Intensity of } (00l)}{\textit{Intensity of All } (hkl)}$$

P_o is the intensity ratio for a non-oriented sample and P' is the intensity ratio for the oriented sample. Using this method, $F=0$ would correspond to a non-oriented structure, while $F=1$ would signify a perfectly oriented c-axis. The factor of P_o , (for a non-oriented pattern), was obtained by using the relative intensities cited by Hasegawa et al.[22]. Any peaks not belonging to the $\text{Pb}_5\text{Ge}_3\text{O}_{11}$ phase were not included in the summations.

Details in regards to x-ray peak shifting and splitting were determined through the use of a peak fitting program (Jandel Scientific Peakfit, Version 3.11).

^a RU-200V, Rigaku Denki Co., Ltd, Japan

3.3.2 Physical Properties

The microstructural characteristics were determined through the use of optical light microscopy^a, scanning electron microscopy, and atomic force microscopy^b. Each technique was advantageous in certain applications. Light microscopy was most useful for analyzing large surface features, both defects and grains. Scanning electron microscopy was most useful for analyzing the features of film cross-sections. Atomic force microscopy proved very useful for resolving the film surface topography.

Profilometry^c was used as a simple means to measure the film thicknesses. Prior to the measurement, a portion of the film was chemically etched away, providing a measurement baseline on the platinum layer of the substrate.

3.3.3 Electrical Properties

Capacitance and dissipation factor measurements were performed between 20 and 200°C at frequencies of 10.0, 100.0 and 1000.0 KHz. These measurements were collected through the use of a precision LCR meter^d and controlled temperature chamber^e. Conversion of capacitance to dielectric constant was then performed according to the equation,

^a aus Jena Neophot 21 Metallograph, Leco Corp., St. Joseph, MI

^b Dimension 3000 Scanning Probe Microscope, Digital Instruments, Inc., Santa Barbara, CA

^c Alpha-Step Profiler, Tencor Instruments, Mountain View, CA

^d HP4284A, Hewlett Packard, Palo Alto, CA

^e Delta 9023, Delta Design, San Diego, CA

$$K = \frac{C \cdot t}{\epsilon_0 \cdot A}$$

Where: K = Dielectric Constant
 C = Capacitance (Farads)
 t = Thickness (cm)
 A = Area (cm²)
 ϵ_0 = Permittivity of Vacuum (8.854x10⁻¹²F/m)

Electrical poling of the films was performed prior to the measurement of ferroelectric and pyroelectric properties. Normally, the ferroelectric hysteresis would be measured on the unpoled material. Cline [91] found that poling of lead germanate was necessary for "opening" up the hysteresis loop. This was also observed by Cornejo [87] and in the present work. Poling was typically performed by applying 10-15KV while cooling the film through the paraelectric-ferroelectric transition, from 185 to 50°C.

Ferroelectric hysteresis loops were measured using a standardized ferroelectric test system^a.

Pyroelectric current versus temperature data were collected by measuring the current generated by poled samples as they were heated between 20 and 100°C at a rate of 2°C/min. Current measurements were performed through the use of a picoampere meter^b. Pyroelectric coefficient values were then calculated according to,

^a RT66A, Radiant Technologies, Albuquerque, NM

^b HP4140B, Hewlett Packard, Palo Alto, CA

$$I = p \cdot A \cdot \frac{\partial T}{\partial t}$$

Where: I = Pyroelectric Current (C/sec)
 p = Pyroelectric Coefficient (C/cm²°C)
 A = Area (cm²)
 $\partial T/\partial t$ = Rate of Temperature Change (°C/sec)

IV. RESULTS AND DISCUSSION

4.1 Phase Development of $\text{Pb}_5\text{Ge}_3\text{O}_{11}$ Thin Films

4.1.1 Pt_{5-7}Pb

The first phase to form in $\text{Pb}_5\text{Ge}_3\text{O}_{11}$ thin films deposited on platinized silicon substrates is a transient intermetallic phase, Pt_{5-7}Pb (Ref. JCPDS 6-574). This phase forms at the platinum/ceramic interface with a (111) orientation of its face-centered cubic structure, matching epitaxially with the (111) orientation of the platinum layer. The (111) x-ray diffraction line is located at $d = 2.34\text{\AA}$, and is the only diffraction line present from this phase over a scan range of 15 to $55^\circ 2\theta$ (Fig. 4.1). This formation is promoted by the reduction of Pb^{2+} during the removal of organics from the as-deposited films. The disappearance of this phase corresponds to the reoxidation of the lead as oxygen diffuses through the film to the electrode/ceramic interface. Figure 4.1 shows that for single layer films annealed for one minute, the transient phase is present only at 300 and 350°C. This transient phase was stable at 300°C for in excess of 10 minutes. At 350°C it persisted up to 120 seconds and by 450°C, this phase was present only in the time frame of 10 seconds (Fig. 4.2).

4.1.2 Metastable $\text{Pb}_5\text{Ge}_3\text{O}_{11}$

The next phase to form appears to be a metastable $\text{Pb}_5\text{Ge}_3\text{O}_{11}$ phase. There is some disagreement as to the exact structural parameters of this

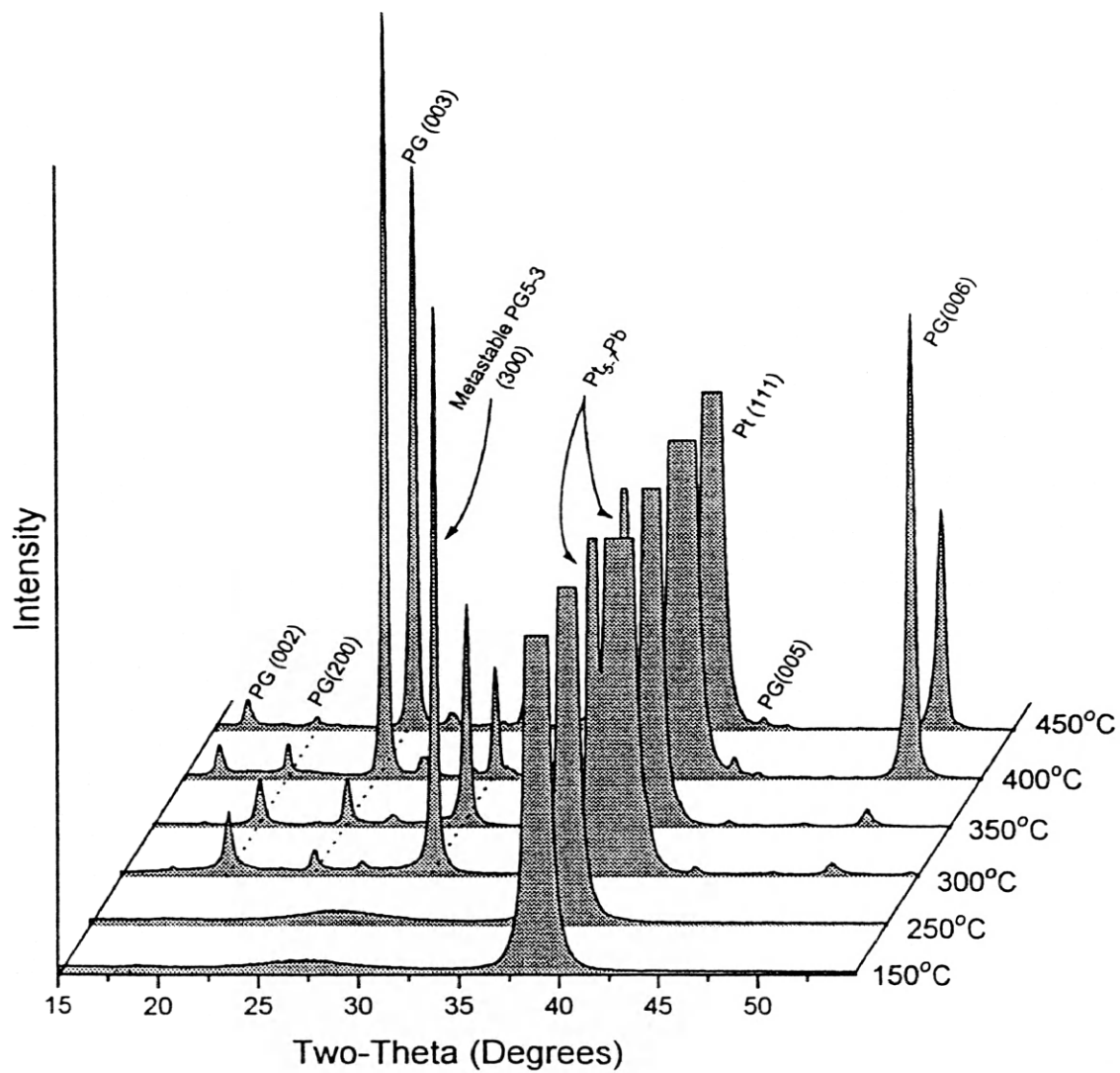


Figure 4.1. X-ray diffraction patterns for single layer $\text{Pb}_5\text{Ge}_3\text{O}_{11}$ films annealed for one minute.

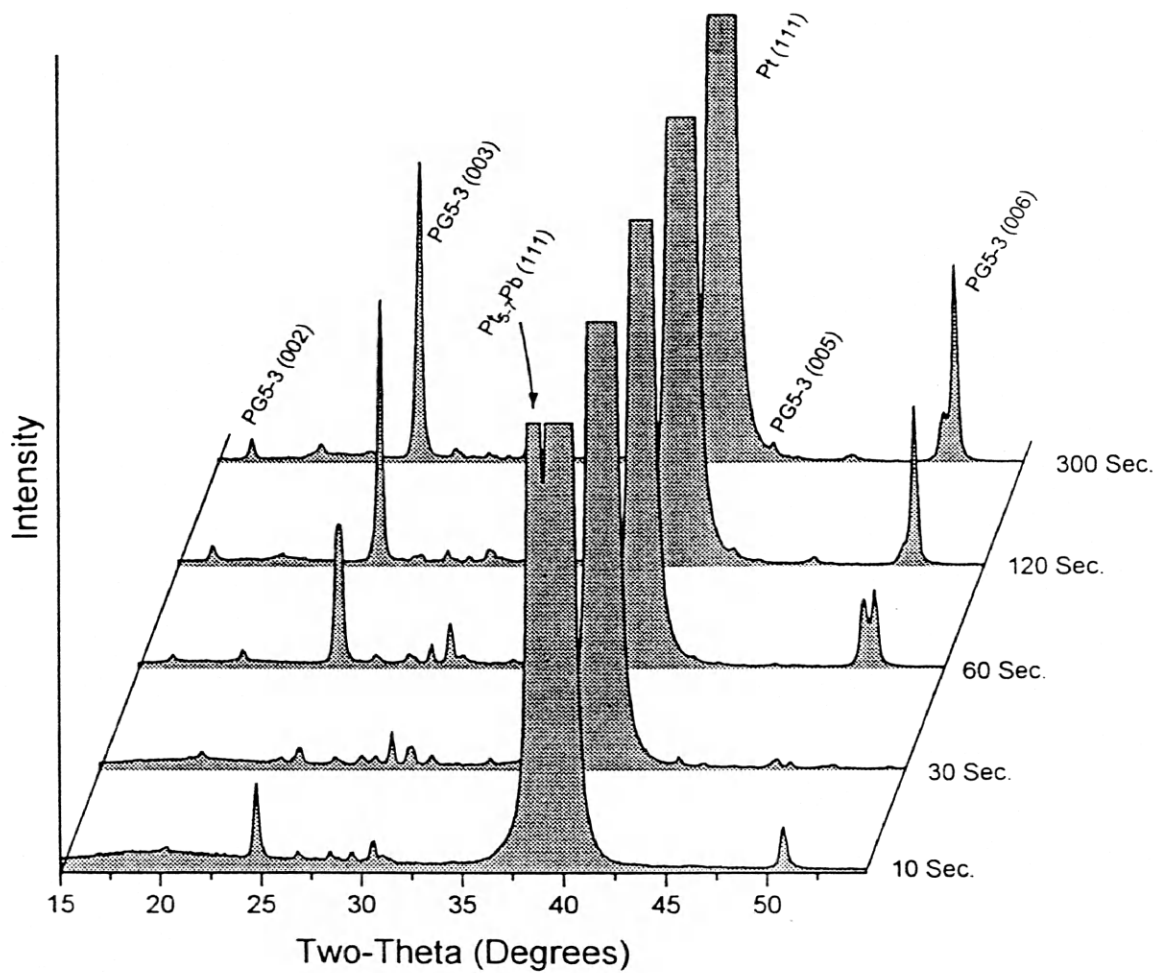


Figure 4.2. X-ray diffraction patterns for single layer $\text{Pb}_5\text{Ge}_3\text{O}_{11}$ films annealed at 450°C .

phase (Section 2.4.1). It appears that there is a certain degree of "continuous" change that occurs. Initially, the phase appears very similar to that reported by Nassau et al. (Ref. JCPDS 33-751) and Otto (Ref. JCPDS 34-51); hexagonal with an a-axis parameter of approximately 10.19Å. Figure 4.1 shows that for single layer films, annealing at 300°C results in a metastable phase with strong a-axis orientation. This could be expected considering that the c-axis cell parameter is reported to be much greater than the a-axis parameter. The positions of the (h00) peaks match those reported in the two standard patterns. With an increase in annealing temperature, the metastable (h00) peaks show a decrease of intensity as well as a shift in their positions to match those of the stable $\text{Pb}_5\text{Ge}_3\text{O}_{11}$ phase (Fig. 4.1).

4.1.3 Stable $\text{Pb}_5\text{Ge}_3\text{O}_{11}$

The transformation of the metastable phase to the stable phase can be followed by observing the shifting of the (200) line which shares a similar position in both metastable and stable phases and doesn't overlap with other peaks. With increased heating, the (200) line shifts from a lower d-spacing, which corresponds to the metastable (200), to a higher d-spacing (lower 2θ) which corresponds to the stable (200). Figures 4.3A and 4.3B show the shifting of the (200) for single layer films annealed at 600°C for 10 and 30 seconds. A peak fitting program was used to examine the peak positions. While the peak fitting was difficult with these data, a shifting is obvious. Figure 4.4 shows the (200) shifting as a function of annealing time and temperature. The magnitude of the (200) shift is similar to what would be expected, approximately 0.05Å which would correspond to an approximate 0.1Å increase in the a-axis unit cell parameter. When the (200) line is

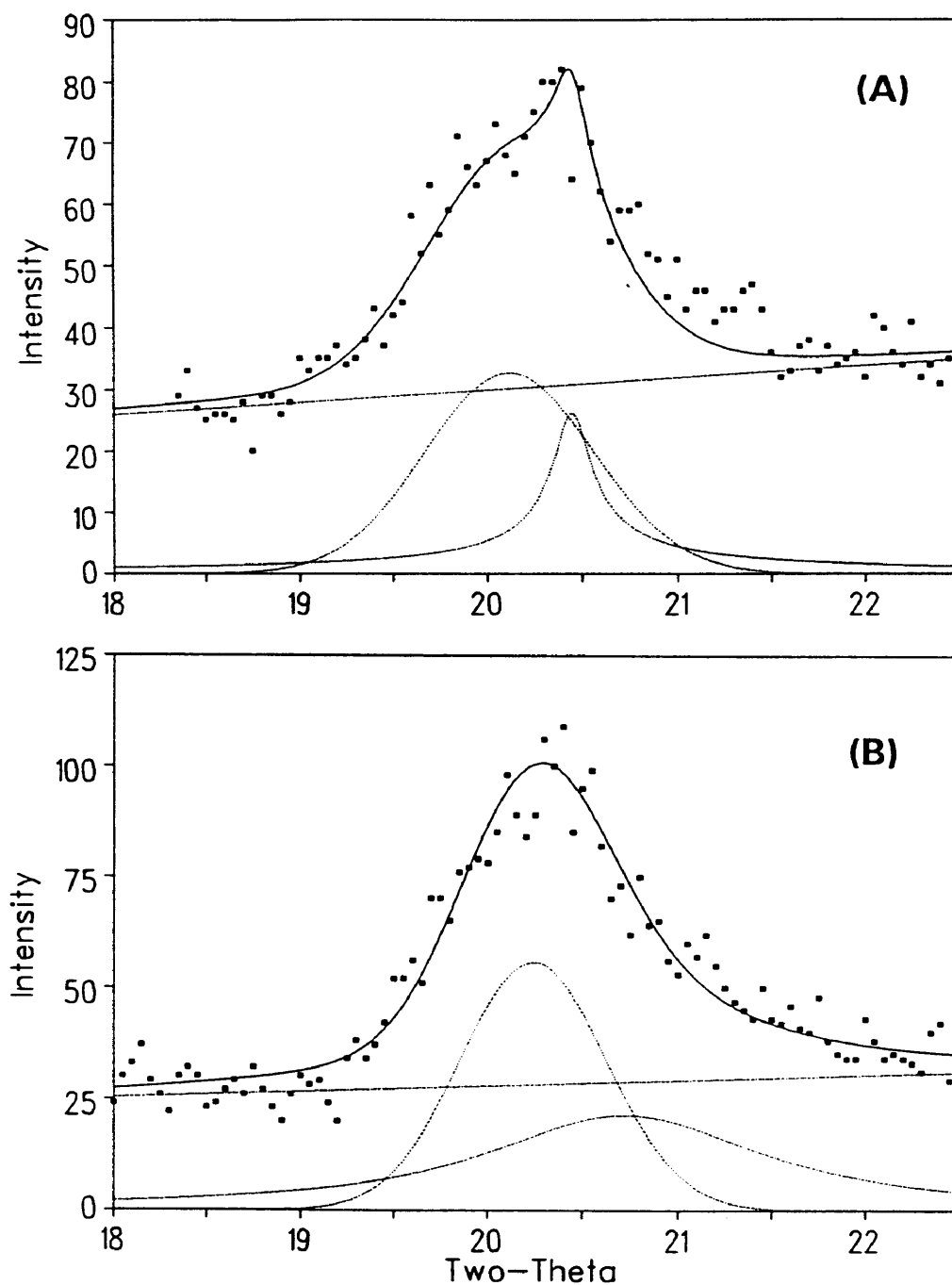


Figure 4.3. X-ray diffraction patterns for the (200) peak and the corresponding fitted curves for (A) a single layer $\text{Pb}_5\text{Ge}_3\text{O}_{11}$ film annealed at 600°C for 10 seconds and (B) a single layer $\text{Pb}_5\text{Ge}_3\text{O}_{11}$ film annealed at 600°C for 30 seconds.

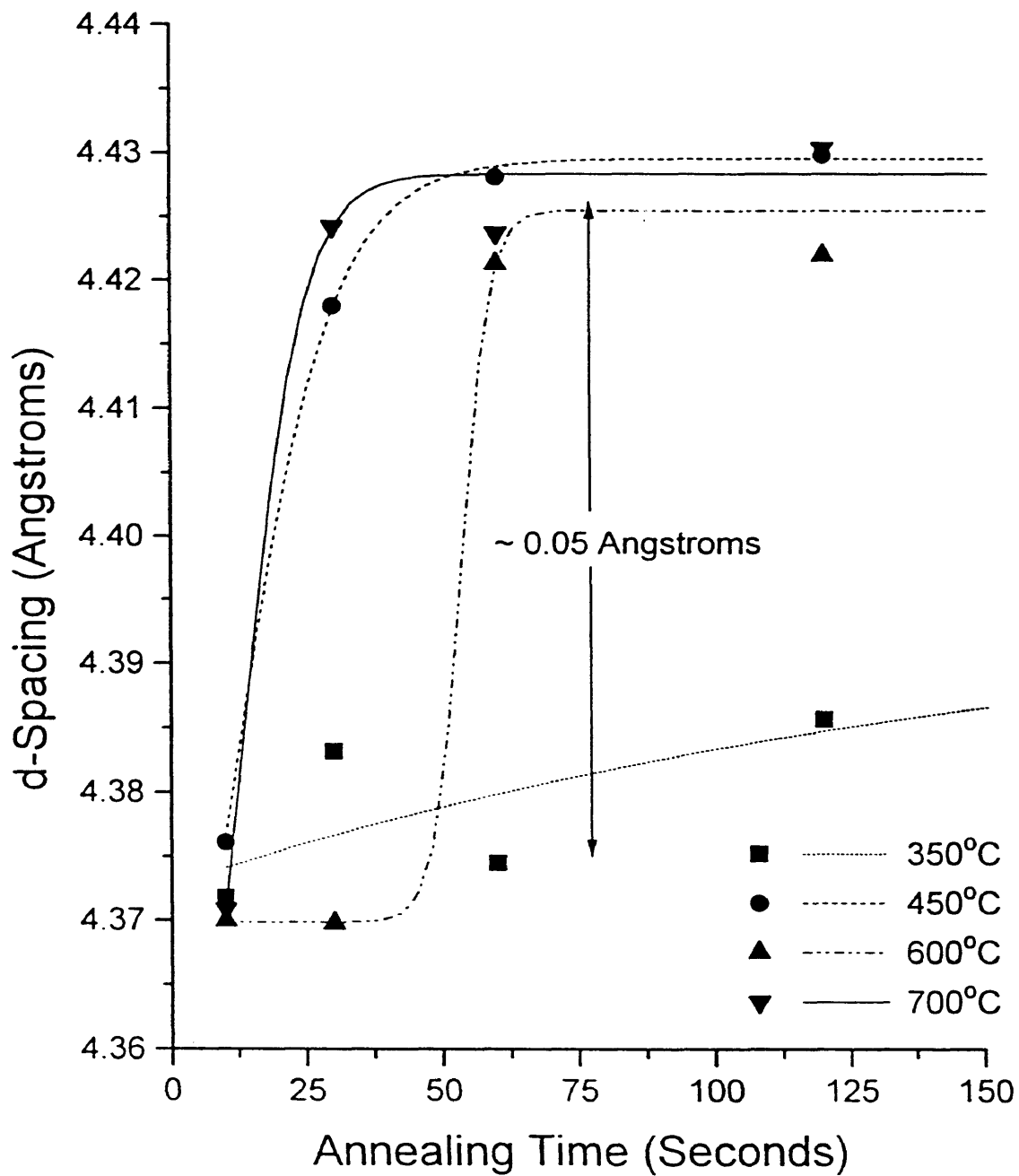


Figure 4.4. The change in the (200) diffraction peak position with annealing time.

completely shifted and occupies the stable position, the diffraction line located at approximately 2.9\AA shows a slight splitting which would correspond to the (300)/(113) peaks for the stable $\text{Pb}_5\text{Ge}_3\text{O}_{11}$ phase (Fig. 4.5). The (300) and (113) peaks represent the two highest intensity diffraction peaks for the stable phase with a random crystallographic orientation.

4.1.4 Shifting of the (00l) Diffraction Peaks

The peaks located at approximately 3.6\AA ($\sim 24.7^\circ 2\theta$) and 1.8\AA ($\sim 50.7^\circ 2\theta$) do not match the reported metastable patterns. It is not certain if these lines belong to the metastable phase or actually represent an initial formation of the oriented stable phase. It does seem reasonable that they are both (00l) type lines.

- They both show a "shifting" to lower d-spacings (higher 2θ).
- The 1.8\AA line undergoes a change of approximately -0.025\AA in all cases and the 3.6\AA line shifts by approximately -0.05\AA . This would correspond to a c-axis change of -0.15\AA , and indicates that these two peaks are related by a factor of $2(hkl)$.

Figure 4.6 shows that for a film annealed at 450°C for 10 seconds, a strong peak is formed at $50.7^\circ 2\theta$ with the possibility of a low intensity peak at a slightly higher two-theta (lower d-spacing). Figures 4.7A and 4.7B show that annealing for 60 seconds results in a definite split in both of the peaks located in the region of the stable $\text{Pb}_5\text{Ge}_3\text{O}_{11}$ (003) and (006) peaks. The split peaks are nearly equal in intensity and width. With an increase in

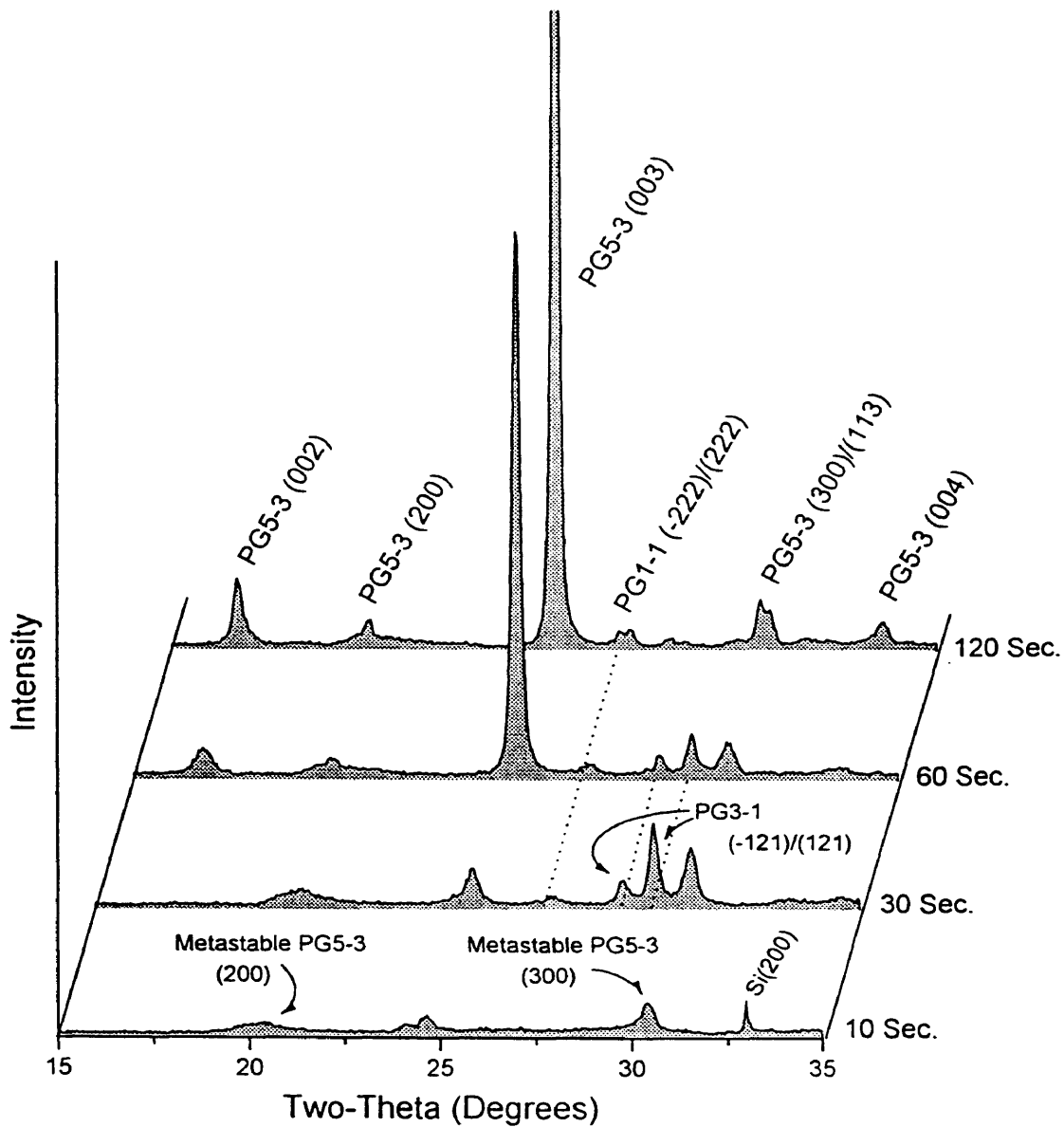


Figure 4.5. X-ray diffraction patterns for single layer $\text{Pb}_5\text{Ge}_3\text{O}_{11}$ films annealed at 600°C .

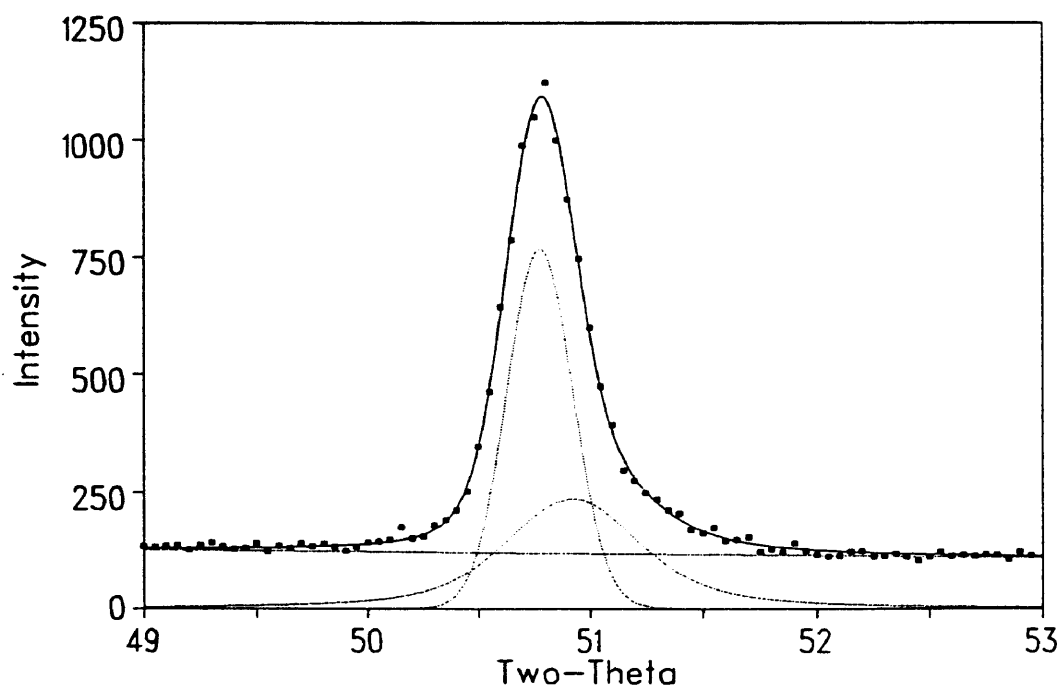


Figure 4.6. The (006) diffraction peak and the corresponding fitted curves for a single layer $\text{Pb}_5\text{Ge}_3\text{O}_{11}$ film annealed at 450°C for 10 seconds.

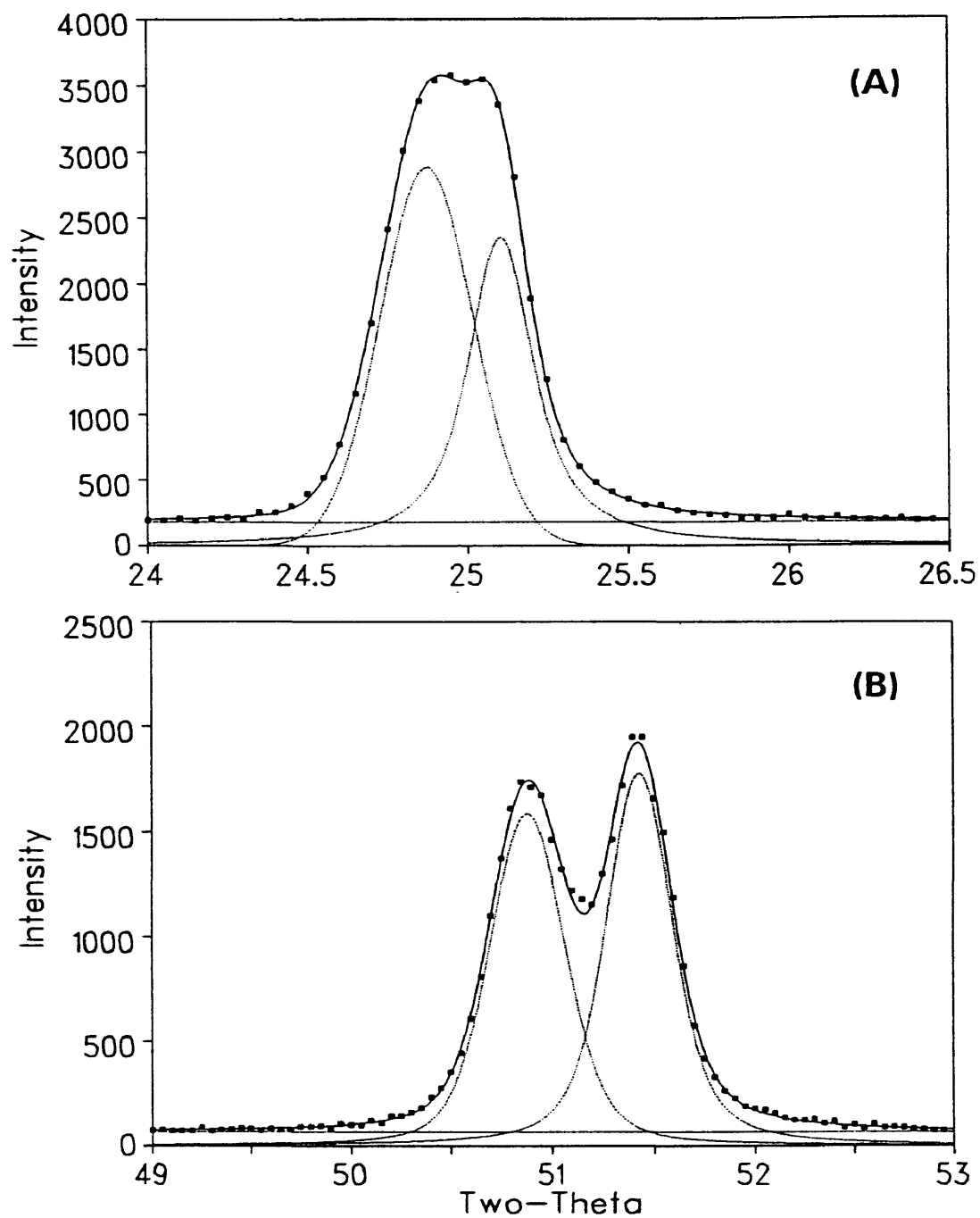


Figure 4.7. X-ray diffraction patterns and the corresponding fitted curves for the (A) (003) and (B) (006) peaks for a single layer $\text{Pb}_5\text{Ge}_3\text{O}_{11}$ film annealed at 450°C for 60 seconds.

annealing time to 120 seconds (Fig. 4.8A,B), the dominant peak for both the (003) and (006) is the higher two-theta (3.55\AA and 1.776\AA respectively) which correspond closely to the stable 5-3 peak positions. This splitting and shifting for 450°C films is summarized in Figure 4.9. The peak splitting was only observed for lead germanate films annealed at 450°C . This is believed to be due to very rapid "transformation" rates for the shifting of the peaks at temperatures higher than 450°C . Figures 4.10A and 4.10B show that at 700°C for 30 seconds, only the "shifted" (003) and (006) peaks are present. The (003) and (006) d-spacings versus annealing time are summarized in Figures 4.11 and 4.12.

Several possible explanations are envisioned for this behavior of the (00l) diffraction lines:

Metastable-Stable Transition

The initial peaks at high d-spacings could represent the (00l) lines of the hexagonal metastable phase. A calculation of all (00l) peaks for the standard metastable phases (JCPDS 33-751 and 34-51) does not result in an exact match. The closest match would be for the metastable phase suggested by Otto (JCPDS 34-51) with a c-axis parameter of 29.01\AA . The (008) line for this phase would be located at 3.62\AA , while the second order (008) line would be at approximately 1.813\AA . However, no other c-axis diffraction lines were observed for the metastable phase.

Stoichiometry

Maiwa [53] reported a very large change of 0.3\AA in the c-axis parameter for lead germanate films (Section 2.4.6). These films showed no

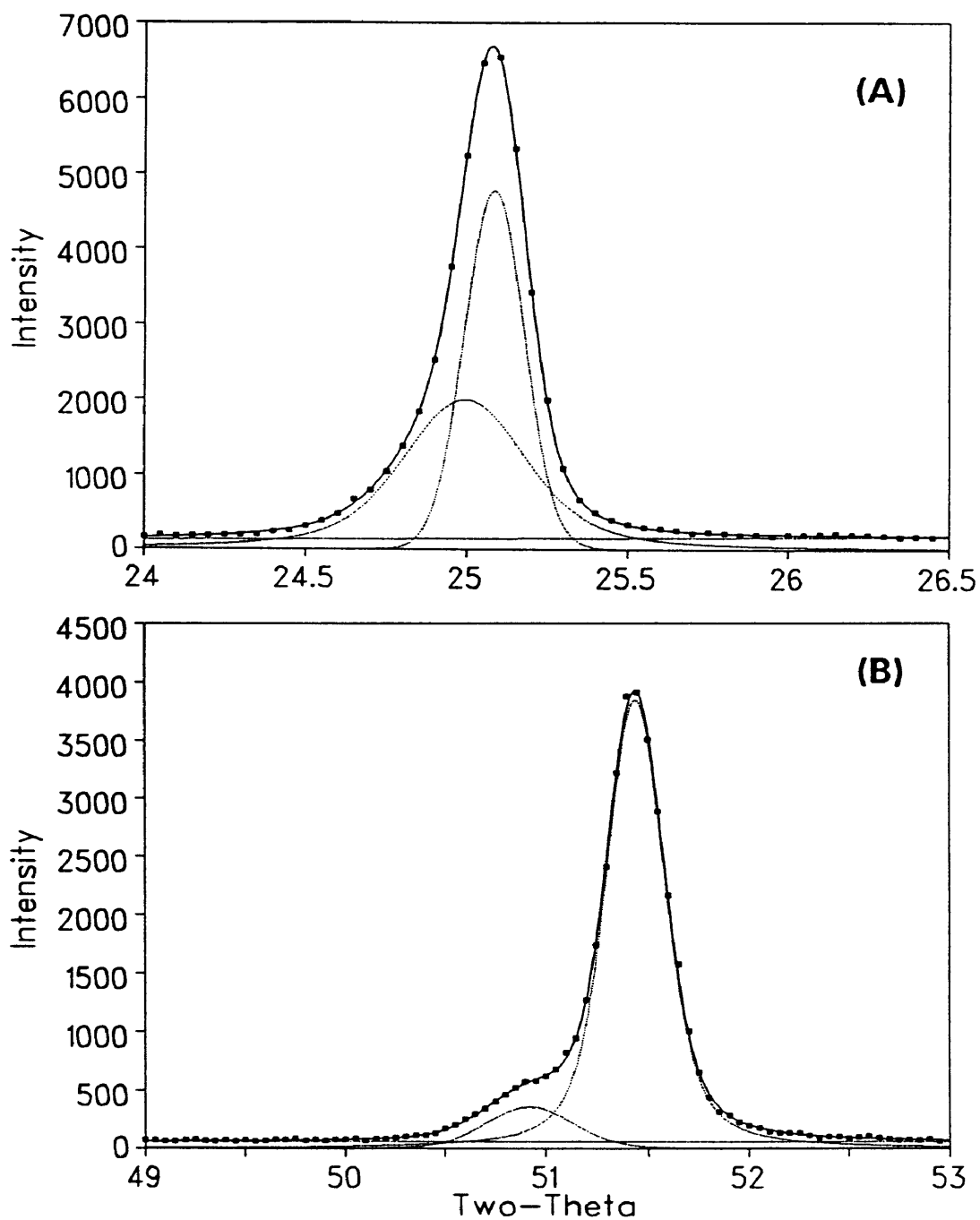


Figure 4.8. X-ray diffraction patterns and the corresponding fitted curves for the (A) (003) and (B) (006) peaks for a single layer $\text{Pb}_5\text{Ge}_3\text{O}_{11}$ film annealed at 450°C for 120 seconds.

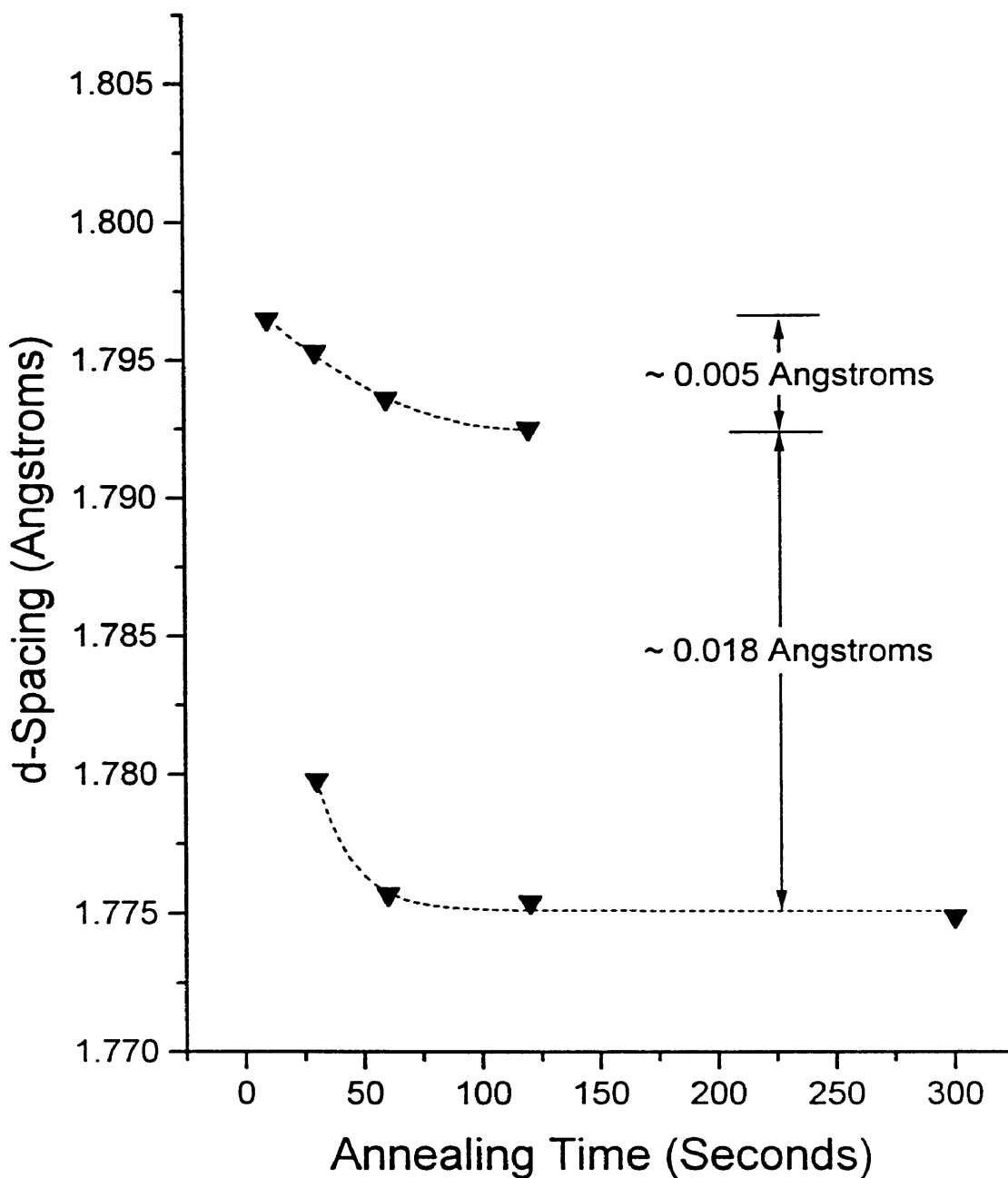


Figure 4.9. The splitting and shifting of the (006) diffraction peak position with annealing time for single layer $\text{Pb}_5\text{Ge}_3\text{O}_{11}$ films annealed at 450°C .

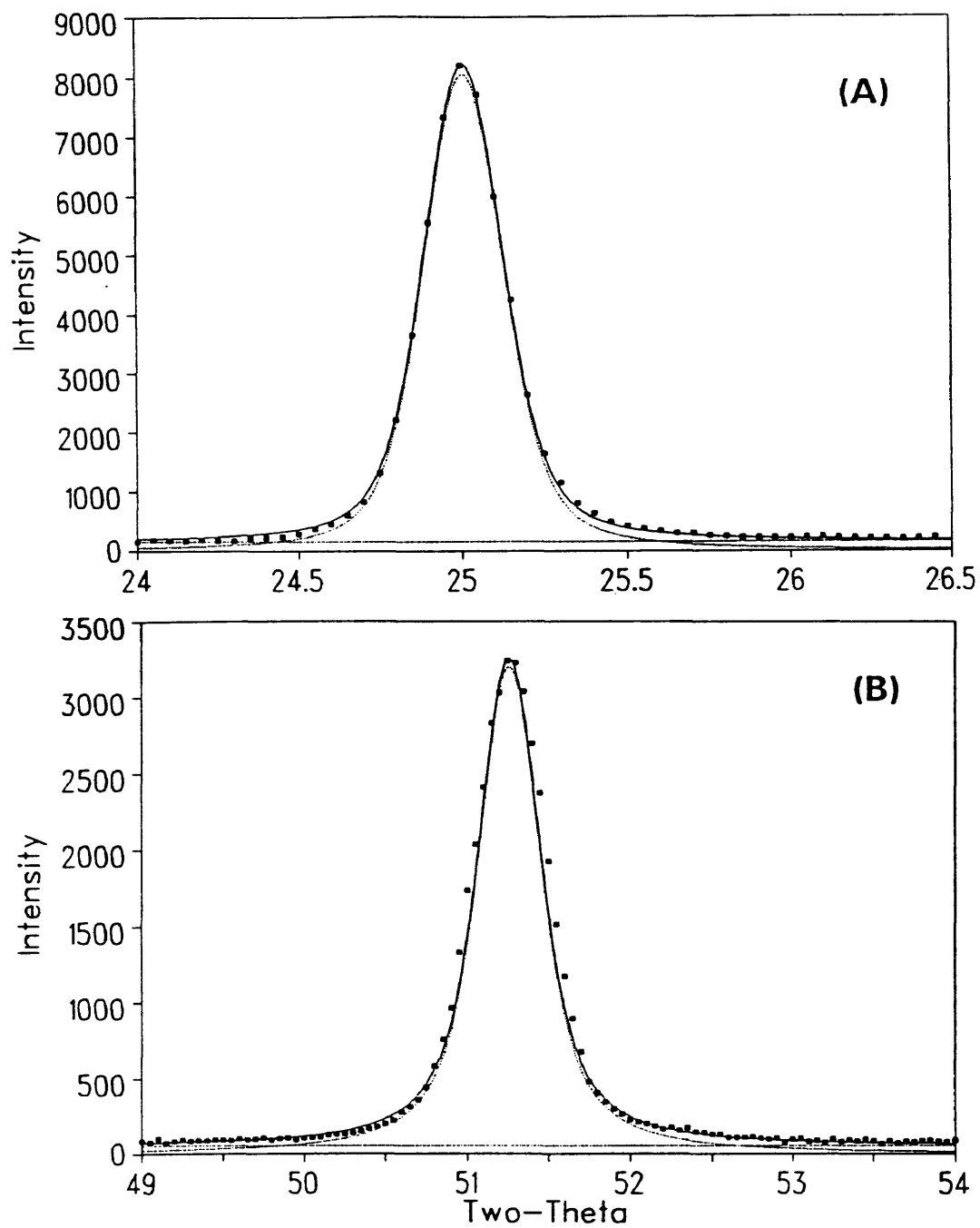


Figure 4.10. X-ray diffraction patterns and the corresponding fitted curves of the (A) (003) and (B) (006) diffraction peaks for a single layer $\text{Pb}_5\text{Ge}_3\text{O}_{11}$ film annealed at 700°C for 30 seconds.

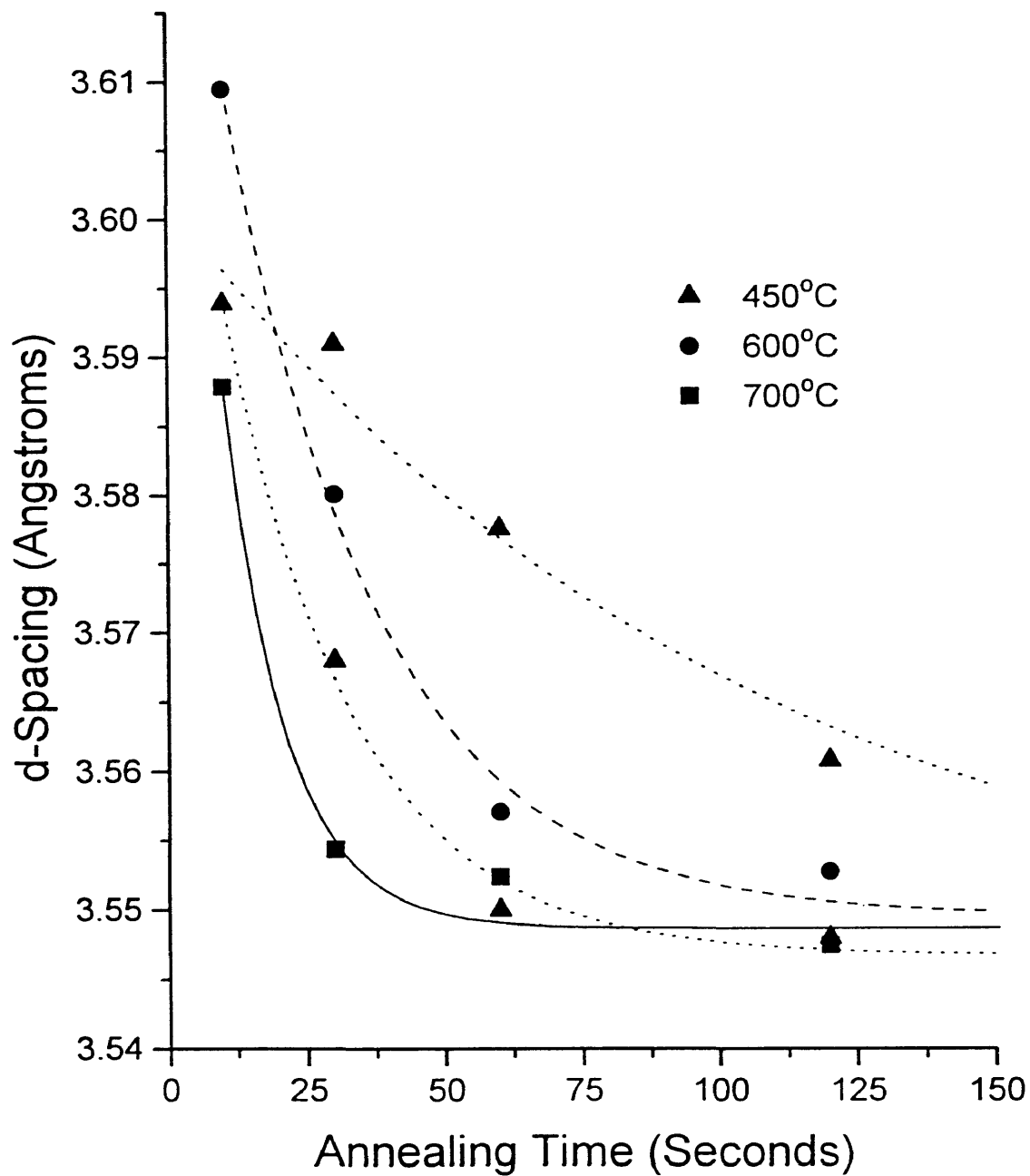


Figure 4.11. The change in the (003) diffraction peak position with annealing time for single layer $\text{Pb}_5\text{Ge}_3\text{O}_{11}$ films. Note that the 450°C annealing temperature is displayed with two curves representing the split peaks.

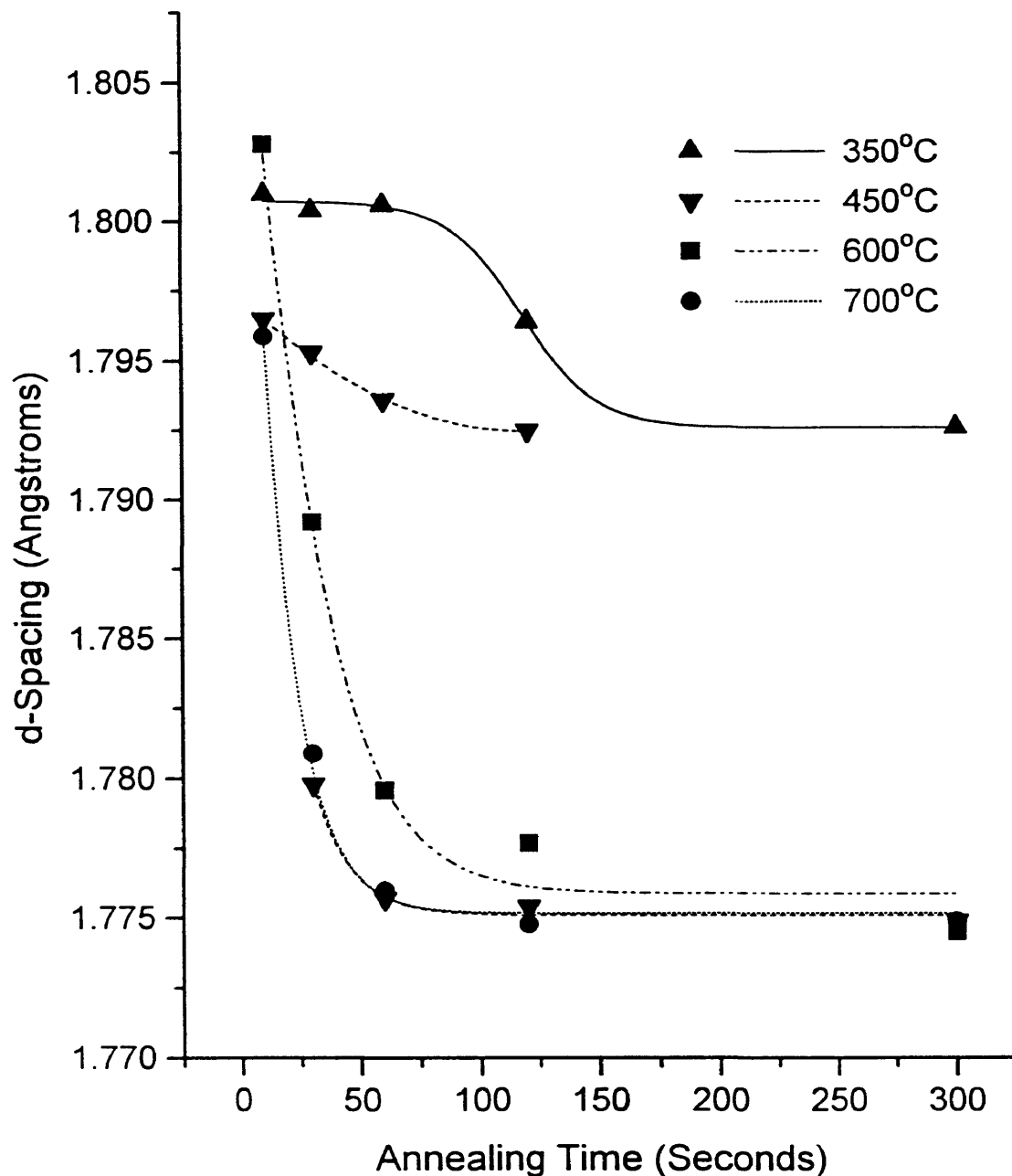


Figure 4.12. The change in the (006) diffraction peak position with annealing time for single layer $\text{Pb}_5\text{Ge}_3\text{O}_{11}$ films. Note that the 450°C annealing temperature is displayed with two curves representing the split peaks.

peak in their dielectric constant. Annealing in oxygen was reported to correct the c-axis parameter difference and resulted in a dielectric peak. Oxygen annealing was attempted in the current investigation. Films initially annealed in air at 700°C for 10 minutes were annealed in an oxygen atmosphere at 600°C for 6 hours. No change was detected in the unit cell parameters of these films after the oxygen annealing.

Stress Induced Shifting

The initial peaks may actually represent the nucleation of the stable phase as a nanophase within a metastable matrix. As the film becomes fully transformed to the stable phase, the stable crystallites are subjected to a highly stressed environment. The strain corresponding to the shifting of the (00l) diffraction peaks is calculated to be approximately -0.013 along the c-axis.

In considering the origin of possible stresses in the films, the thermal expansion mismatch between the silicon and the lead germanate must be considered. This difference in thermal expansion would result in the film being put into a biaxial state of tension during cooling. Iwasaki et al.[18] gave the thermal expansion for lead germanate along the a-axis to be $7.75 \times 10^{-6}/^{\circ}\text{C}$ below the transition temperature and $13.8 \times 10^{-6}/^{\circ}\text{C}$ above the transition temperature. Assuming that thermally induced stresses develop to a significant extent only below $\sim \frac{1}{2} T_{\text{melt}}$, the temperature change in the paraelectric state would be 200°C and in the ferroelectric state, 150°C. Using the equation,

$$\epsilon_{\text{therm}} = (\alpha_f - \alpha_s)(\Delta T)$$

the thermal strain is calculated to be approximately -0.003. This calculation also assumed a constant silicon thermal expansion coefficient of $3 \times 10^{-6}/^{\circ}\text{C}$ over the entire temperature range and constant lead germanate expansion coefficients within the paraelectric and ferroelectric phases. A further assumption is that the films are oriented perfectly with the a-axis in the plane of the substrate and the c-axis perpendicular. Knowing the strain in the plane of the film, $\epsilon_{1 \text{ therm}} = \epsilon_{2 \text{ therm}} = -0.003$, the thermal strain along the c-axis, $\epsilon_{3 \text{ therm}}$ can be calculated. The ferroelectric trigonal phase has seven independent elastic constants, however C_{14} and C_{25} have been found to be over twenty times smaller than the other constants [92]. Assuming these constants to be zero allows hexagonal symmetry to be used for both the ferroelectric and paraelectric phases. In approximation then,

$$\begin{aligned}\epsilon_{1 \text{ therm}} &= S_{11}\sigma_{1 \text{ therm}} + S_{12}\sigma_{2 \text{ therm}} + S_{13}\sigma_{3 \text{ therm}} \\ \epsilon_{2 \text{ therm}} &= S_{12}\sigma_{1 \text{ therm}} + S_{11}\sigma_{2 \text{ therm}} + S_{13}\sigma_{3 \text{ therm}} \\ \epsilon_{3 \text{ therm}} &= S_{13}\sigma_{1 \text{ therm}} + S_{13}\sigma_{2 \text{ therm}} + S_{33}\sigma_{3 \text{ therm}}\end{aligned}$$

Due to the biaxial nature of the stress, $\sigma_{1 \text{ therm}} = \sigma_{2 \text{ therm}} \neq 0$ and $\sigma_{3 \text{ therm}} = 0$. The compliance terms have been determined to be, $S_{11} = 1.77 \times 10^{-11} \text{m}^2/\text{N}$, $S_{12} = -0.64 \times 10^{-11} \text{m}^2/\text{N}$, $S_{13} = -0.22 \times 10^{-11} \text{m}^2/\text{N}$ and $S_{33} = 1.14 \times 10^{-11} \text{m}^2/\text{N}$ [92]. The thermal stress is therefore calculated to be $\sim 270 \text{MN}/\text{m}^2$, and the thermal strain along the c-axis is approximately -0.0012. This thermal strain is an order of magnitude less than that calculated from the shifting and splitting of the diffraction peaks (-0.013). A biaxial stress of approximately $3000 \text{MN}/\text{m}^2$ would be required to produce the strain observed. This may not be entirely unreasonable. Kwok and Desu [93] reported sol gel derived PZT thin films with tensile stresses of $1200 \text{MN}/\text{m}^2$. The calculated thermal stress

of 270MN/m^2 is sufficient to shift the transition temperature to approximately 135°C according to the relation given by Kirk et al.[29] (Section 2.4.4). Dielectric peaks have been observed in this temperature range in the current work (Section 4.4). It is proposed here that only the initial peak shifting ($\sim 0.005\text{\AA}$ for the (006) peak in Figure 4.9) is the result of internal stress. The peak splitting that results in two distinct diffraction peaks immediately following the shifting (Figure 4.9) would most probably be the result of two distinct structures.

Structural Change Within the $\text{Pb}_5\text{Ge}_3\text{O}_{11}$ Phase

A possible explanation for the large change in the c-axis lattice parameter involves the ferroelectric-paraelectric phase transition. It is proposed that the internal stress of the film may be high enough to prevent "part" of the ferroelectric-paraelectric phase transition from occurring and the corresponding change in the unit cell dimensions. Gavrilov et al.[31] proposed that the phase transition of lead germanate occurs as a two-step process. Their findings are described with more detail in Section 2.4.2. Basically, the rotation of the Ge_2O_7 double tetrahedra was described as occurring at 177°C (the accepted transition temperature for $\text{Pb}_5\text{Ge}_3\text{O}_{11}$) while the relaxation motions within the GeO_4 single tetrahedra are not halted until approximately 136°C , which then results in a large displacement of one of the oxygen ions thereby triggering a displacement of the lead ions. These researchers state that the Ge_2O_7 rotation is solely responsible for the symmetry change of hexagonal to trigonal.

Sal'nikov et al.[25,33] and Stefanovich et al.[94] report the existence of a $\text{Pb}_3\text{Ge}_2\text{O}_7$ ferroelectric phase. This phase is very similar in properties

and composition to the $\text{Pb}_5\text{Ge}_3\text{O}_{11}$ phase. Their reported data shows that the transition temperature for the $\text{Pb}_3\text{Ge}_2\text{O}_7$ is very close to that of $\text{Pb}_5\text{Ge}_3\text{O}_{11}$ ($\sim 177^\circ\text{C}$). The structure for the $\text{Pb}_3\text{Ge}_2\text{O}_7$ phase is also given as hexagonal in the paraelectric state and trigonal in the ferroelectric state. Other researchers have questioned the existence of this phase raising the possibility that it is simply the $\text{Pb}_5\text{Ge}_3\text{O}_{11}$ phase [32].

If the structure reported by Sal'nikov et al.[25,33] and Stefanovich et al.[94] is in fact based on a 3:2 Pb/Ge ratio, its transformation and ferroelectric properties may be based entirely on the Ge_2O_7 rotation since the GeO_4 structural unit would not be present. According to Gavrilov et al.[31], this transition occurs at approximately 177°C .

Sal'nikov et al.[25,33] and Stefanovich et al.[94] also experimented with silicon substitutions for germanium according to $\text{Pb}_3(\text{Ge}_{1-x}\text{Si}_x)_2\text{O}_7$. They show that increasing substitutions of Si for Ge caused a steady decrease in the transition temperature. This has also been reported for $\text{Pb}_5\text{Ge}_3\text{O}_{11}$ [18]. At a substitution of approximately 35 mole percent Si, Sal'nikov et al. report that the transition temperature lowered to approximately room temperature. Their data at this amount of silicon substitution also show a dramatic drop in the lattice parameters of $\text{Pb}_3\text{Ge}_2\text{O}_7$ (Fig. 4.13). They attribute this to the disappearance of the spontaneous polarization. The low transition temperature means that the data for the cell dimensions suddenly switched to that of the paraelectric phase. Iwasaki et al.[18] show a transition temperature of approximately 60°C for the same degree of silicon substitution in $\text{Pb}_5\text{Ge}_3\text{O}_{11}$.

It is therefore proposed that a possible explanation for the splitting and shifting observed in the $\text{Pb}_5\text{Ge}_3\text{O}_{11}$ films may be due to the elimination of one mechanism of the phase transition. The possibilities are as follows:

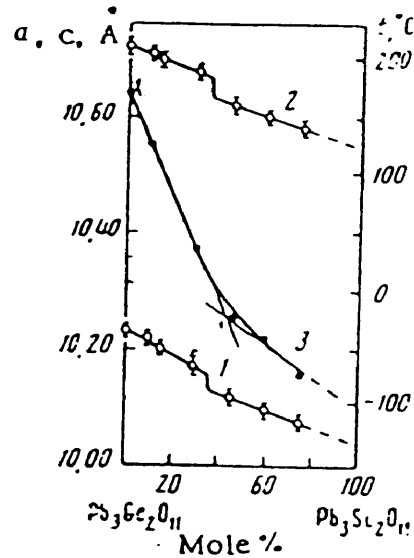


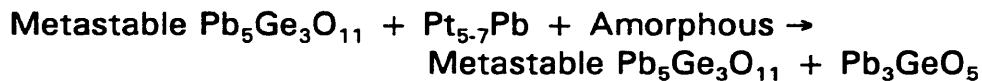
Figure 4.13. The variation of lattice parameters, (1 = a-axis, 2 = c-axis and 3 = transition temperature) with composition for $\text{Pb}_3\text{Ge}_{2-x}\text{Si}_x\text{O}_7$ [25].

- The Ge_2O_7 rotation could be eliminated due to the large internal stresses of the films. The films may still be ferroelectric because unlike the composition of Sal'nikov et al., the GeO_4 single tetrahedra structural units are present. The transformation due to these GeO_4 tetrahedra would then occur at approximately 135°C . This transition temperature has been observed through dielectric constant measurements in this research.
- The Ge_2O_7 rotation may occur, however the transition temperature has been shifted from 177°C to 135°C due to the thermally induced stresses. In this case, the strain may be large enough to prevent the large displacement of the oxygen atom in the GeO_4 tetrahedra. This would correspond to an elimination of the movement of the lead ions.

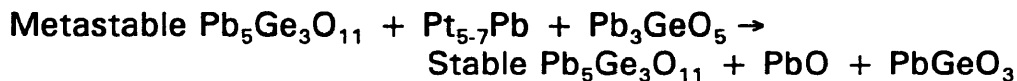
Elimination of either of these mechanisms would result in a reduction of the unit cell size.

Structural Change of $Pb_3Ge_2O_7$ to $Pb_5Ge_3O_{11}$

As stated earlier, Salnikov et al.[25,33] and Stefanovich et al.[94] support the existence of ferroelectric $Pb_3Ge_2O_7$ as well as $Pb_5Ge_3O_{11}$. These two phases have a very similar structure and identical symmetry change at the ferroelectric-paraelectric transition. For single layer lead germanate films annealed at 600°C, it appears that the reaction,



occurs between 10 and 30 seconds annealing time. Single layer lead germanate films annealed at 700°C show the reaction,



between 10 and 30 seconds annealing time. These equations are not balanced for a starting composition with a 5Pb:3Ge ratio. It is believed that the Pb_3GeO_5 formation is promoted by the reoxidation of $Pt_{5.7}Pb$ (Section 4.1.5). The remaining composition is then deficient in lead (Ge rich). $Pb_5Ge_3O_{11}$ has been shown to exist over a very narrow compositional range. A slight excess of germanium would result in a compositional formula that could be described by $(1-x)Pb_5Ge_3O_{11} \cdot (x)Pb_3Ge_2O_7$. The possibility therefore exists that the (00l) peaks that form initially at a high d-spacing belong to

the $\text{Pb}_3\text{Ge}_2\text{O}_7$ phase. With higher annealing temperatures or longer annealing times, Pb^{2+} from the $\text{Pt}_{5.7}\text{Pb}$, PbO and Pb_3GeO_5 phases is made available resulting in $\text{Pb}_5\text{Ge}_3\text{O}_{11}$ formation and a very slight alteration of the structure resulting in a shift of the (00l) peaks. The data presented by Sal'nikov et al.[23] in regards to the lattice parameter of pure $\text{Pb}_3\text{Ge}_2\text{O}_7$ clearly indicates that the c-axis lattice parameter of this phase is greater than 10.7\AA (Fig.4.13 on p.79). The c-axis lattice parameter of $\text{Pb}_5\text{Ge}_3\text{O}_{11}$ has been reported over the range of 10.54 to 10.685\AA (Section 2.4.2). The initial shifting of $\sim -0.005\text{\AA}$ described in Figure 4.9 (on p.71) is believed to possibly be due to film stress. The $\sim -0.018\text{\AA}$ shift of the (006) peak that follows after is believed to be due to the transformation from $\text{Pb}_3\text{Ge}_2\text{O}_{11}$ to $\text{Pb}_5\text{Ge}_3\text{O}_{11}$. This shifting would correspond to an approximate 0.11\AA reduction of the c-axis and closely agrees with the difference between the c-axis lattice parameters of these two structures.

4.1.5 PbO , PbGeO_3 , and Pb_3GeO_7

Other phases that are present under certain conditions include, PbO , PbGeO_3 and Pb_3GeO_5 (Fig. 4.14 and 4.15). The formation of $\text{Pt}_{5.7}\text{Pb}$ would temporarily leave the overall composition deficient in lead. As discussed in the previous section, this lead deficiency in the film composition is believed to promote the formation of $\text{Pb}_3\text{Ge}_2\text{O}_7$ as an intermediate to the formation of stable $\text{Pb}_5\text{Ge}_3\text{O}_{11}$. When the $\text{Pt}_{5.7}\text{Pb}$ reoxidizes, a lead rich region would be created at the platinum/ceramic interface. The lead-rich region appears to promote the formation of PbO and Pb_3GeO_5 . Figure 4.15 shows that at 450°C , the Pb_3GeO_5 peaks have a maximum intensity after 30 seconds of annealing which corresponds to the complete disappearance of $\text{Pt}_{5.7}\text{Pb}$

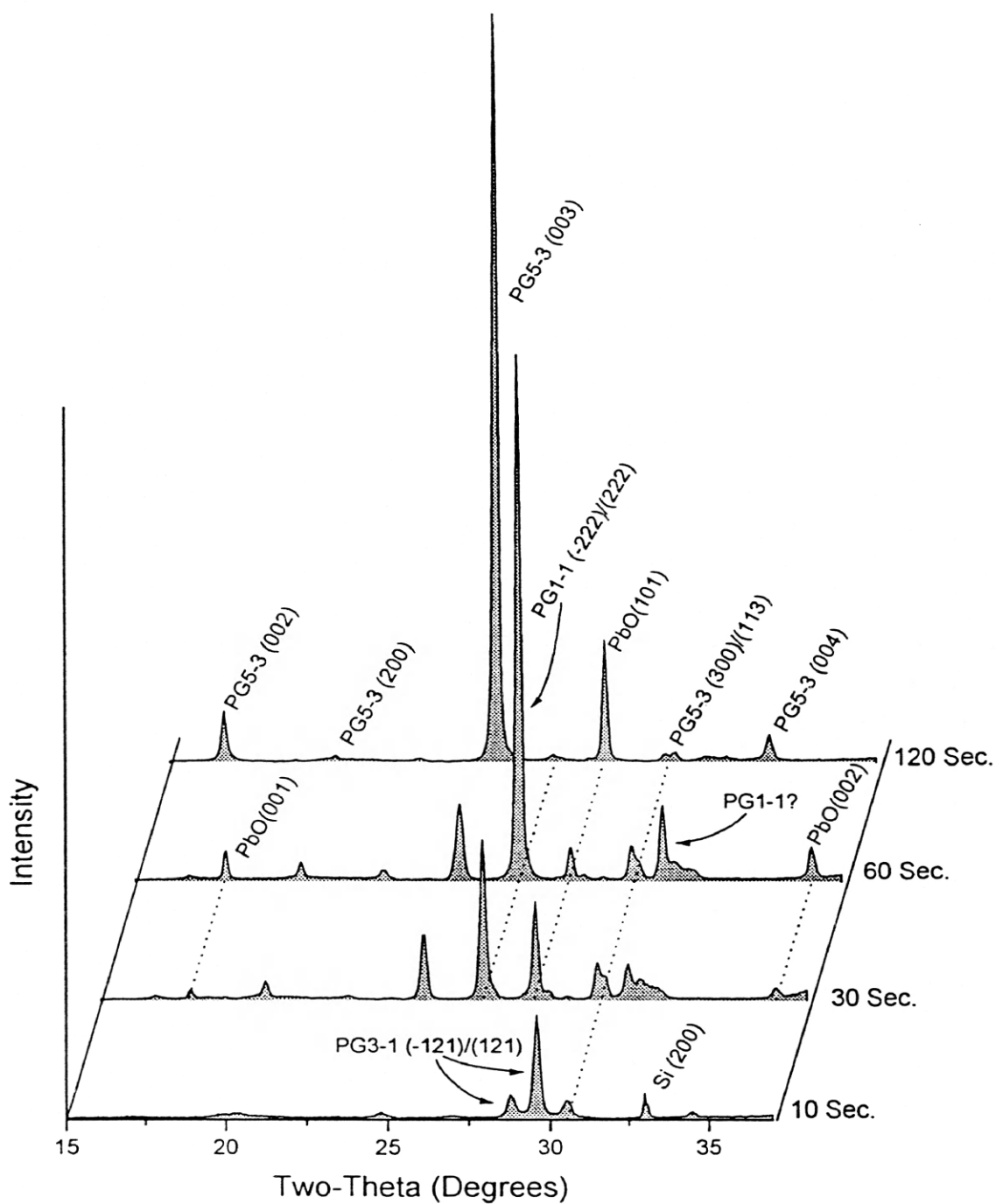


Figure 4.14. X-ray diffraction patterns for single layer $\text{Pb}_5\text{Ge}_3\text{O}_{11}$ films annealed at 700°C .

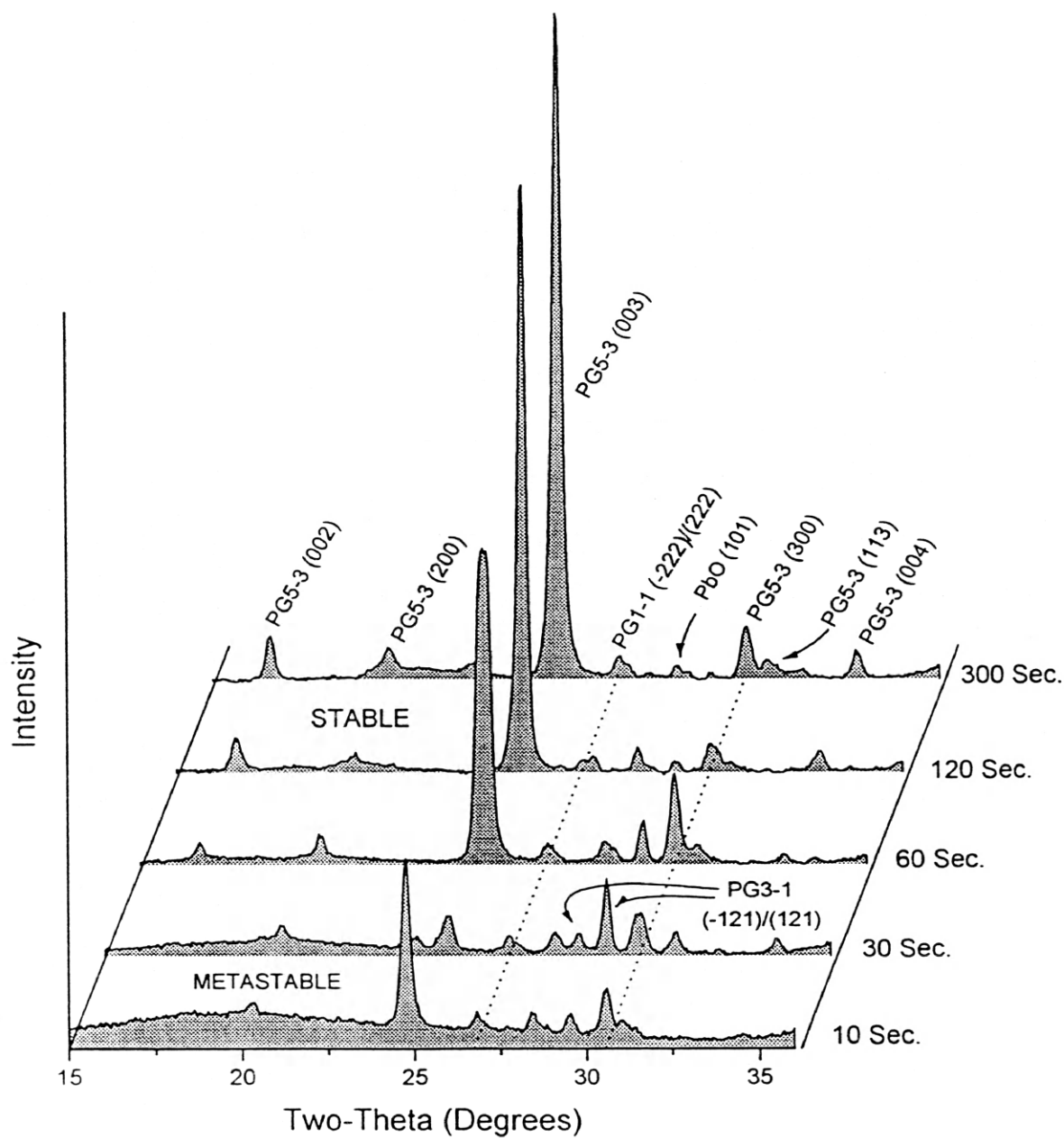


Figure 4.15. X-ray diffraction patterns for single layer $\text{Pb}_5\text{Ge}_3\text{O}_{11}$ films annealed at 450°C .

(Fig.4.2 on p.61). With increased annealing time, the Pb_3GeO_5 phase disappears as the diffusion process increases the $\text{Pb}_5\text{Ge}_3\text{O}_{11}$ formation.

If the temperature is high enough, ie. 700°C , PbGeO_3 is observed to form (Fig. 4.14). This formation at 700°C is probably due to a more rapid PbGeO_3 formation compared to the Pb^{2+} diffusion from the lead-rich regions of PbO and Pb_3GeO_5 . The lead deficient PbGeO_3 phase serves to balance the overall composition. At 600°C and below, the PbGeO_3 formation is slow enough that $\text{Pb}_5\text{Ge}_3\text{O}_{11}$ forms directly from the Pb^{2+} . Figures 4.5 (on p.66) and 4.15 show that the PbGeO_3 phase does not form significantly below 600°C . The Pb^{2+} diffusion does eventually cause the PbGeO_3 to transform into stable $\text{Pb}_5\text{Ge}_3\text{O}_{11}$, however the additional step delays the $\text{Pb}_5\text{Ge}_3\text{O}_{11}$ formation until approximately 120 seconds for a 700°C annealing temperature. It is also interesting to note that the PbO phase goes to a (001) orientation between 30 and 60 seconds at 700°C (Fig.4.14). Any PbO , PbGeO_3 , or Pb_3GeO_5 still left after 300 seconds annealing time may reflect a stoichiometry problem.

4.2 Phase Development in $\text{Pb}_5\text{Ge}_3\text{O}_{11}$ - $\text{PbZr}_x\text{Ti}_{1-x}\text{O}_3$ Thin Films

Thin films in the $\text{Pb}_5\text{Ge}_3\text{O}_{11}$ - $\text{PbZr}_x\text{Ti}_{1-x}\text{O}_3$ (PG-PZT) system crystallize into separate phases (Fig.4.16). As with the pure lead germanate, the first phase to appear is the $\text{Pt}_{5.7}\text{Pb}$ intermetallic phase. The final phases appear to be a (111) oriented perovskite PZT and an (001) oriented lead germanate which shows a high degree of peak splitting (Fig.4.16). The development of the lead germanate phases is much more difficult to determine in these mixed systems.

In the $4\text{Pb}_5\text{Ge}_3\text{O}_{11}$ - $\text{PbZr}_{0.5}\text{Ti}_{0.5}\text{O}_3$ composition, annealing temperatures

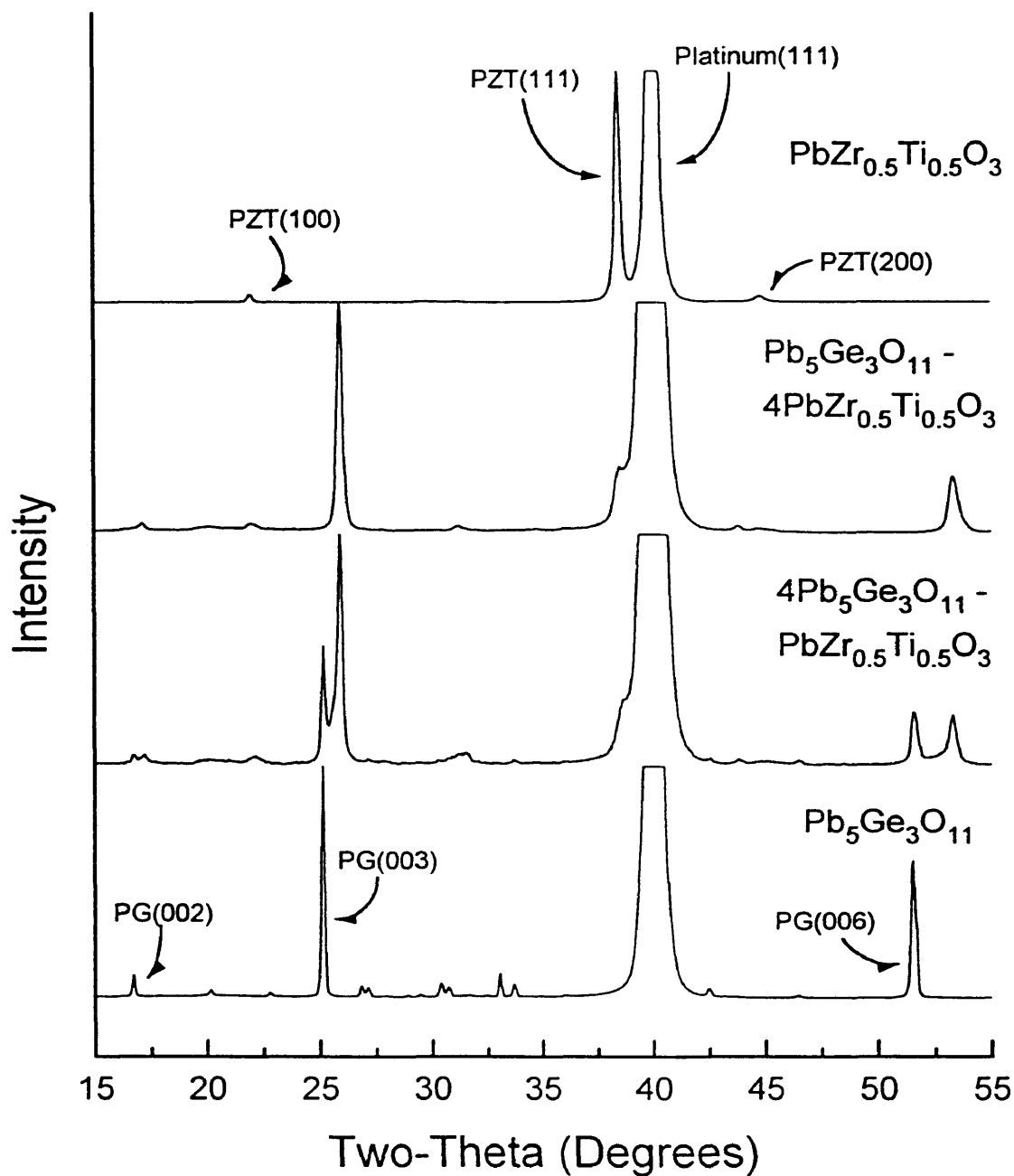


Figure 4.16. X-ray diffraction patterns for four layer films of varying composition, annealed at 500°C for 60 seconds after each layer and 700°C for 10 minutes after the final layer. Note the splitting of the PG (003) and (006) peaks in the $4\text{Pb}_5\text{Ge}_3\text{O}_{11}-\text{PbZr}_{0.5}\text{Ti}_{0.5}\text{O}_3$ composition and the shifted (003) and (006) peak positions in the $\text{Pb}_5\text{Ge}_3\text{O}_{11}-4\text{PbZr}_{0.5}\text{Ti}_{0.5}\text{O}_3$ composition.

of 600 or 700°C appear to result in oriented $\text{Pb}_5\text{Ge}_3\text{O}_{11}$ with the peaks shifted to slightly lower d-spacings (Figs.4.17 and 4.18). The peak at approximately $34.5^\circ 2\theta$ ($\sim 2.6\text{\AA}$) corresponds well with the (400) peak of the pyrochlore PZT. The high intensity of this peak would indicate an orientation of the (h00) type planes. The peak at approximately 5.19\AA matches well with the pyrochlore (200). The (600) peak would be located in the region of 1.74\AA . By 60 seconds at 600°C, peaks at 3.10\AA and 3.02\AA appear. These peaks could correspond to the pyrochlore (311) and (222) which are cited as having relative intensities of 50% and 100% respectively (Ref. JCPDS 26-142). Several difficulties become apparent when assigning the previous peaks to the pyrochlore phase of PZT.

- It would be surprising that the pyrochlore phase would show a preferred orientation prior to the development of its 100% diffraction peak (222).
- Films in the pure $\text{PbZr}_{0.5}\text{Ti}_{0.5}\text{O}_3$ and $\text{Pb}_5\text{Ge}_3\text{O}_{11}$ - $4\text{PbZr}_{0.5}\text{Ti}_{0.5}\text{O}_3$ systems showed the initial development of a randomly oriented pyrochlore (Fig.4.19).
- The intensity of the peaks are relatively high compared to those of the lead germanate peaks considering that the PZT in the 4PG-PZT composition is only 5 volume percent.

Another possible explanation would be to assign the 3.10 and 3.02\AA peaks to the Pb_3GeO_5 phase. The $(121)/(\bar{1}21)$ peaks for that phase are cited to be 3.114 and 3.023\AA with relative intensities of 95 and 100% respectively. The presence of extra Pb^{2+} would promote the formation of

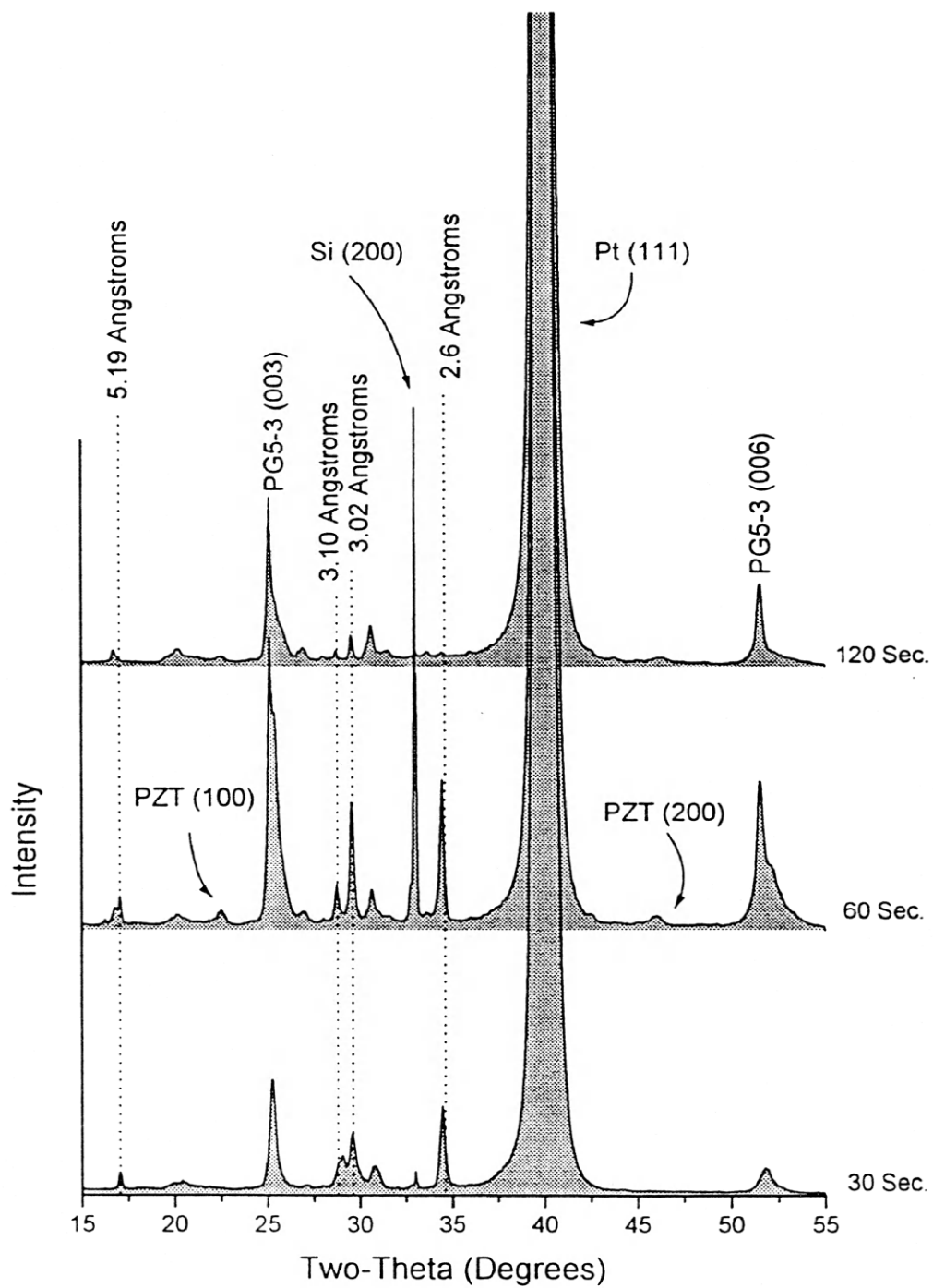


Figure 4.17. X-ray diffraction patterns for single layer $4\text{Pb}_5\text{Ge}_3\text{O}_{11}\text{-PbZr}_{0.5}\text{Ti}_{0.5}\text{O}_3$ films annealed at 600°C .

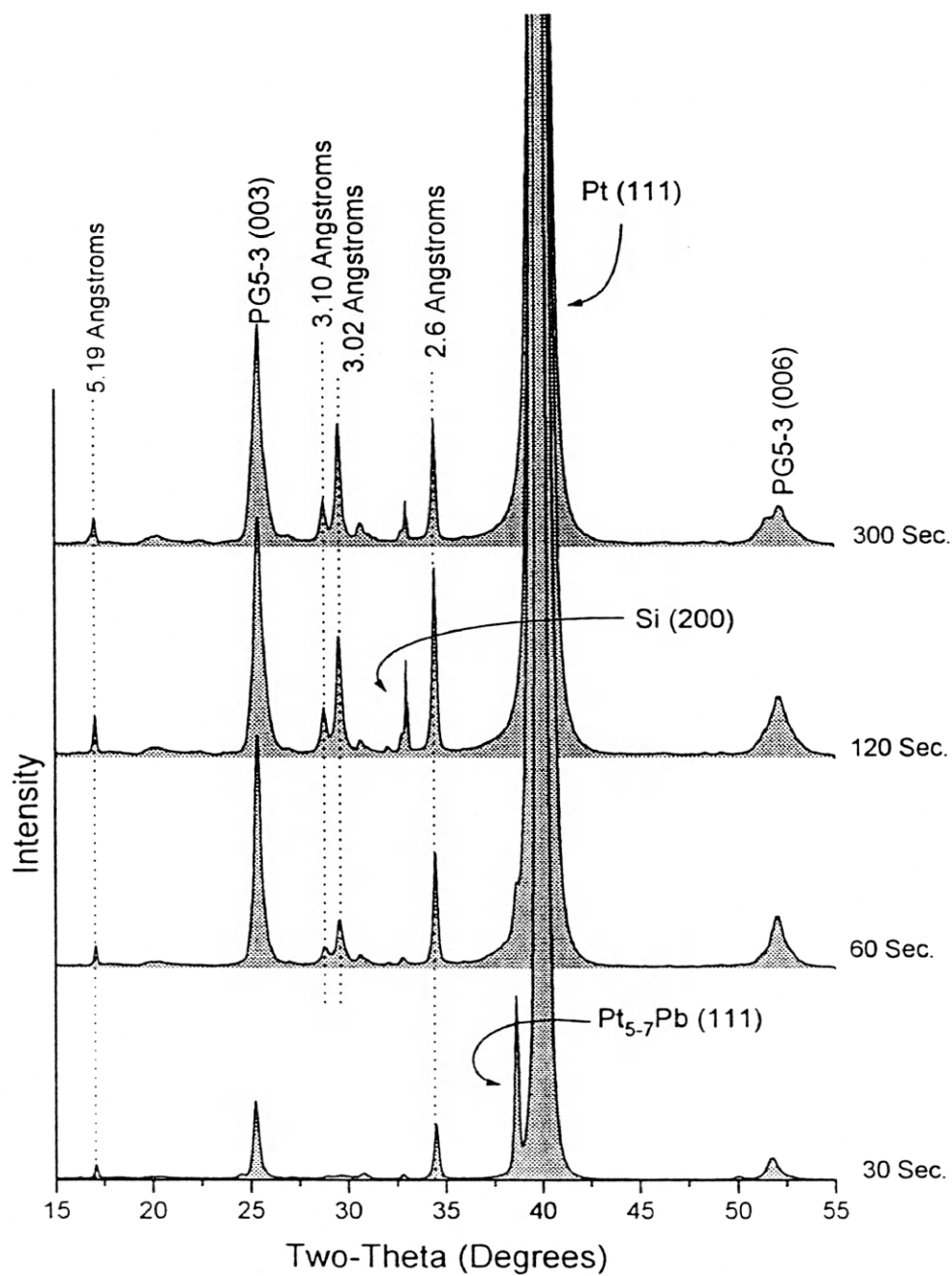


Figure 4.18. X-ray diffraction patterns for single layer $4\text{Pb}_5\text{Ge}_3\text{O}_{11}\text{-PbZr}_{0.5}\text{Ti}_{0.5}\text{O}_3$ films annealed at 700°C .

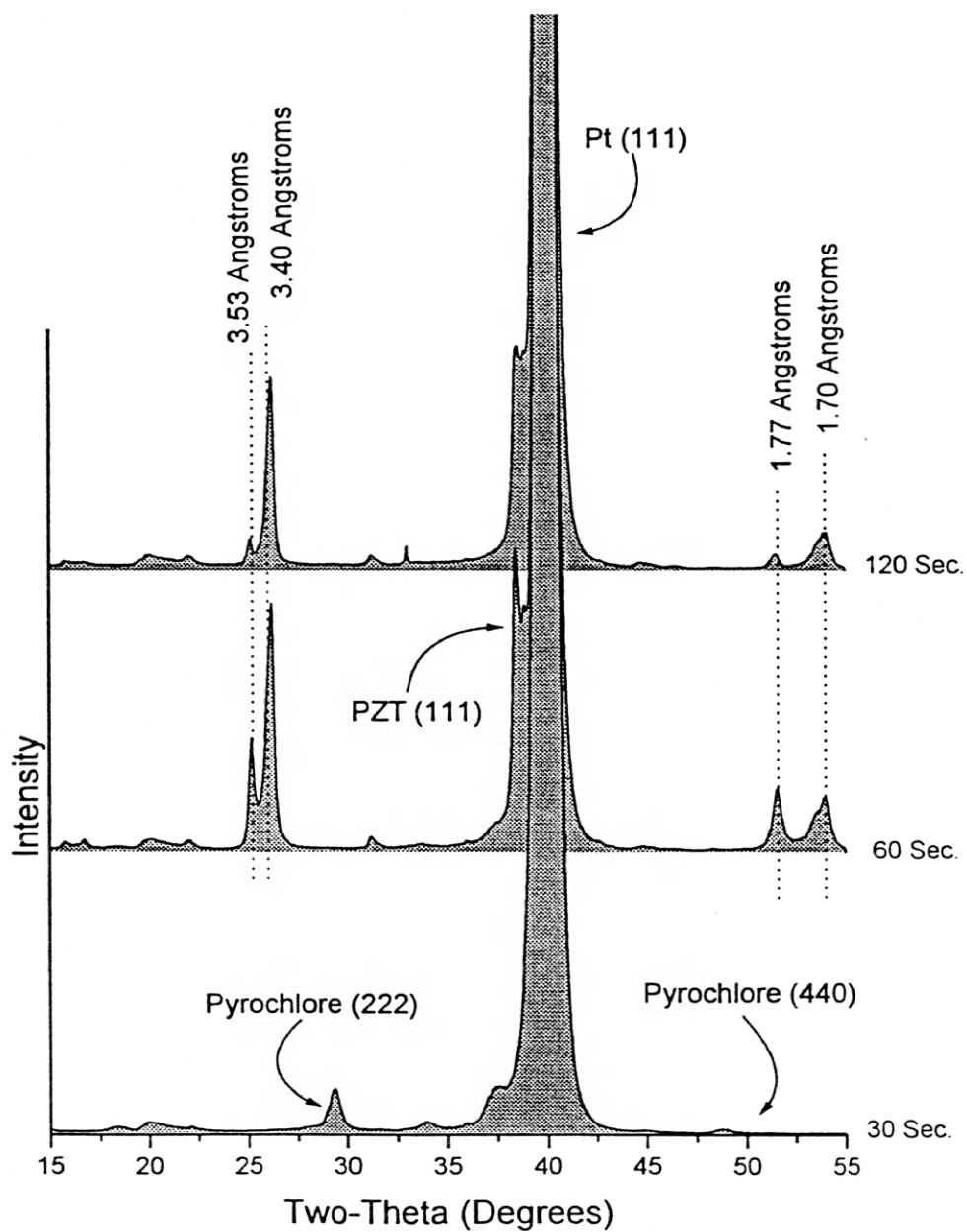


Figure 4.19. X-ray diffraction patterns for single layer $\text{Pb}_5\text{Ge}_3\text{O}_{11}-4\text{PbZr}_{0.5}\text{Ti}_{0.5}\text{O}_{11}$ films annealed at 700°C .

Pb_3GeO_5 if its reaction preceded the formation of PZT. This was observed by Schulze and Biggers [84] (Section 2.6). It is also possible that the line located at 2.6\AA is in fact the (200) of the Pb_3GeO_5 . The strong intensity of the line would indicate a preferred orientation of the (h00). It would follow then that the (100) and (300) peaks should be present. These are located at 5.254 and 1.751\AA respectively and correspond well to the observed patterns. Difficulties are also encountered when assigning these peaks to the Pb_3GeO_5 .

- The Pb_3GeO_5 phase was detected in the pure lead germanate films, however the peak at 2.6\AA and therefore the (h00) orientation was not observed.
- The Pb_3GeO_5 phase does not appear in the PG-4PZT composition. If this phase is promoted by an excess of Pb^{2+} , its formation in the PG-4PZT composition would be expected.

The perovskite PZT phase developed by 60 seconds at 700°C in both the $4\text{Pb}_5\text{Ge}_3\text{O}_{11}\text{-PbZr}_{0.5}\text{Ti}_{0.5}\text{O}_3$ and $\text{Pb}_5\text{Ge}_3\text{O}_{11}\text{-4PbZr}_{0.5}\text{Ti}_{0.5}\text{O}_3$ systems (Figs. 4.18 and 4.19).

The nature of the splitting and shifting of the (003) and (006) lead germanate peaks in these mixed systems is difficult to explain. The splitting is much more pronounced than in the pure lead germanate. Figure 4.16 (on p.85) summarizes the effect of composition on the splitting of these peaks for four layer films annealed at 700°C . For single layer $4\text{Pb}_5\text{Ge}_3\text{O}_{11}\text{-PbZr}_{0.5}\text{Ti}_{0.5}\text{O}_3$ films annealed at 600°C , three x-ray peaks are detected in the vicinity of the $\text{Pb}_5\text{Ge}_3\text{O}_{11}$ (006) peak position (Figs. 4.20A,B and 4.21A,B). These were measured at approximately 1.78 , 1.75 and 1.74\AA . If as for the

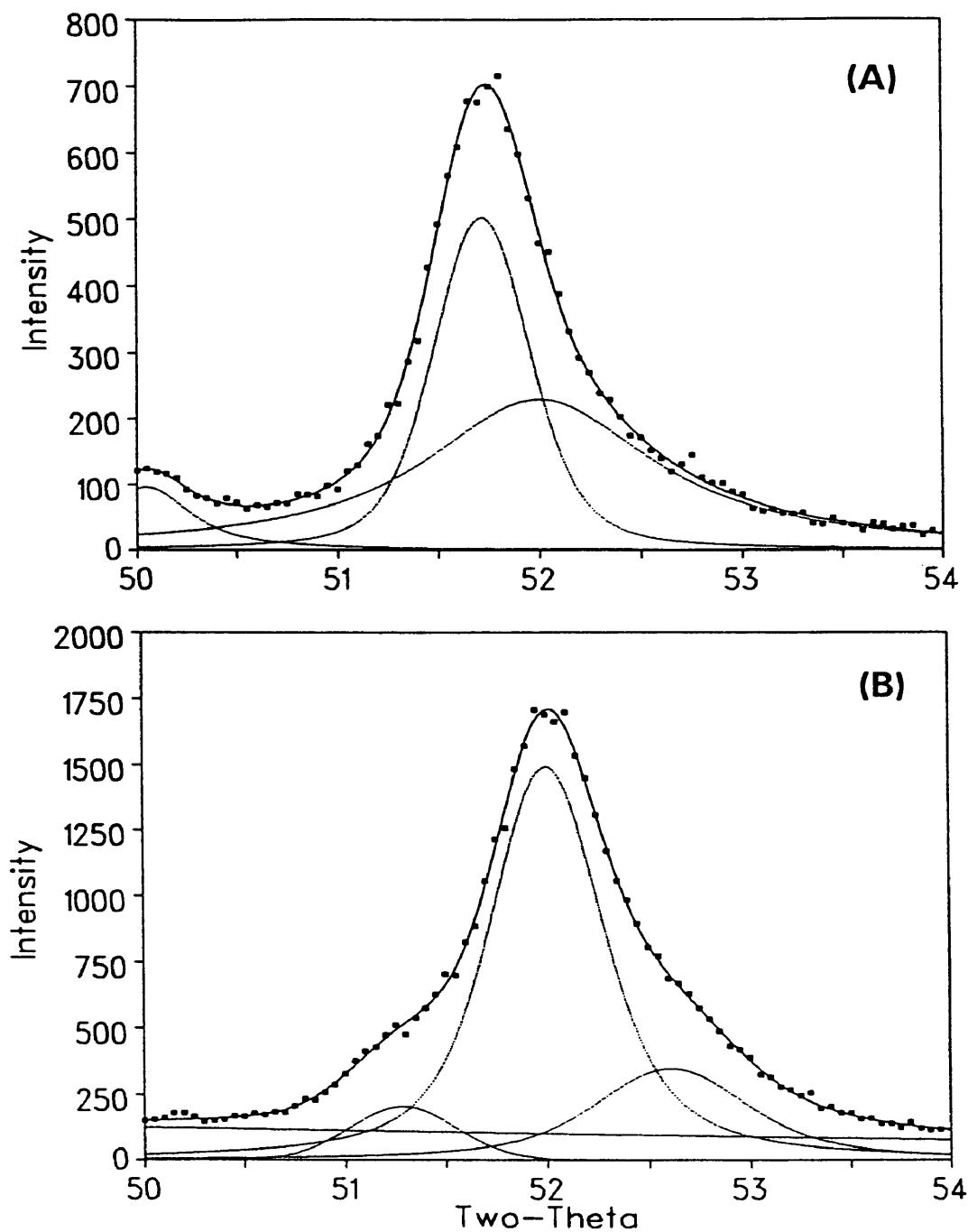


Figure 4.20. X-ray diffraction patterns for $4\text{Pb}_5\text{Ge}_3\text{O}_{11}\text{-PbZr}_{0.5}\text{Ti}_{0.5}\text{O}_3$ films and the corresponding fitted curves in the region of the PG(006). (A) A single layer film annealed at 600°C for 30 seconds. (B) A single layer film annealed at 600°C for 60 seconds.

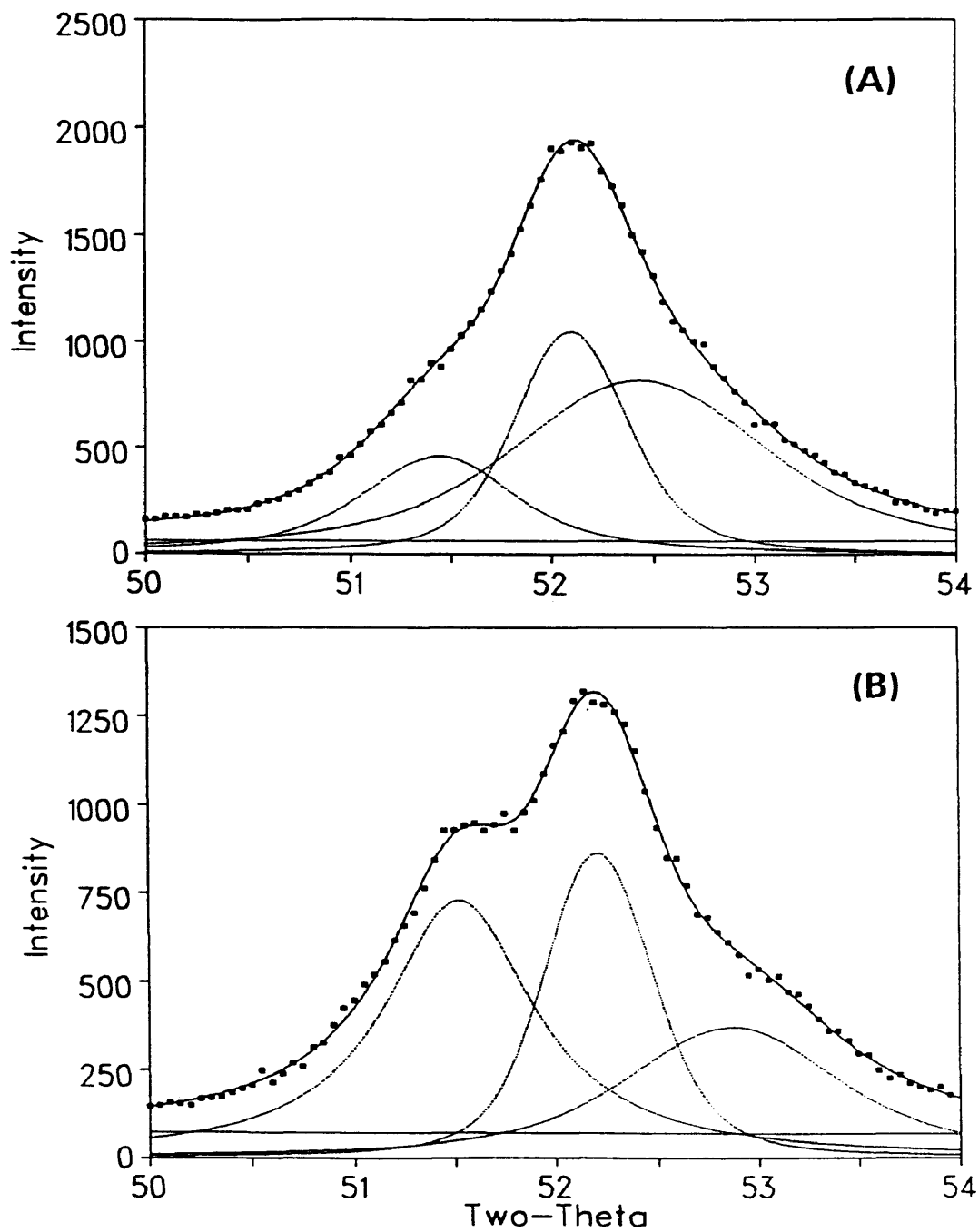


Figure 4.21. X-ray diffraction patterns for $4\text{Pb}_5\text{Ge}_3\text{O}_{11}\text{-PbZr}_{0.5}\text{Ti}_{0.5}\text{O}_3$ films and the corresponding fitted curves in the region of the PG(006). (A) A single layer film annealed at 600°C for 120 seconds. (B) A single layer film annealed at 600°C for 300 seconds.

pure lead germanate, these peaks are assumed to be characteristic of the $\text{Pb}_5\text{Ge}_3\text{O}_{11}$ phase, the separation between the first and third peaks would represent an approximate 0.24\AA change in the c-axis cell parameter. This is very similar to Maiwa et al.[53] (Section 2.4.6) who reported a 0.3\AA change which was reversible by oxygen annealing. They therefore attributed the structural change to nonstoichiometry. Attempts to anneal the current films in oxygen had no effect on the peak positions.

Currently, three possible explanations are considered for the source of the splitting of these peaks:

- There could be a stoichiometry problem similar to that reported by Maiwa et al.[53]. However, they observed this behavior in pure lead germanate films using a different deposition technique. Additionally, they did not report the coexistence of both peak positions. The current work did not indicate any reversible nature of the splitting by oxygen annealing as previously reported.

- The Pb_3GeO_5 phase has its $(\bar{1}11)/(111)$ peaks located at $3.634/3.493\text{\AA}$. Its (222) peaks are located in the region of 1.747\AA . If the Pb_3GeO_5 phase showed both (100) and (111) type orientations, the diffraction peaks observed could be accounted for by the Pb_3GeO_5 and PZT phases alone. The presence of the lead-rich Pb_3GeO_5 could be expected due to the inclusion of $\text{PbZr}_{0.5}\text{Ti}_{0.5}\text{O}_3$ in the composition. A preferred orientation of (100) and (111) would not be expected and is viewed as very unlikely.

- The magnitude of the split between the first and second peaks is very similar to that observed in the pure lead germanate, $\sim 0.15\text{\AA}$ change in the c-axis dimension. The final peak would indicate a further $\sim 0.06\text{\AA}$ change in the c-axis lattice parameter. It is suspected that the peak with the largest d-spacing (lowest 2θ) corresponds to the $\text{Pb}_3\text{Ge}_2\text{O}_7$ phase while the middle peak represents the stable $\text{Pb}_5\text{Ge}_3\text{O}_{11}$ phase. The rationale behind these assignments is discussed in Section 4.1.4. These two peaks are shifted to slightly higher 2θ positions (lower d-spacings) when compared to the pure $\text{Pb}_5\text{Ge}_3\text{O}_{11}$ composition. This shifting is believed to be due to an increase in the film stresses caused by the presence of the PZT phase. The third peak at the lowest d-spacing (highest 2θ) in the diphasic system may represent a nonferroelectric phase (ie. Pb_3GeO_5). This could be attributed to an increase in the availability of lead due the incorporation of $\text{PbZr}_{0.5}\text{Ti}_{0.5}\text{O}_3$ in the composition.

4.3 Microstructure and Preferred Orientation

4.3.1 Time / Temperature Relationships

Lead germanate ($\text{Pb}_5\text{Ge}_3\text{O}_{11}$) shows a very rapid orientation of its polar c-axis perpendicular to the plane of the film. Figure 4.22 compares the x-ray diffraction patterns for oriented and non-oriented lead germanate samples. Figure 4.23 shows the x-ray diffraction patterns for single layer $\text{Pb}_5\text{Ge}_3\text{O}_{11}$ films annealed for one minute. These data show that the films achieve c-axis orientations greater than 80% by 400°C (according to the calculation procedure described in Section 3.3.1). Orientations increase with

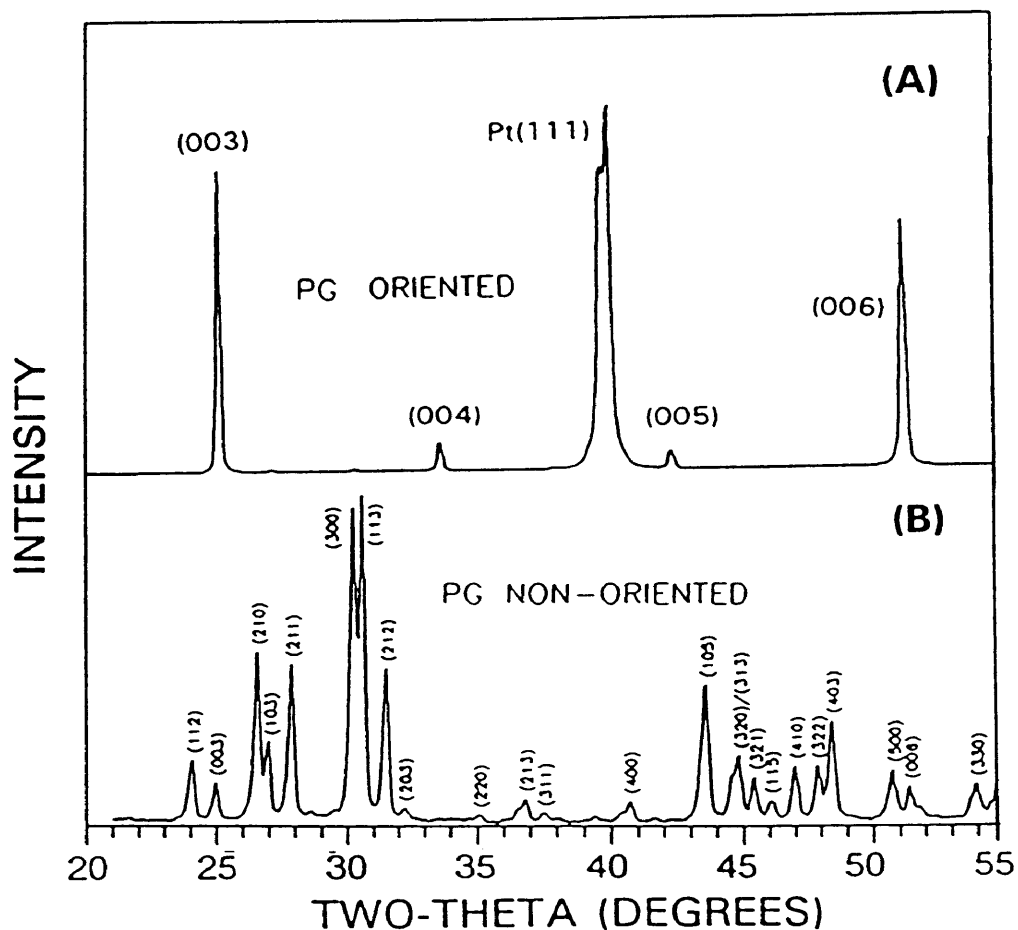


Figure 4.22. X-ray diffraction patterns comparing c-axis oriented to non-oriented $\text{Pb}_5\text{Ge}_3\text{O}_{11}$ microstructures. **(A)** A c-axis oriented lead germanate thin film annealed at 700°C for 10 minutes. **(B)** A non-oriented lead germanate bulk sample prepared by glass recrystallization [85].

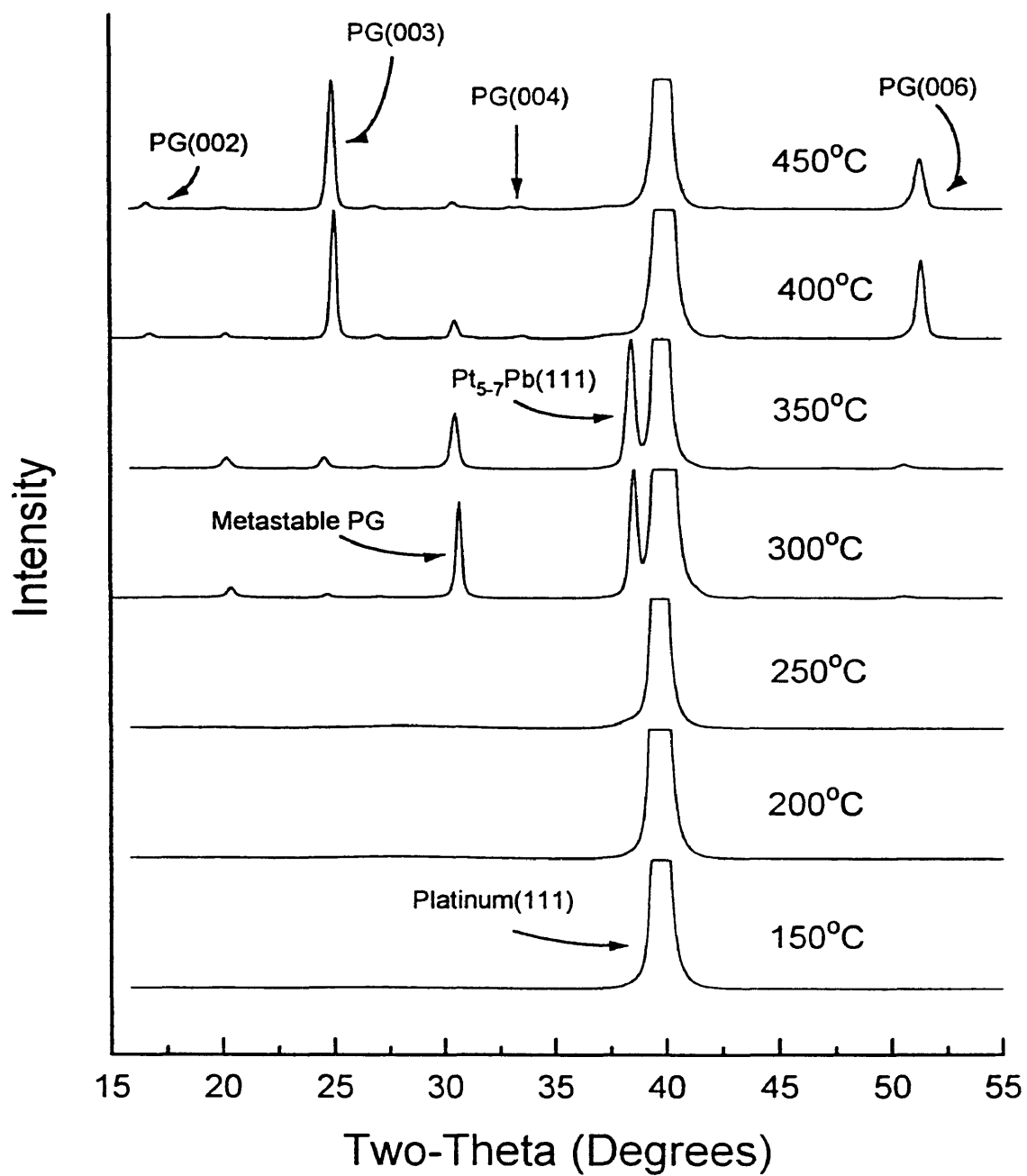


Figure 4.23. X-ray diffraction patterns for single layer $\text{Pb}_5\text{Ge}_3\text{O}_{11}$ films annealed for one minute.

increasing annealing temperatures and successive film layers. Figure 4.24 shows that 4-layer films annealed at 700°C achieved a c-axis orientation greater than 98%.

The annealing temperature and time also significantly impacted the grain size of lead germanate thin films. Below 500°C, the grains were not easily distinguished by atomic force microscopy (AFM) or scanning electron microscopy (SEM). AFM work in the current research allowed imaging of surface structural features with dimensions down to approximately 0.1 microns. It is therefore estimated that the grain size for these films was less than 0.1 microns.

Table 6 gives the approximate surface grain size for thin films annealed at 700 and 730°C. Films annealed at 700°C for 10 minutes had grain sizes on the order of 0.5 to 1.0 μm (Fig. 4.25). Increasing the annealing time to 20 minutes resulted in grain sizes of approximately 1-3 μm (Fig. 4.26) while 30 minutes yielded grain sizes of approximately 2-5 μm (Fig. 4.27). Figure 4.28 shows the surface of a 15-layer film annealed at 700°C for 30 minutes. Extensive "mud-cracking" is observed. This cracking is a function of the film thickness. Given the solution processing parameters followed in this research, 8-12 layers could be reproducibly applied without evidence of this form of cracking.

Table 6. Approximate surface grain size for $\text{Pb}_5\text{Ge}_3\text{O}_{11}$ thin films as a function of annealing time and temperature.

Annealing Temperature	Annealing Time					
	3 Min.	4 Min.	6 Min.	10 Min.	20 Min.	30 Min.
700°C	---	---	---	~ 1 μm	~ 3 μm	~ 5 μm
730°C	~ 2 μm	~ 3 μm	~ 5 μm	~ 15 μm	~ 30 μm	---

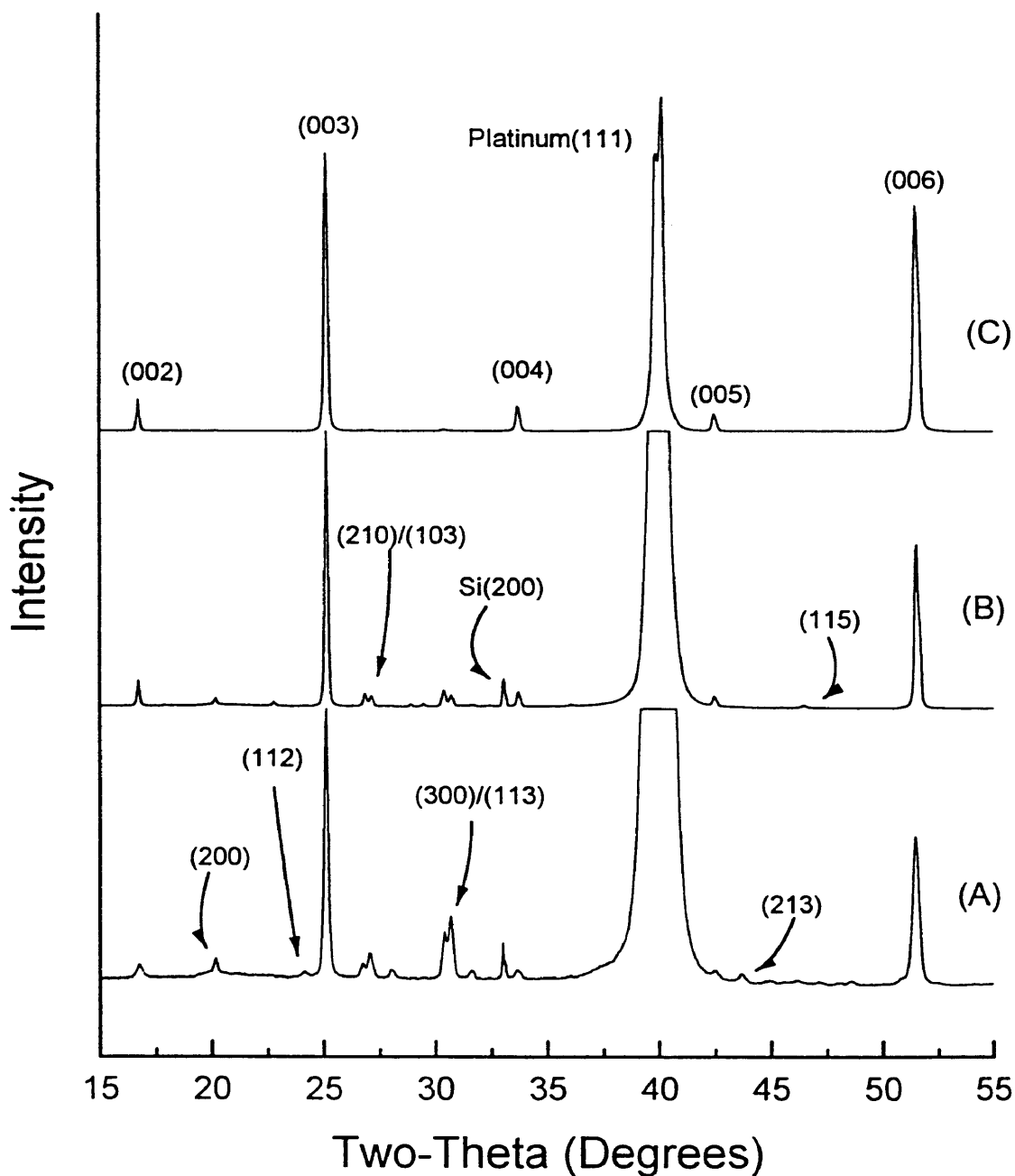


Figure 4.24. X-ray diffraction patterns for four layer $\text{Pb}_5\text{Ge}_3\text{O}_{11}$ films. (A) 500°C for one minute after each layer, 500°C for ten minutes after the final layer. (B) 500°C for one minute after each layer, 700°C for ten minutes after the final layer. (C) 700°C for one minute after each layer, 700°C for ten minutes after the final layer. Note that unless otherwise labeled, all identified diffraction lines belong to the $\text{Pb}_5\text{Ge}_3\text{O}_{11}$ phase.

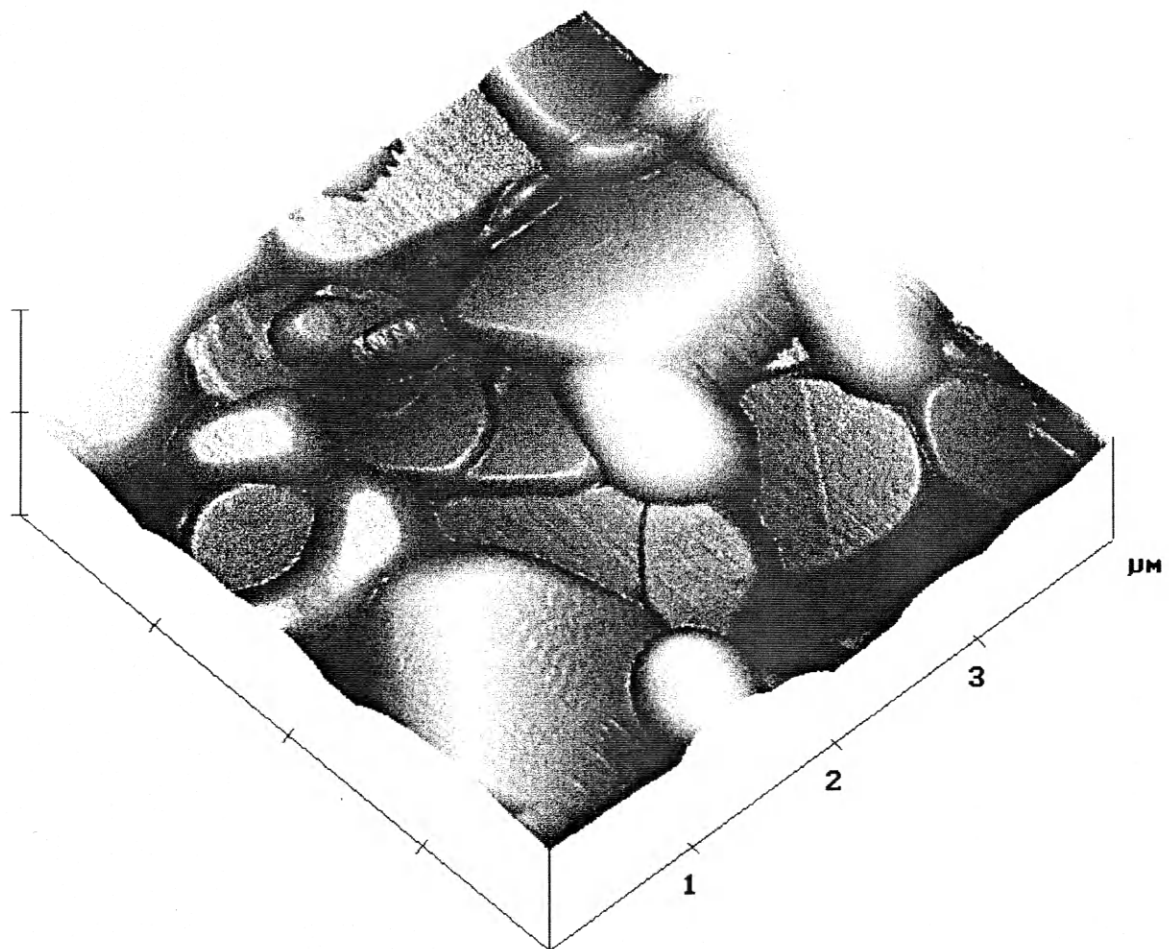


Figure 4.25. AFM micrograph of the surface of a two layer $\text{Pb}_5\text{Ge}_3\text{O}_{11}$ film annealed at 350°C for one minute after each layer and 700°C for ten minutes after the final layer.

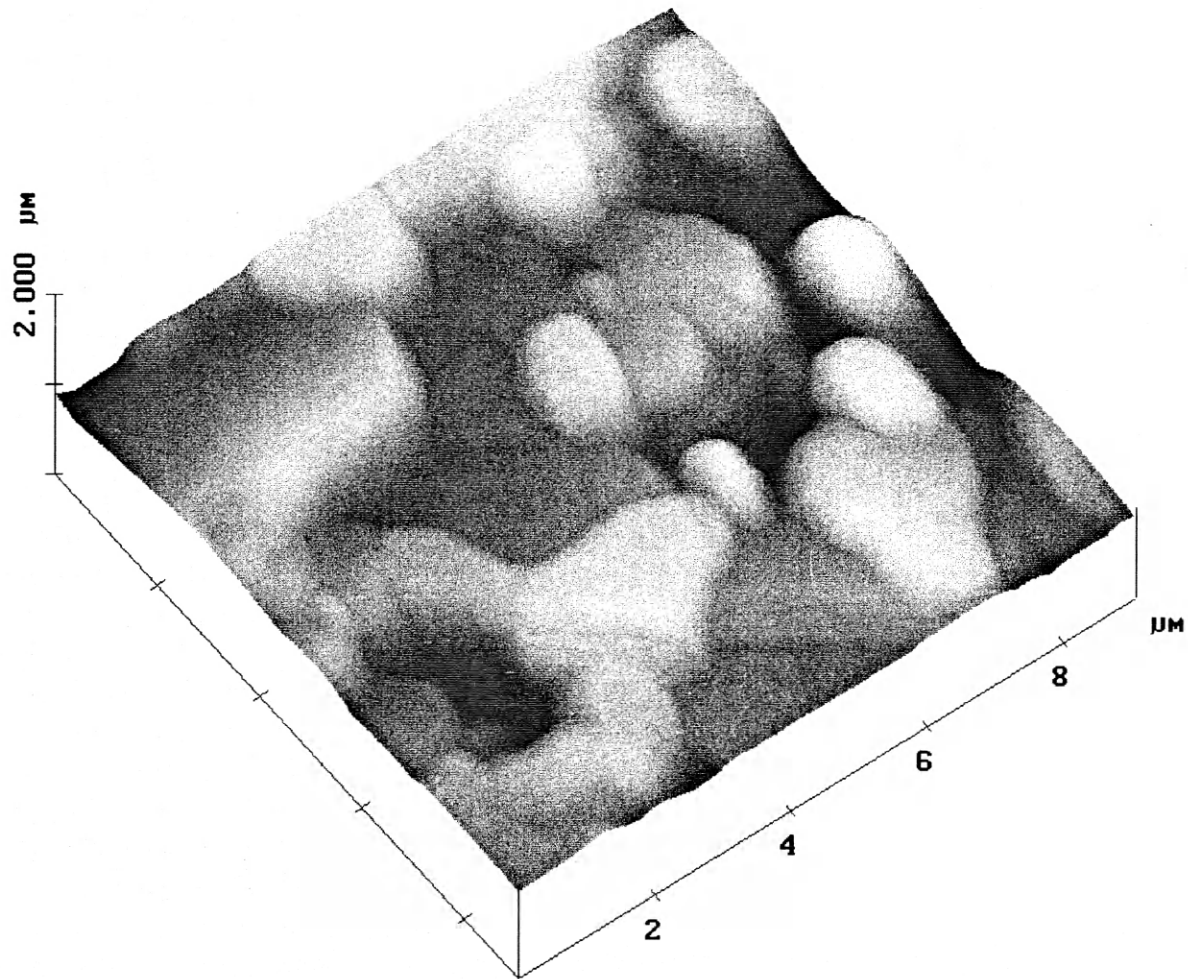


Figure 4.26. AFM micrograph of the surface of a 15-layer $\text{Pb}_5\text{Ge}_3\text{O}_{11}$ film annealed at 450°C for one minute after each layer and 700°C for 20 minutes after the final layer.

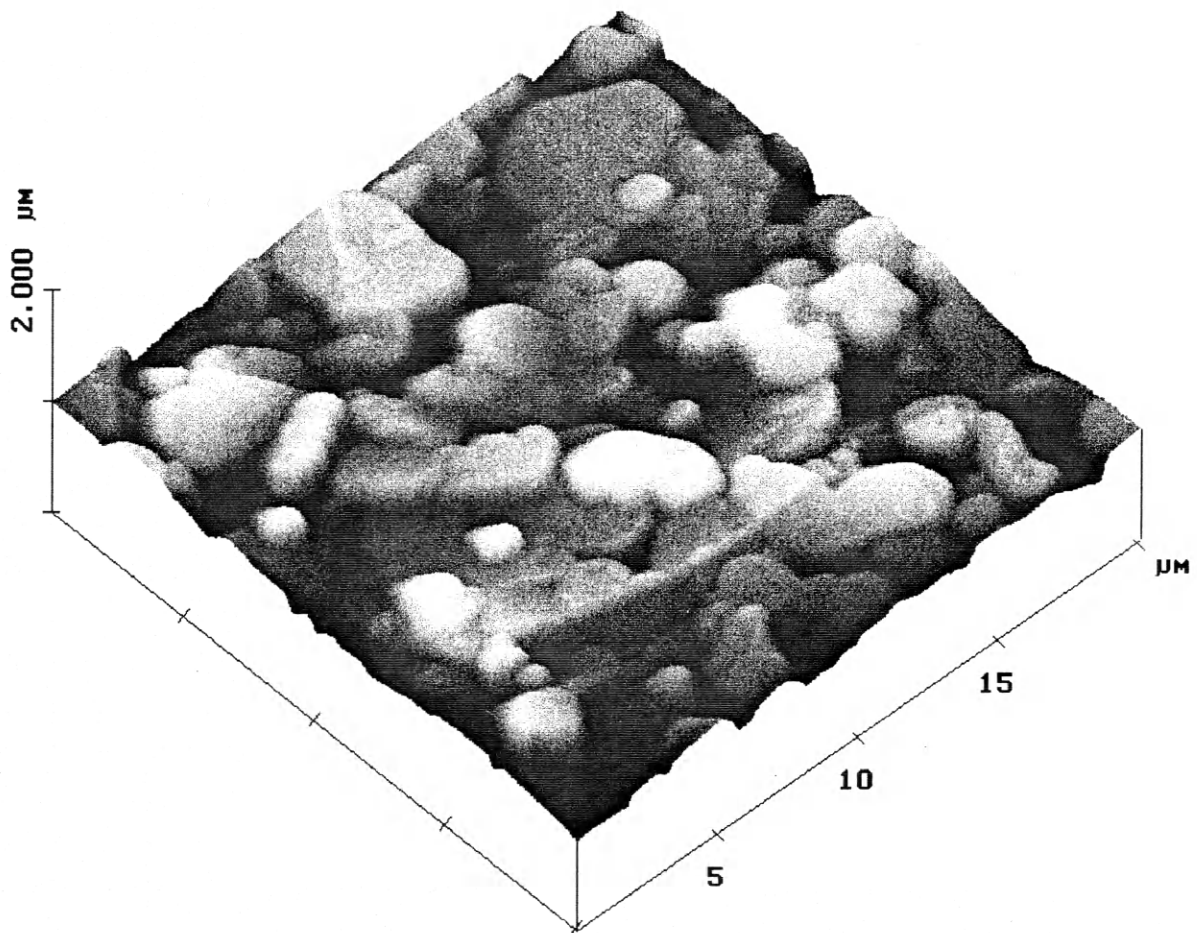


Figure 4.27. AFM micrograph of the surface of a 15-layer $\text{Pb}_5\text{Ge}_3\text{O}_{11}$ film annealed at 450°C for one minute after each layer and 700°C for 30 minutes after the final layer.

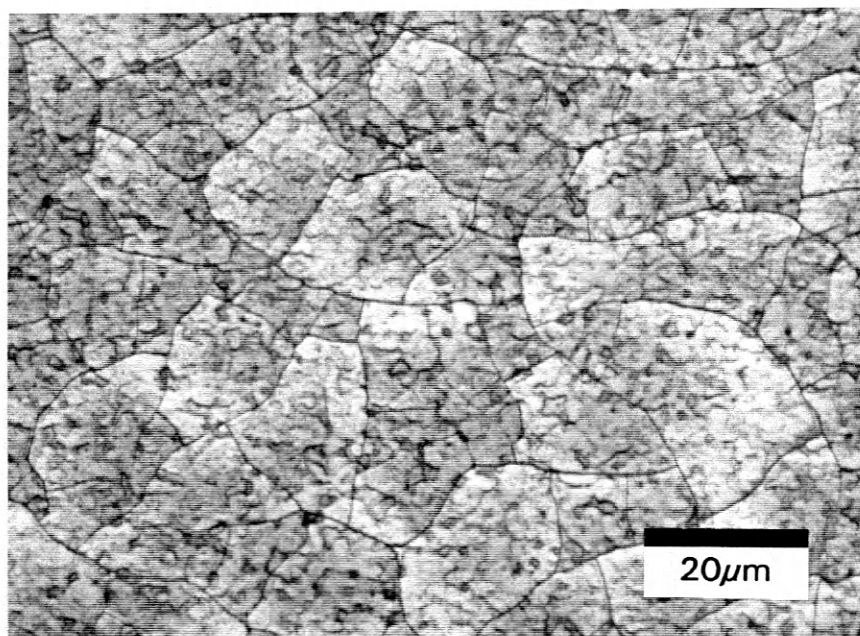


Figure 4.28. Optical micrograph of a 15-layer $\text{Pb}_5\text{Ge}_3\text{O}_{11}$ film annealed at 450°C for one minute after each layer and 700°C for 30 minutes after the final layer (1000X).

Annealing at 730°C, just below the melting point of 738°C, resulted in an approximate one order of magnitude increase in the rate of grain growth for lead germanate thin films (Table 6 on p.97). After annealing at 730°C for 3 minutes, grain sizes of approximately 1-2 μm were observed (Fig. 4.29). After 4 minutes, the surface grain size was determined to be 2-3 μm (Fig. 4.30). By 6 minutes, grain sizes of approximately 3-5 μm uniformly covered the film surface (Fig. 4.31). Figure 4.32A and B shows optical micrographs of films annealed at 730°C for 4 and 6 minutes respectively. The hexagonal (trigonal) symmetry of the grain structure is easily observed. X-ray diffraction patterns for these two films indicate c-axis orientations greater than 98% for both films (Fig. 4.33A and B). Increasing the annealing time at 730°C beyond 6 minutes results in a decrease of grain size uniformity. Figure 4.34A shows that after annealing at 730°C for 10 minutes, large grains on the order of 15 μm are observed in a matrix of much finer grained material. Annealing for 20 minutes at 730°C allowed grains to grow to approximately 30 μm in size (Fig. 4.34B).

Investigations were also performed in regards to processing lead germanate films at temperatures above the melting point of lead germanate. All annealing profiles above the melting temperature were performed at 760°C. Films were initially annealed at 450°C for one minute after the deposition of each layer for the removal of organics and the formation of $\text{Pb}_5\text{Ge}_3\text{O}_{11}$ as a nanocrystalline phase. Figure 4.35A shows the surface of a 2-layer film annealed at 760°C for 10 seconds. Figure 4.35B shows a 2-layer film annealed at 760°C for 5 minutes. With complete melting of the film at these longer annealing times, the lead germanate appears to "de-wet" the platinum surface of the substrate and forms as isolated "islands" of highly crystalline material. Figure 4.36A and B shows the surface of a

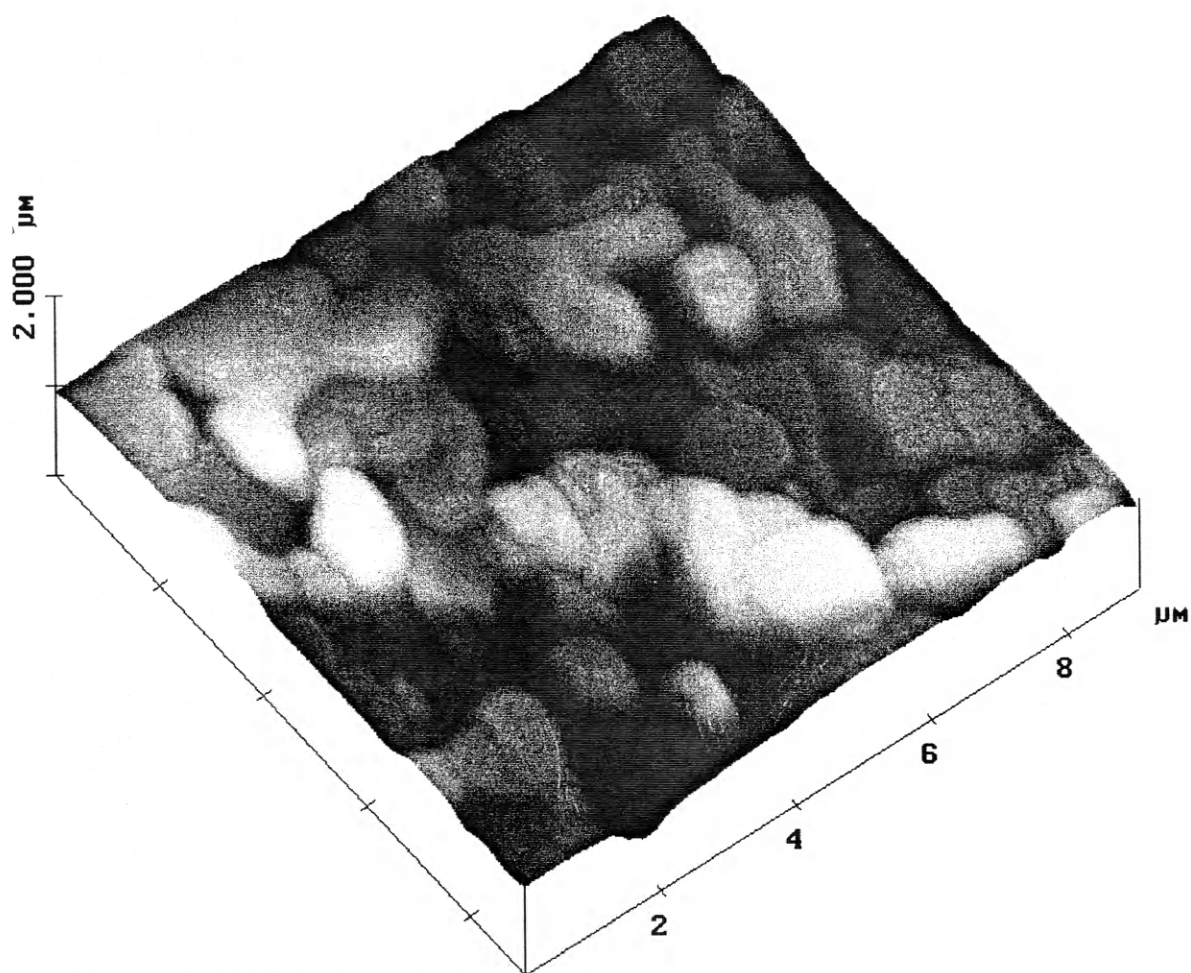


Figure 4.29. AFM micrograph of the surface of a 12-layer $\text{Pb}_5\text{Ge}_3\text{O}_{11}$ film annealed at 450°C for one minute after each layer and 730°C for 3 minutes after the final layer.

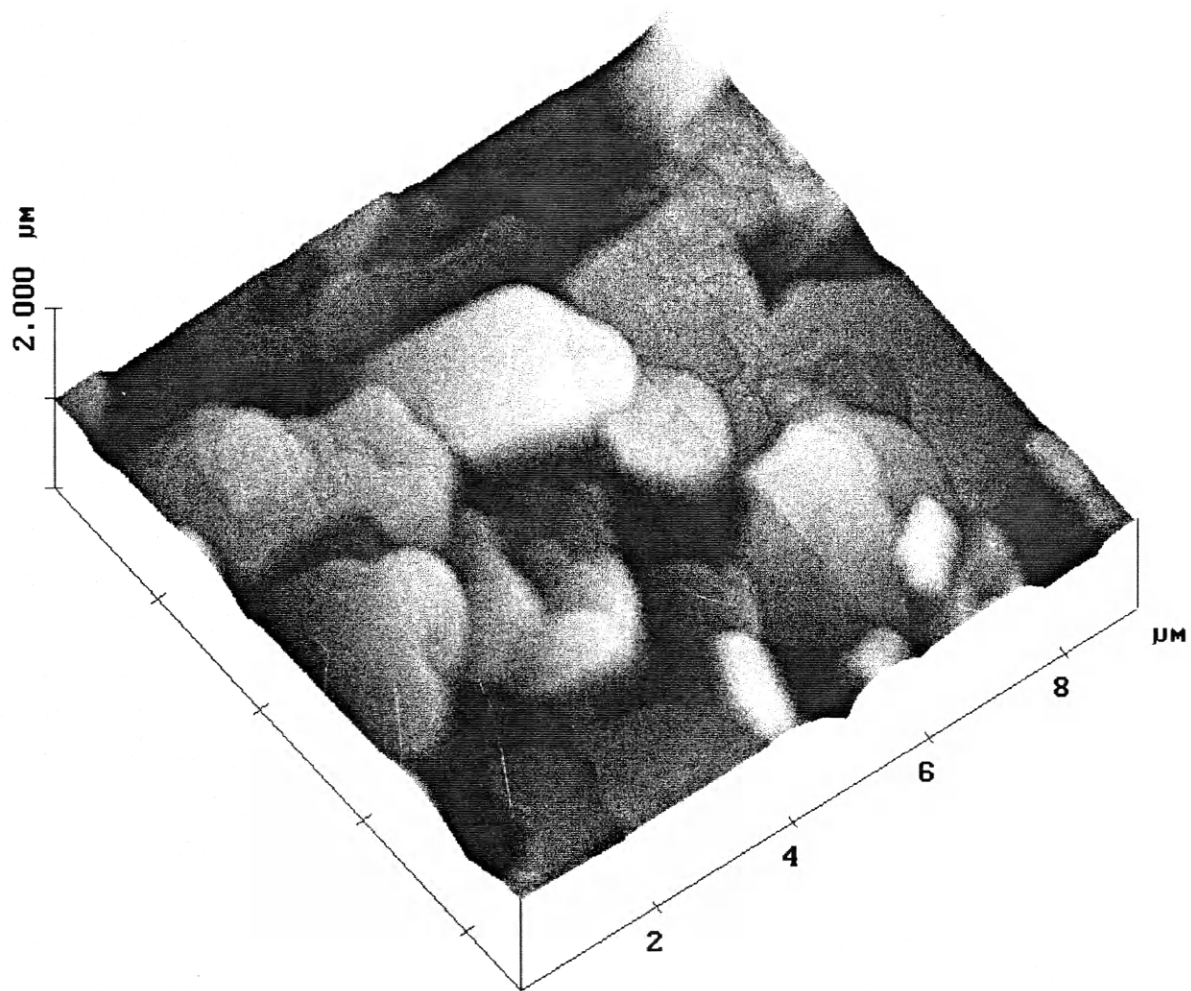


Figure 4.30. AFM micrograph of the surface of a 12-layer $\text{Pb}_5\text{Ge}_3\text{O}_{11}$ film annealed at 450°C for one minute after each layer and 730°C for 4 minutes after the final layer.

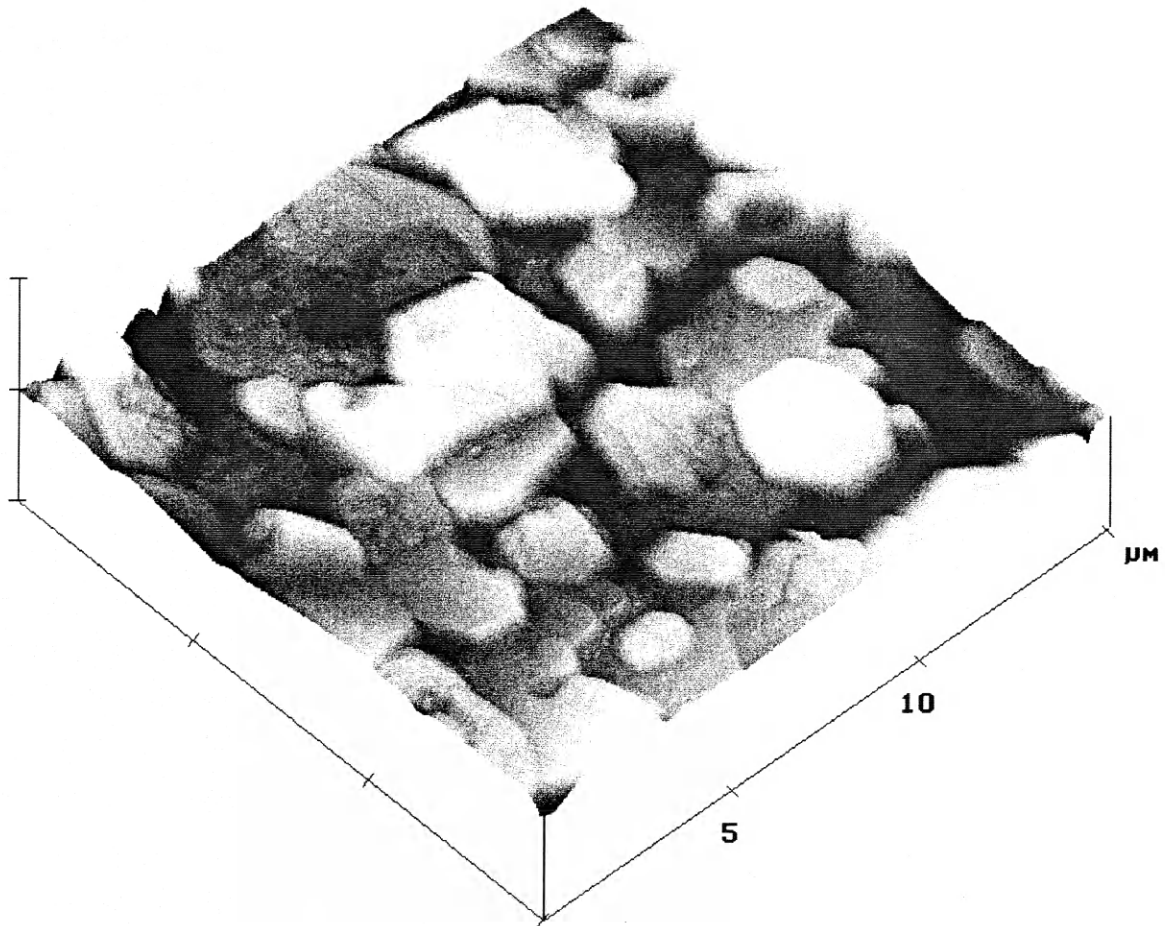


Figure 4.31. AFM micrograph of the surface of a 12-layer $\text{Pb}_5\text{Ge}_3\text{O}_{11}$ film annealed at 450°C for one minute after each layer and 730°C for 6 minutes after the final layer.

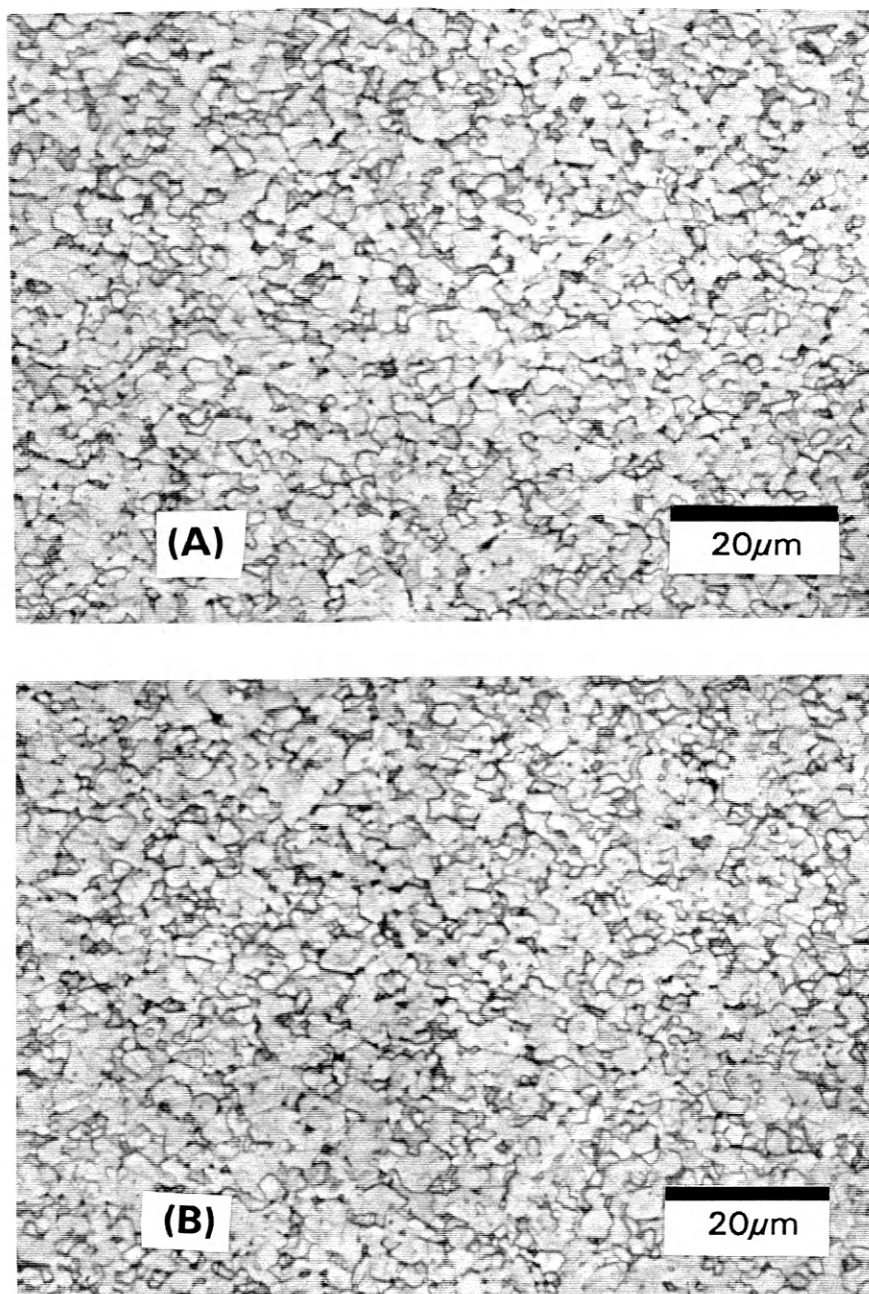


Figure 4.32. Optical micrographs of four layer $\text{Pb}_5\text{Ge}_3\text{O}_{11}$ films annealed at 450°C for one minute after each layer and (A) 730°C for 4 minutes after the final layer (1000X) (B) 730°C for 6 minutes after the final layer (1000X).

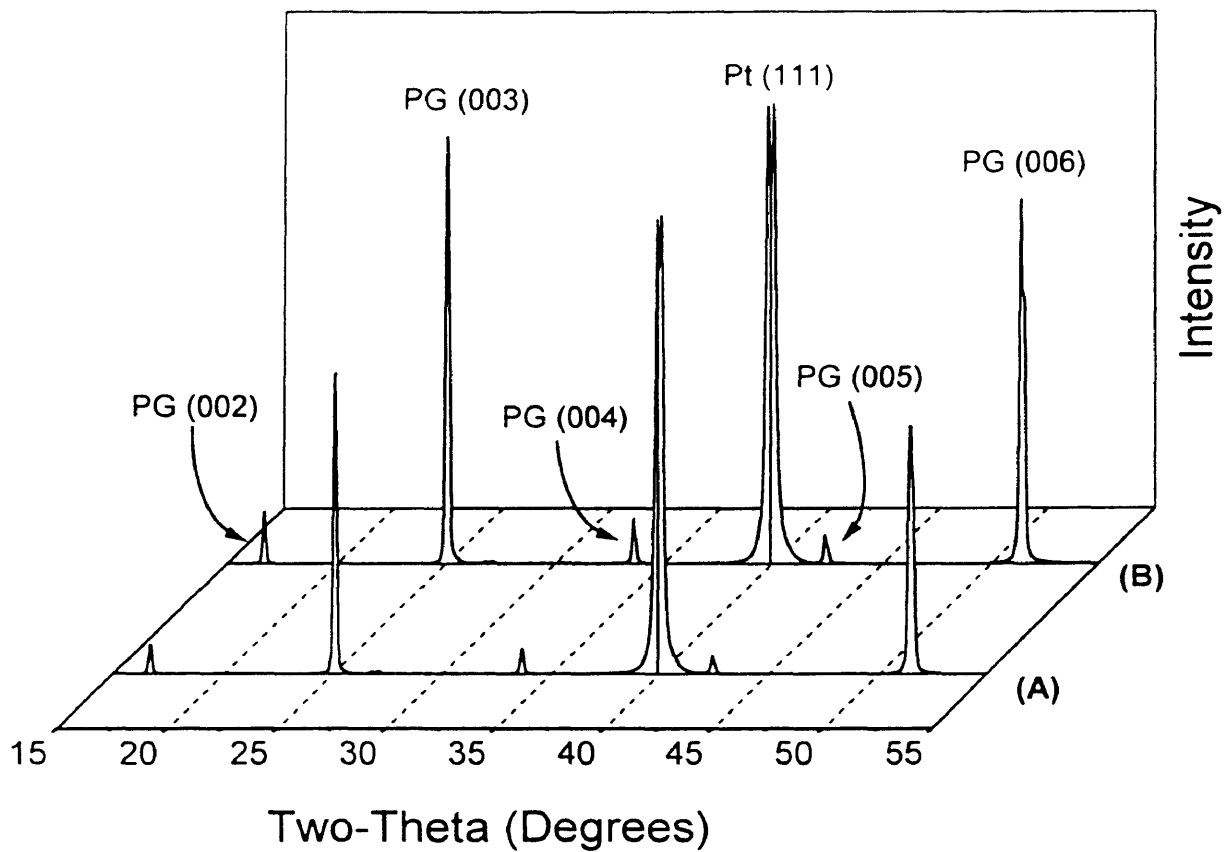


Figure 4.33. X-ray diffraction patterns for 12-layer $\text{Pb}_5\text{Ge}_3\text{O}_{11}$ films annealed at 450°C for one minute after each layer and (A) 730°C for 4 minutes after the final layer (B) 730°C for 6 minutes after the final layer.

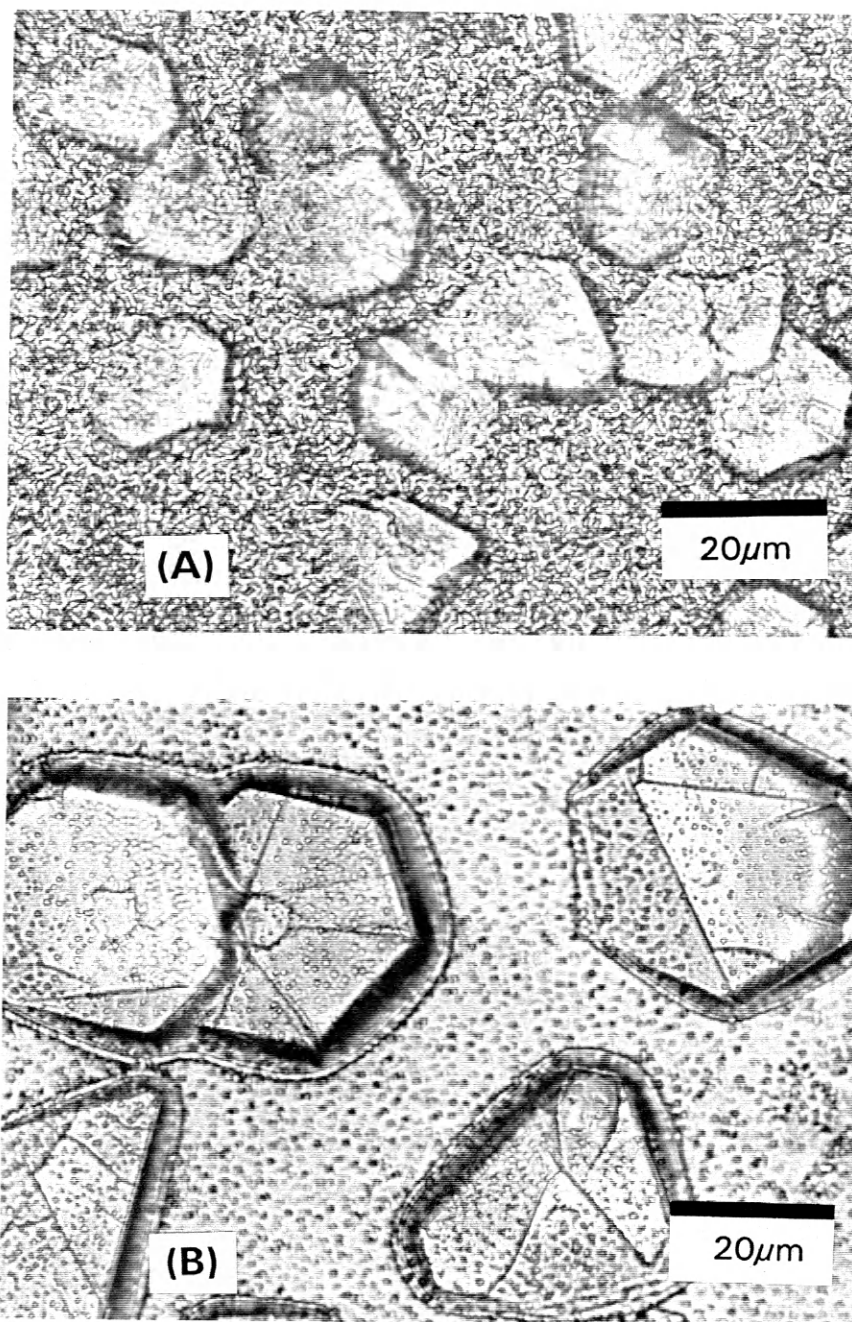


Figure 4.34. Optical micrographs of four layer $\text{Pb}_5\text{Ge}_3\text{O}_{11}$ films annealed at 350°C for one minute after each layer and (A) 730°C for 10 minutes after the final layer (1000X) (B) 730°C for 20 minutes after the final layer (1000X).

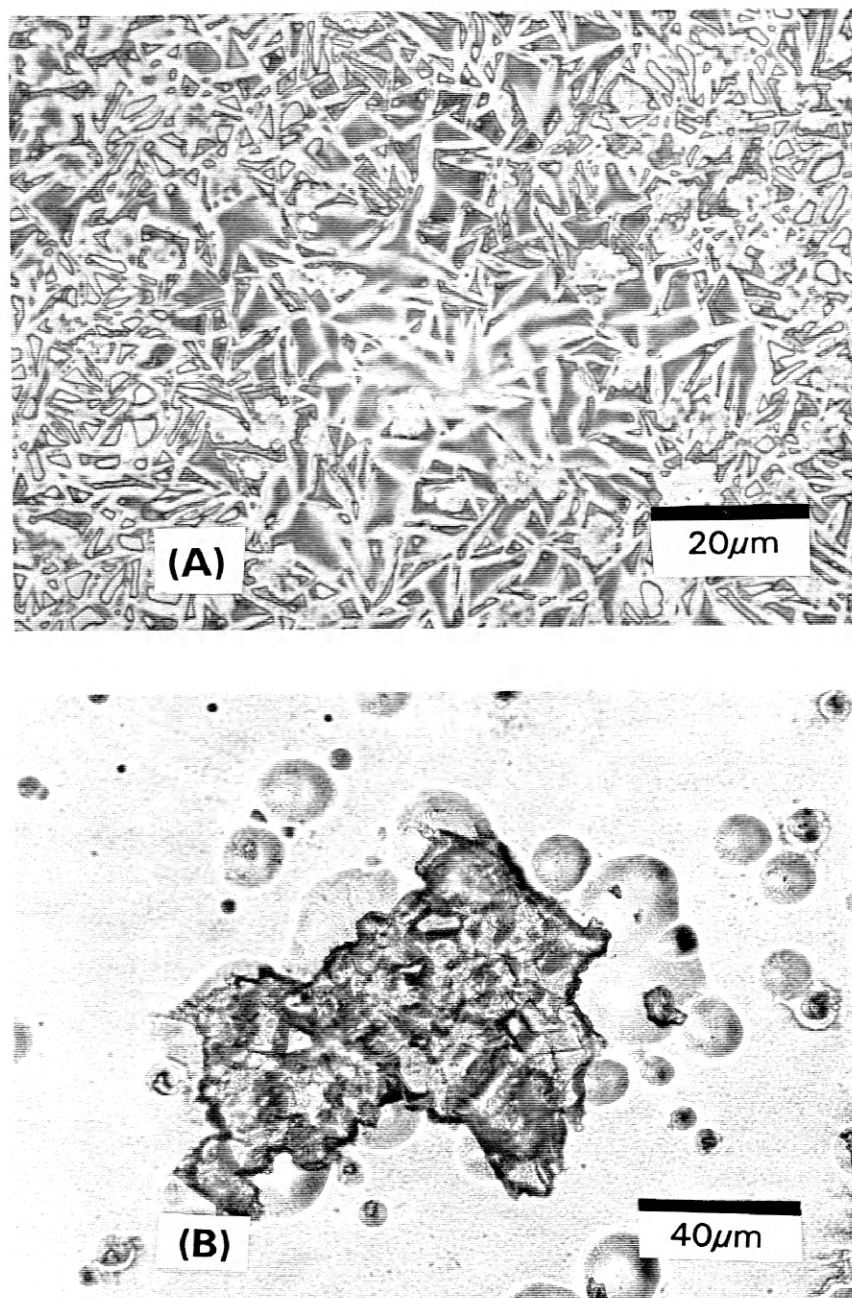


Figure 4.35. Optical micrographs of two layer $\text{Pb}_5\text{Ge}_3\text{O}_{11}$ films annealed at 450°C for one minute after each layer and (A) 760°C for 10 seconds after the final layer (1000X) (B) 760°C for 5 minutes after the final layer (500X).

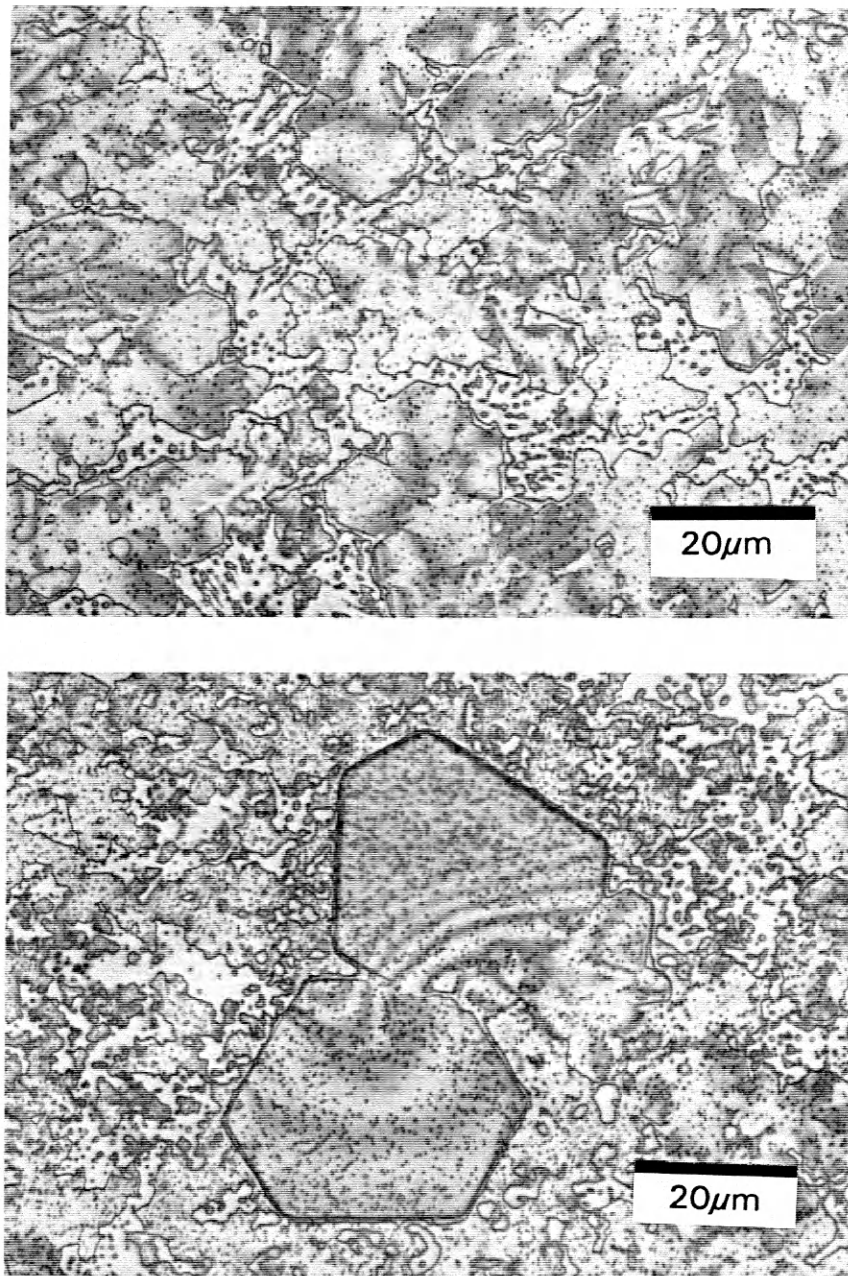


Figure 4.36. Optical micrographs of two layer $\text{Pb}_5\text{Ge}_3\text{O}_{11}$ films annealed at 450°C for one minute after each layer and 760°C for one minute after the final layer (1000X).

2-layer film annealed at 760°C for one minute. Definite hexagonal grains can be seen forming over the entire film surface with grain sizes on the order of 5-10 μ m. Several larger isolated grains on the order of 20 μ m were also present. The film has not completely de-wetted from the substrate, however the coverage is not complete. Figure 4.37A shows the surface of a film annealed at 760°C for two minutes. An interesting feature of this film was the extreme dendritic crystal growth originating from film defects. These dendrites formed macroscopic hexagonal patterns with diameters on the order of 2 to 4 millimeters and were easily identified visually. Evidently, withdrawal of the film from the furnace resulted in supercooling of the melt. The defects served as nucleation sites. The heat of solidification must be diffused through the liquid phase. This heat removal will occur most rapidly for the dendrite spikes due to the small radius of curvature. These spikes will then serve as the advancing crystalline front. The x-ray diffraction data for this film confirms the $\text{Pb}_5\text{Ge}_3\text{O}_{11}$ phase with a c-axis orientation (Fig.4.38). Figure 4.37B shows the surface of a 2-layer film annealed at 760°C for three minutes. Exaggerated grain growth was present with grain sizes as large as 50 μ m.

Films in the $\text{Pb}_5\text{Ge}_3\text{O}_{11}$ - $\text{PbZr}_x\text{Ti}_{1-x}\text{O}_3$ system also showed c-axis orientation of the lead germanate phase. Determination of the amount of this orientation is complicated by the splitting of the (00l) peaks. The PZT phase showed (111) orientation, both as a pure phase and when mixed with lead germanate (Fig.4.16 on p.85). When PZT or lead titanate was deposited on top of a lead germanate film, these phases formed with a random orientation. This indicates a dependence on the substrate or intermetallic phase for the PZT orientation. In contrast, lead germanate displayed strong c-axis orientation when deposited on PZT or lead titanate.

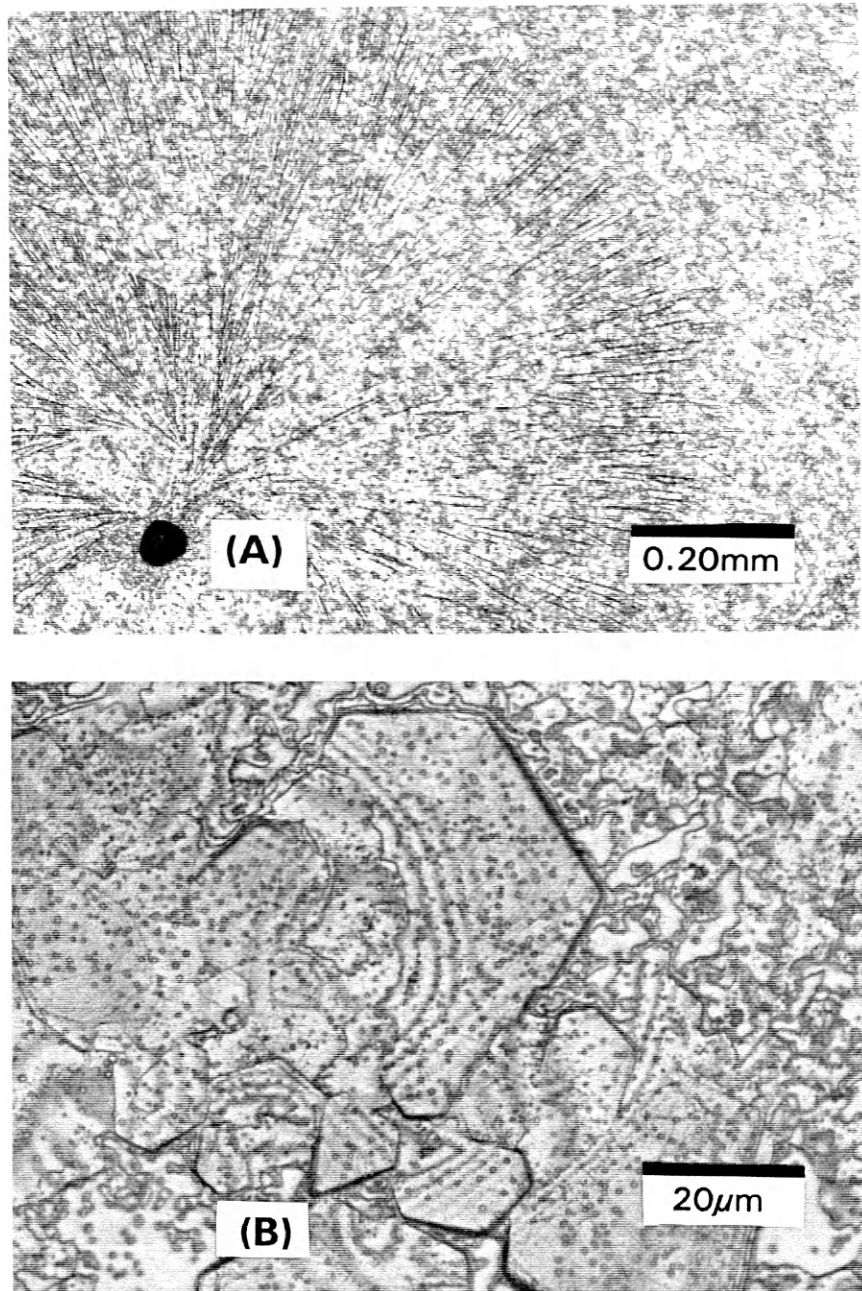


Figure 4.37. Optical micrographs of two layer $\text{Pb}_5\text{Ge}_3\text{O}_{11}$ films annealed at 450°C for one minute after each layer and (A) 760°C for 2 minutes after the final layer (125X) (B) 760°C for 3 minutes after the final layer (1000X).

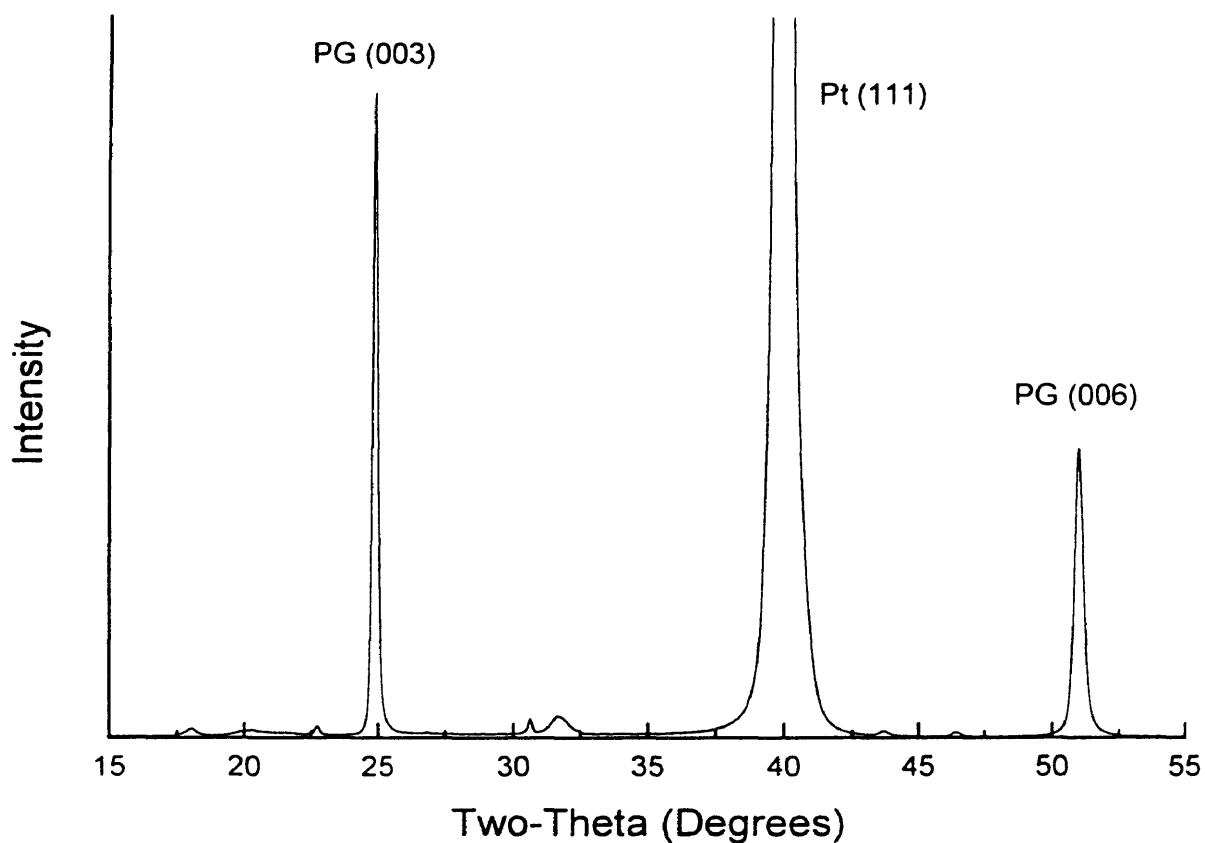


Figure 4.38. X-ray diffraction pattern for a two layer $\text{Pb}_5\text{Ge}_3\text{O}_{11}$ film annealed at 450°C for one minute after each layer and 760°C for two minutes after the final layer.

This indicates that the $\text{Pb}_5\text{Ge}_3\text{O}_{11}$ orientation is not dependent on the substrate.

It was interesting that lead germanate thin films deposited on lead titanate thin films appear to show a more uniform grain growth. These films were prepared by first depositing two layers of lead titanate on the substrate with an annealing condition of 700°C for 10 minutes. The lead titanate had a grain size of approximately 100nm (Fig. 4.39). Two layers of lead germanate were then deposited on the lead titanate layers with the same annealing conditions, 700°C for 10 minutes. The resulting microstructure (Fig. 4.40) appears to be more uniform when compared to lead germanate deposited directly on the substrate (Fig. 4.25 on p.99). This is believed to be due to the lead titanate grains serving as nucleation sites for the lead germanate.

4.3.2 Microstructure Optimization

The primary difficulty observed up to this point in attempting to attain an optimized film microstructure is the lack of macroscopic "density". Films annealed at 450°C attained c-axis orientation and were dense, however the grain size is very small ($<0.1\mu\text{m}$) and the films do not show normal ferroelectric properties (Section 4.4). An optimal grain size in terms of electrical properties is expected to be in the range of $5\mu\text{m}$. Growing the grains to this size, however, resulted in the films having a very "open" microstructure (Fig. 4.41) that will inevitably lead to electrical shorting.

Several novel processing methods were investigated as possible solutions to this problem of film density. These included annealing at temperatures above the melting point of lead germanate and altered

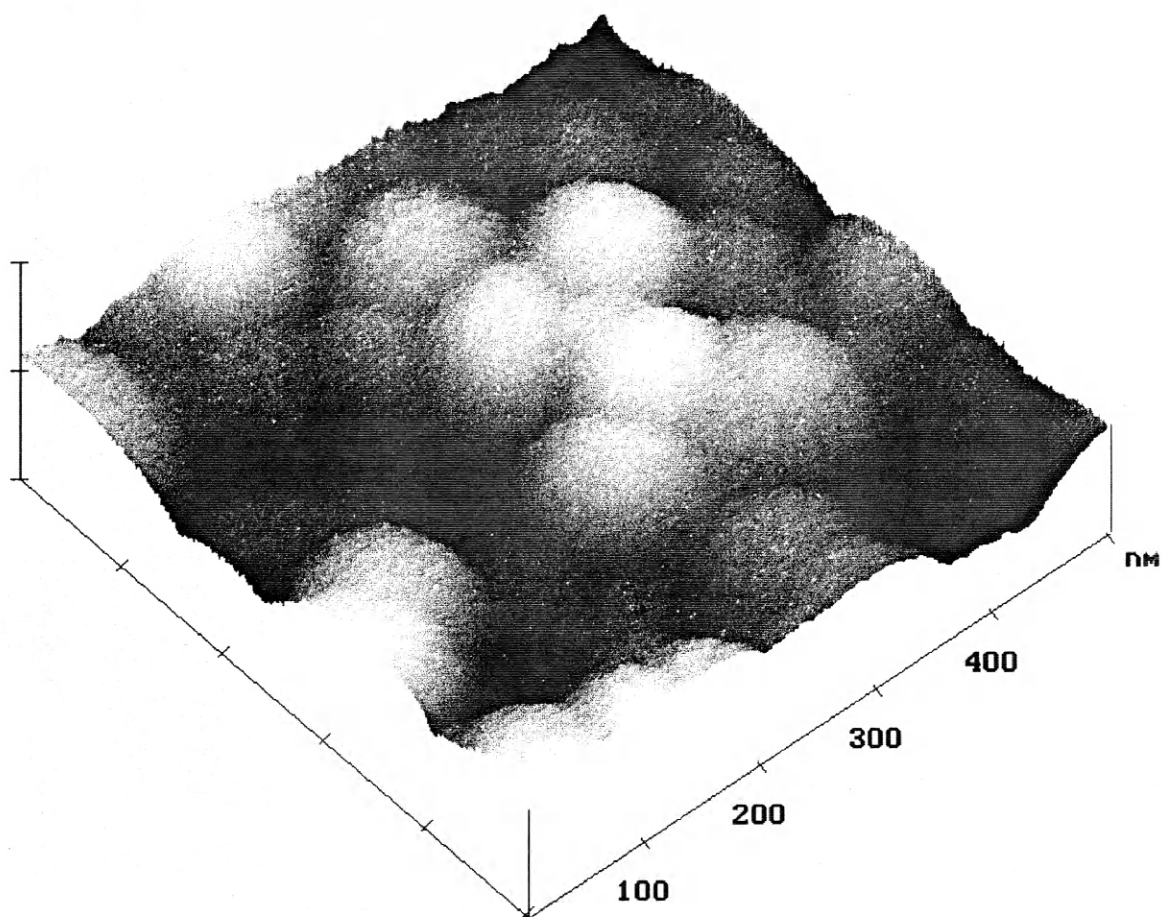


Figure 4.39. AFM micrograph of a two layer PbTiO_3 film annealed at 350°C for one minute after each layer and 700°C for 10 minutes after the final layer.

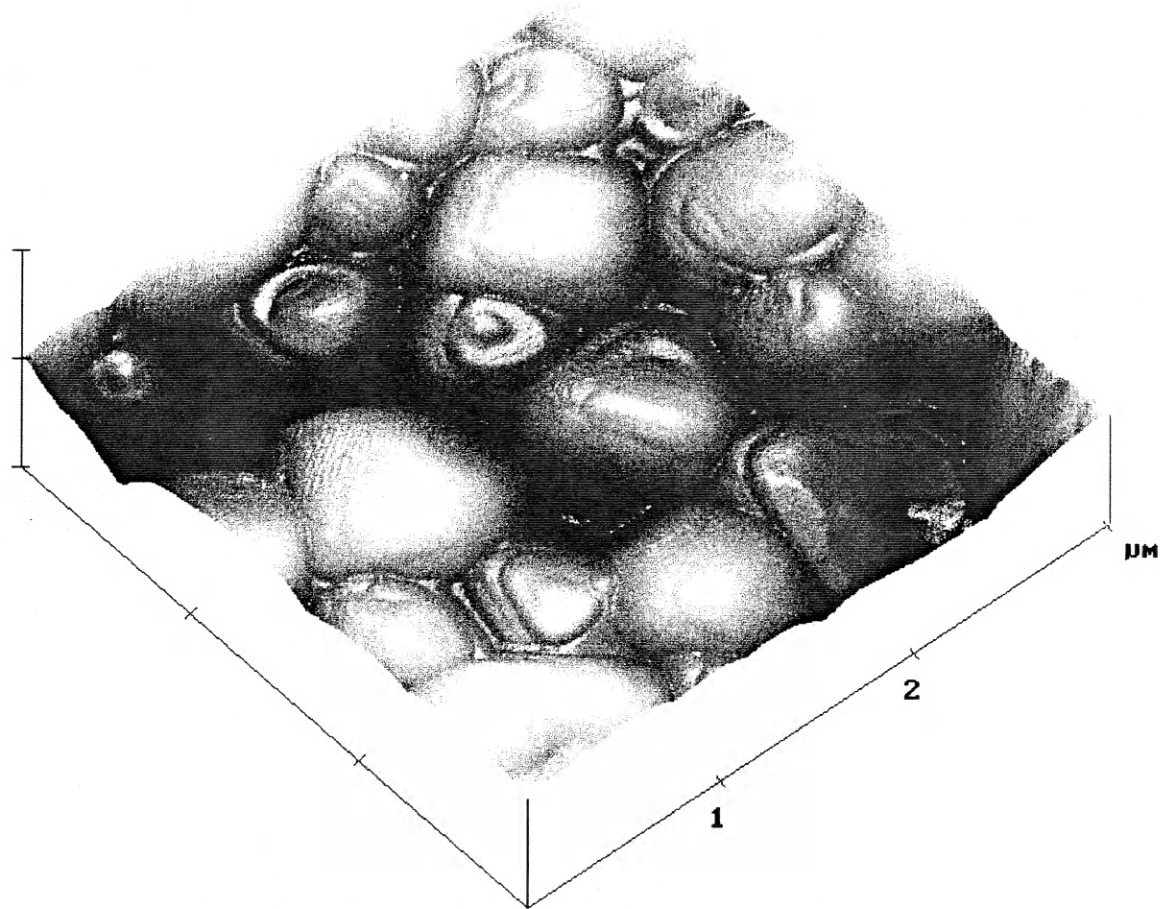


Figure 4.40. AFM micrograph of a film consisting of two layers of $\text{Pb}_5\text{Ge}_3\text{O}_{11}$ annealed at 350°C for one minute after each layer and 700°C for 10 minutes after the final layer. This $\text{Pb}_5\text{Ge}_3\text{O}_{11}$ film was deposited on a two layer PbTiO_3 film with identical processing conditions.

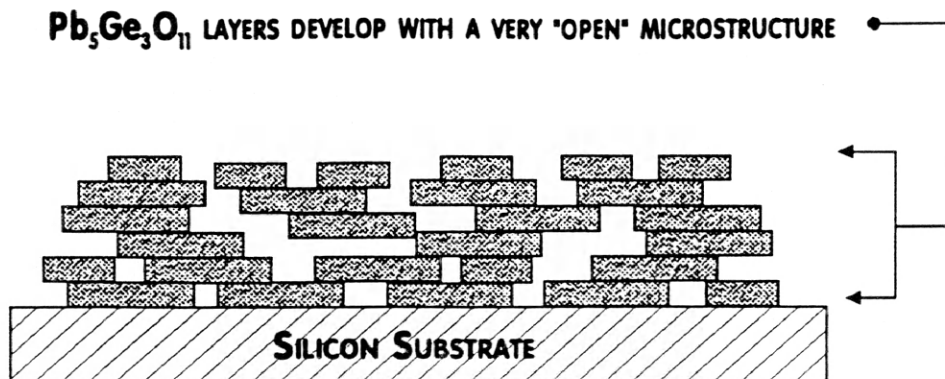


Figure 4.41. Schematic diagram of the proposed "open" microstructure that develops in Pb₅Ge₃O₁₁ films annealed to develop a large grain size.

microstructures at the surface of the films. The "nonhomogeneous" film configurations investigated are shown in Figure 4.42B-E. Figure 4.42A diagrams a film annealed at 730°C for 5 minutes. The grain size is desirable ($\sim 5\mu\text{m}$), however the films displayed shorting when surface electrodes were applied. Figure 4.42B shows the same configuration as in Figure 4.42A, however after the 730°C annealing, the film was annealed at 760°C for one minute. This annealing above the melting temperature was investigated as a means to increase the film density, particularly at the film surface. A more "dense" microstructure may be attained by allowing material transport through viscous flow mechanisms. Figure 4.43 shows the microstructure of a film with the configuration diagrammed in Figure 4.42B. The brief annealing above the melting point did not appear to completely melt the film. Grain size at the film surface increased from approximately $5\mu\text{m}$ to approximately $8\mu\text{m}$ after the 760° annealing step. These films showed a definite improvement in regards to their ability to be electrically

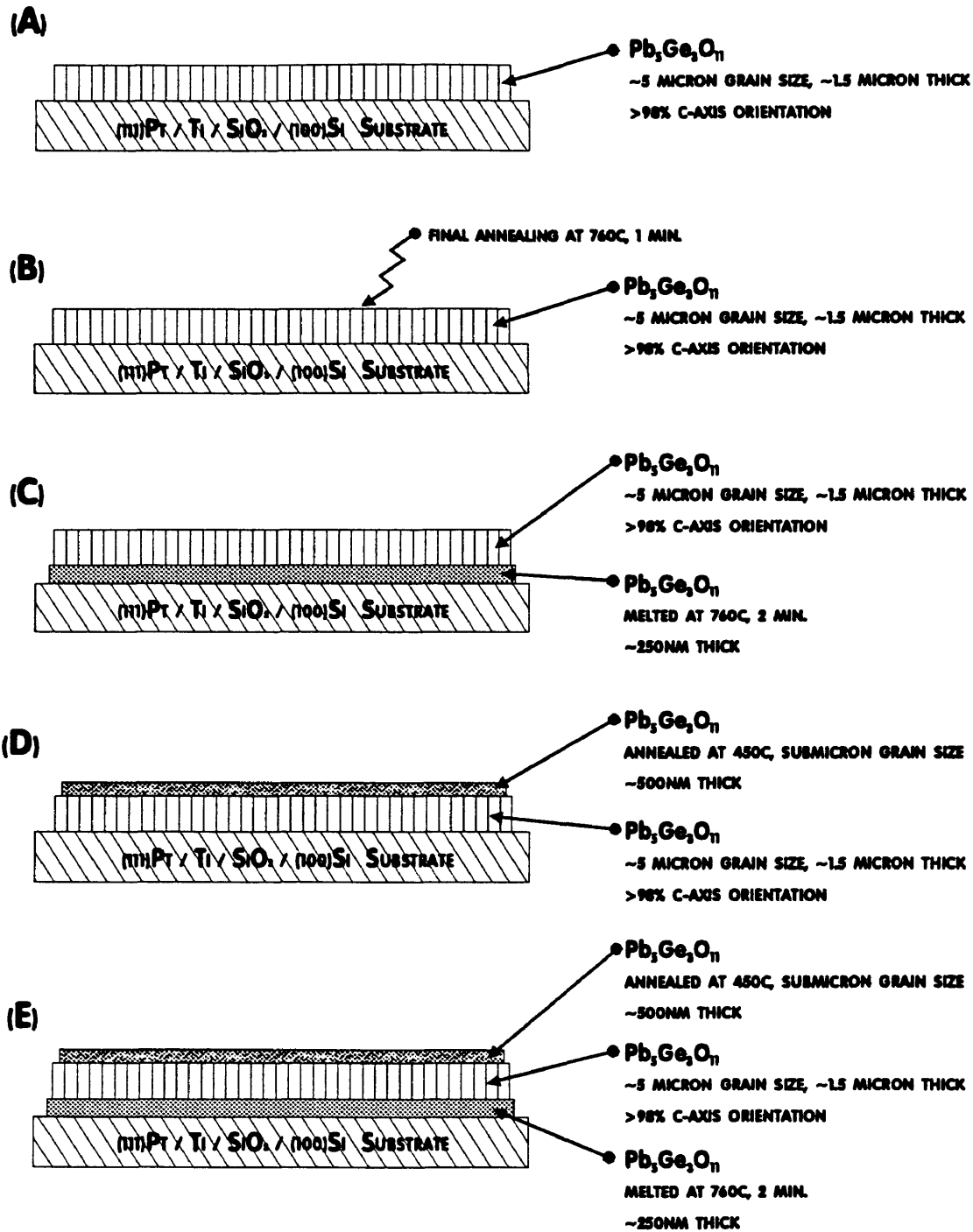


Figure 4.42. $\text{Pb}_5\text{Ge}_3\text{O}_{11}$ film configurations for microstructural optimization.

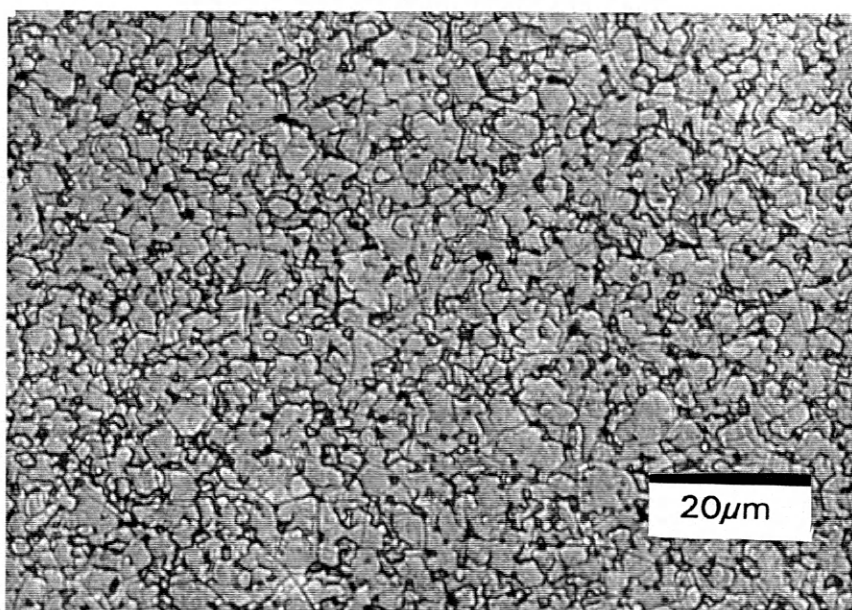


Figure 4.43. Optical micrograph of a 12-layer $\text{Pb}_5\text{Ge}_3\text{O}_{11}$ film annealed at 450°C for one minute after each layer, then 730°C for 5 minutes and 760°C for one minute after the final layer (1000X).

contacted at the surface without shorting. Approximately 50% of the attempted contact points did not short out.

Figure 4.42C shows an alternative film configuration for utilizing "melt" processing. Approximately 250nm of lead germanate was initially melted on the platinum surface of the substrate. Additional layers were then applied on top of this melted layer with a final annealing at 730°C for 5 minutes to grow the grain size to approximately 5 μ m. The idea pursued here was to create a dense, adhered layer initially on the substrate. This may be followed by a more uniform grain growth of subsequent layers, reducing the degree of "open" porosity. The degree of success in making electrical contacts with these films, however, was not improved over that of the configuration in Figure 4.42A.

The film configurations diagramed in Figure 4.42D and E utilize a "capping" layer of submicron lead germanate on the surface of the large grained material. It was previously found that amorphous films annealed at 450°C developed a c-axis oriented $\text{Pb}_5\text{Ge}_3\text{O}_{11}$ microstructure with submicron grain sizes. These films, annealed at 450°C, were easily contacted without electrical shorting, however the extremely small grain size of the films resulted in an absence of the desired electrical properties. In the configurations diagramed in Figure 4.42D and E, a 1.5 μ m thick lead germanate film was first grown to a grain size of approximately 5 μ m. An additional 500nm thick layer of lead germanate was deposited on the surface and annealed at 450°C. This additional layer of submicron grain sized lead germanate effectively "sealed" the voids in the surface of the large-grained layer. The incorporation of a melted layer as diagramed in Figure 4.42E did not alter the successfulness of contacting the films when compared to the configuration in Figure 4.42D. The success rate of electrically contacting

these films was much higher than with any other configuration (better than 80%).

4.4 Electrical Properties

Difficulties were encountered in the measurement of electrical properties of lead germanate thin films due to electrical shorting. Defects due to the "open" nature of the microstructure (Section 4.3.2) or possibly due to the thermal expansion mismatch between the film and the substrate are expected to have contributed to the shorting. As reported in Section 4.3.2, films annealed at 400 to 500°C were easily contacted without shorting. The microstructure for these annealing temperatures consisted of submicron grain sizes. Films annealed at 700°C or above, with grain sizes greater than 1 μ m were very difficult to contact. For films with grain sizes greater than 1 μ m, it was found that a "capping" layer of submicron lead germanate at the surface greatly improved the integrity of the film and the success rate of making electrical contact (Section 4.3.2).

The dielectric constant and dissipation factor for 8-layer (1 μ m) lead germanate films annealed at 450, 500 and 700°C are given in Figures 4.44, 4.45 and 4.46. As expected, the dielectric constant increases with increasing annealing temperature while the dissipation factor decreased with increasing annealing temperature. Figure 4.44 shows that annealing at 450°C results in a very broad increase of the dielectric constant with temperature. A distinctive peak is not easily distinguished. Figure 4.45 shows that a 500°C annealing temperature results in dielectric data which appears to display two maxima. One peak results in a maximum near 100°C while the other is located at approximately 170°C. The dielectric

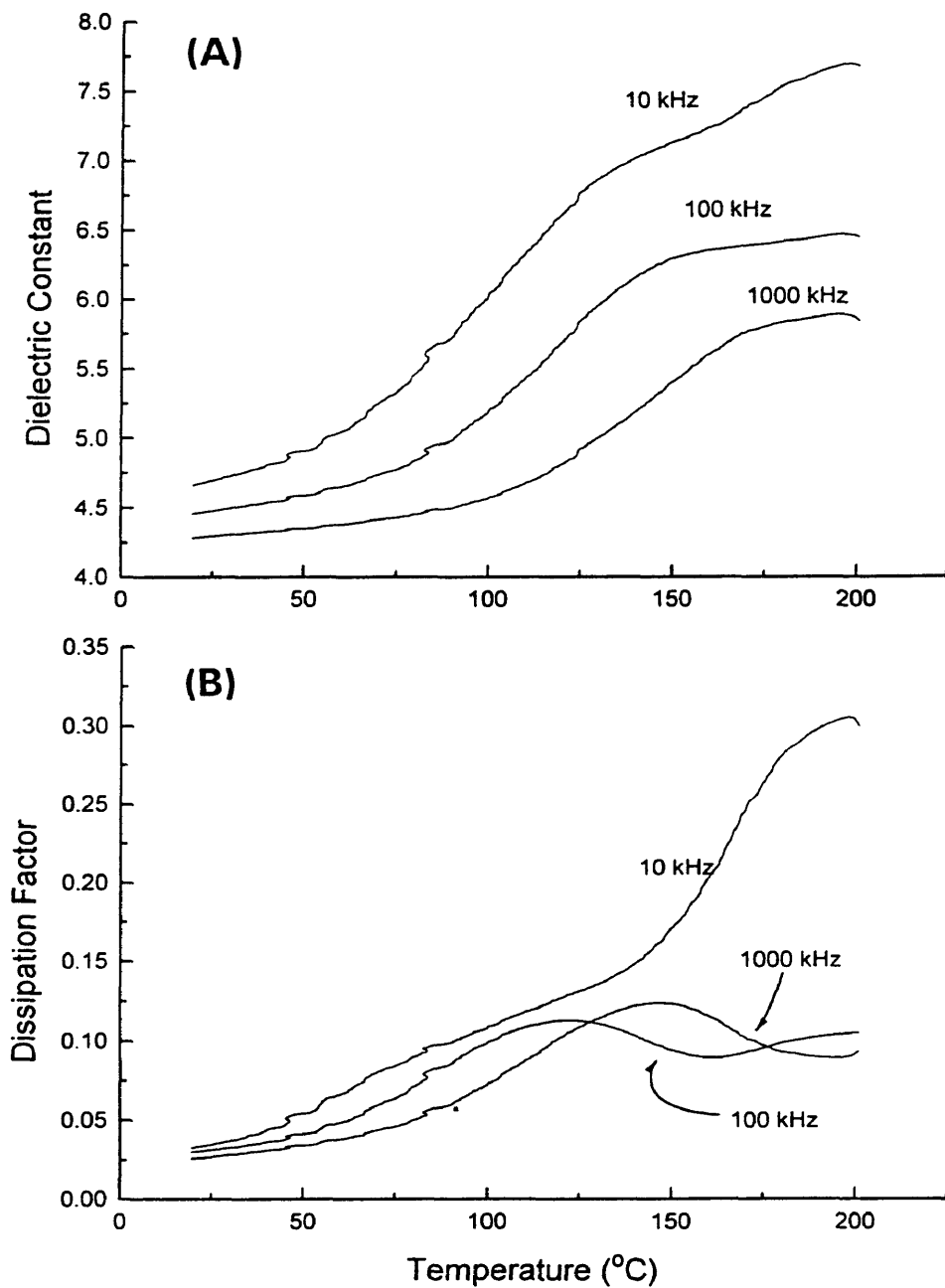


Figure 4.44. Dielectric data for an 8-layer $\text{Pb}_5\text{Ge}_3\text{O}_{11}$ film annealed at 450°C for one minute after each layer and 450°C for 10 minutes after the final layer. (A) Dielectric constant versus temperature. (B) Dissipation factor versus temperature.

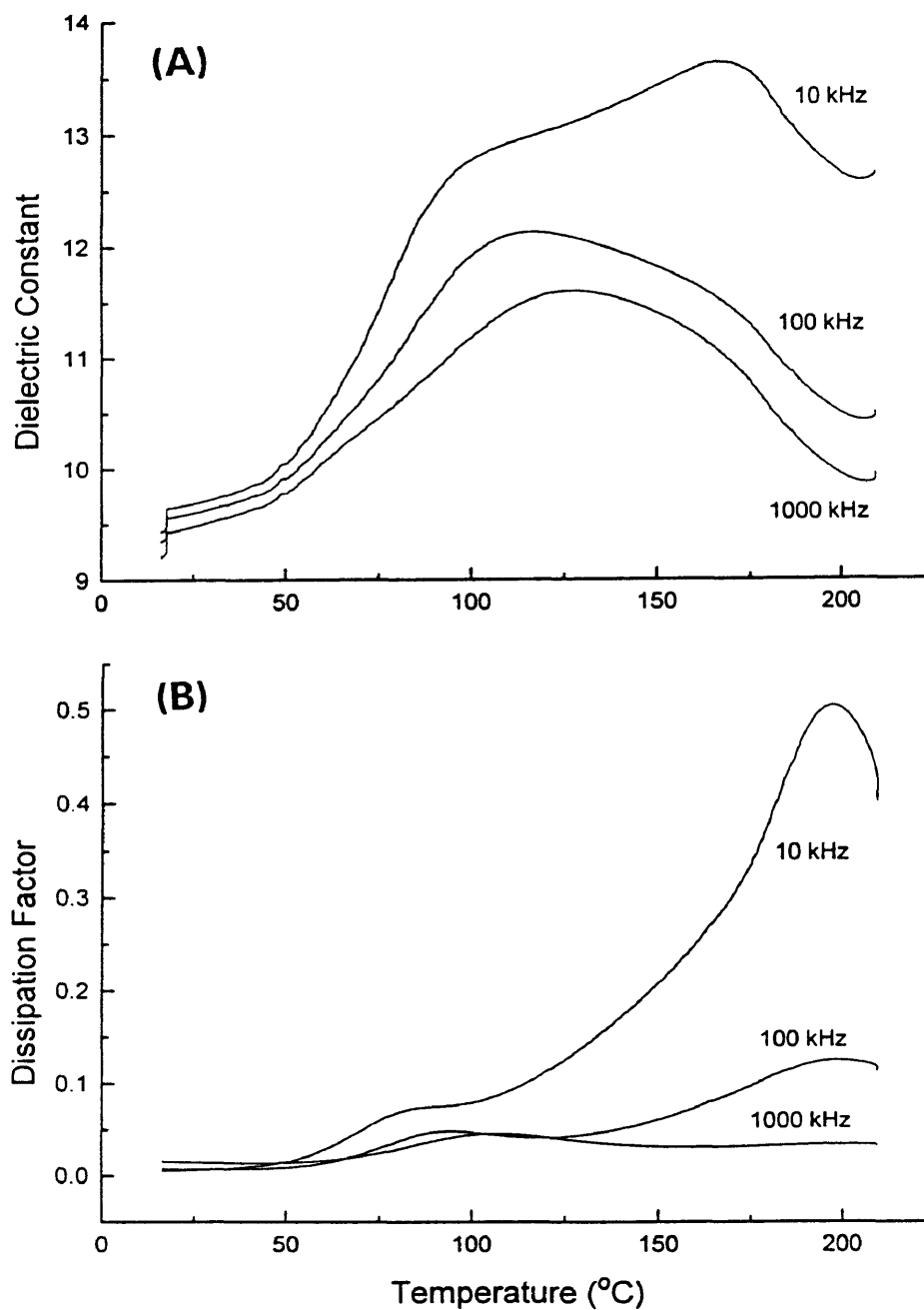


Figure 4.45. Dielectric data for an 8-layer $\text{Pb}_5\text{Ge}_3\text{O}_{11}$ film annealed at 500°C for one minute after each layer and 500°C for 10 minutes after the final layer. (A) Dielectric constant versus temperature. (B) Dissipation factor versus temperature.

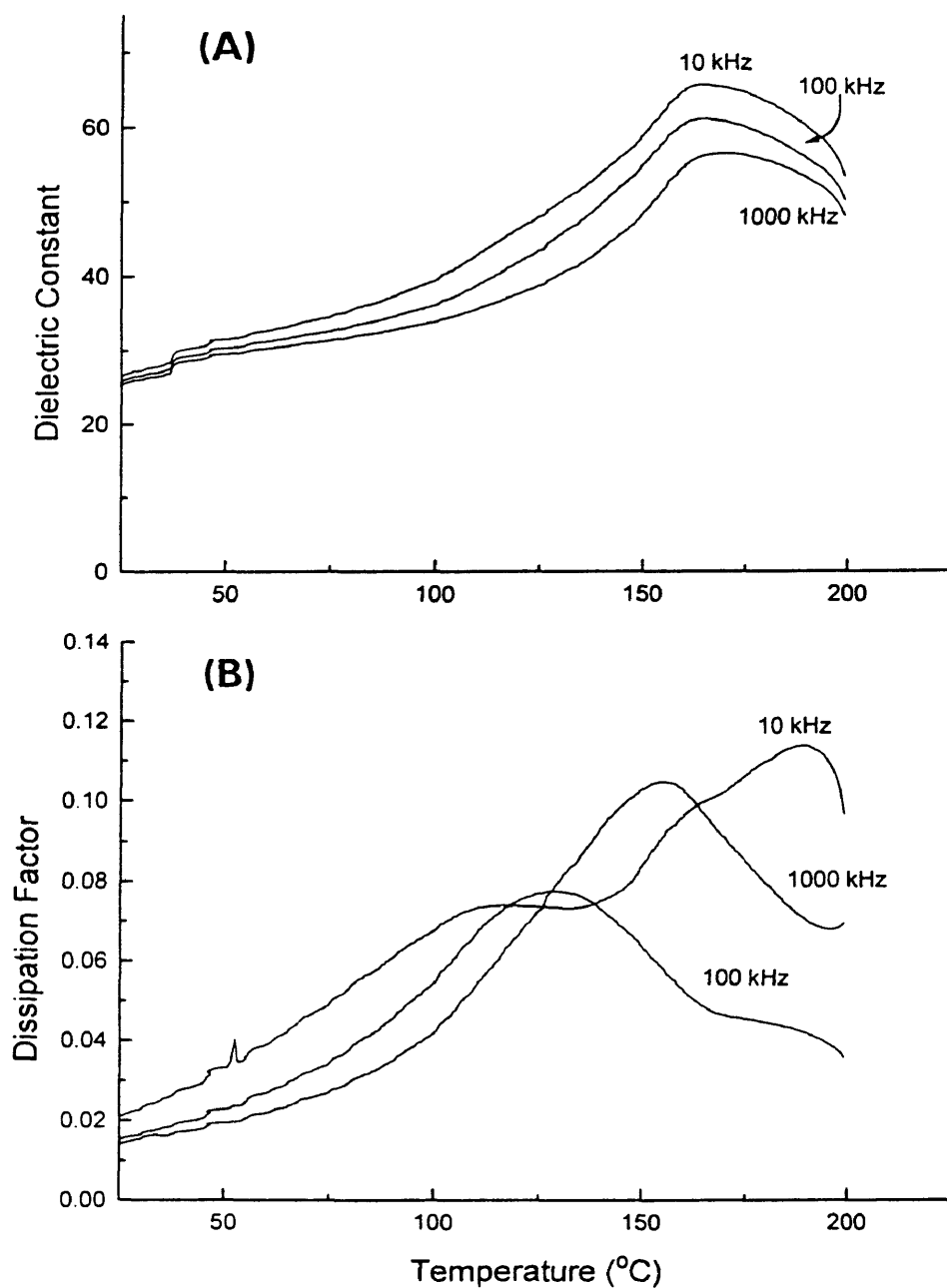


Figure 4.46. Dielectric data for an 8-layer $\text{Pb}_5\text{Ge}_3\text{O}_{11}$ film annealed at 700°C for one minute after each layer and 700°C for 10 minutes after the final layer. **(A)** Dielectric constant versus temperature. **(B)** Dissipation factor versus temperature.

constant magnitudes were extremely low for samples annealed at 450 or 500°C.

Films annealed at 700°C showed a distinct maximum of the dielectric constant in the region of 170°C, close to the reported single crystal value of 177°C, corresponding to the ferroelectric to paraelectric phase transition. At a frequency of 100KHz, the dielectric constant reached a maximum of approximately 60 (Fig. 4.45). The room temperature dielectric constant was approximately 25. These dielectric properties are significantly lower than for single crystal lead germanate (Fig.2.11 on p.34), however they are very similar to those reported by Schmitt et al.[50] and by Mansingh and Krupanidhi [54] for thin films fabricated by sputtering and evaporation respectively.

Ferroelectric and pyroelectric properties were not successfully obtained for films thinner than 1 μ m or for films with annealing temperatures less than 700°C. This could perhaps be attributed to a grain size that is not sufficient to stabilize spontaneous ferroelectric order (Sections 2.2.1 and 2.4.4). Glass et al.[21] studied the recrystallization of lead germanate glass and found that grain sizes on the order of 1 μ m resulted in stable ferroelectric behavior. Samples with grain sizes on the order of 10nm, which they obtained by annealing the glass for one minute at 520°C, showed no evidence of a ferroelectric transition. Schmitt et al.[50] reported that a grain size of at least 2 μ m and a film thickness greater than 1 μ m were required to obtain ferroelectric hysteresis loops in sputtered lead germanate thin films. The increased critical dimensions reported by Schmitt et al. may be due to contributions from surface effects to the depolarization energy (Section 2.2.2). In the current work, lead germanate films annealed at 700°C for 10 minutes (dielectric data shown in Figure 4.46) had a grain size in the range

of $1.0\mu\text{m}$ (Section 4.3). According to the previous research discussed above, these dimensions are at the lower limit for obtaining ferroelectric properties.

The ferroelectric hysteresis loop for a lead germanate film annealed at 700°C for 10 minutes is shown in Figure 4.47. The hysteresis loop has developed a relatively square shape characteristic of uniaxial ferroelectrics. A remnant polarization (P_r) of approximately $0.7\mu\text{C}/\text{cm}^2$, a saturation polarization (P_s) of approximately $1.25\mu\text{C}/\text{cm}^2$ and a coercive field (E_c) of approximately $4.5\text{kV}/\text{cm}$ were observed prior to the breakdown of the sample. Single crystal $\text{Pb}_5\text{Ge}_3\text{O}_{11}$ has been reported to have a spontaneous polarization of $4.8\mu\text{C}/\text{cm}^2$ at room temperature [18]. Thin film polarizations as high as $P_r = 3.3\mu\text{C}/\text{cm}^2$ and $P_s = 3.7\mu\text{C}/\text{cm}^2$ have been reported [59]. Considering the applied electrical field of $13\text{kV}/\text{cm}$, this $1.5\mu\text{m}$ film switches at 2 volts.

Figure 4.48 shows the pyroelectric current and pyroelectric coefficient as a function of temperature after poling at $15\text{kV}/\text{cm}$ for a $1.2\mu\text{m}$ film annealed at 700°C . The pyroelectric coefficient for this film at 25°C is calculated to be $0.86 \times 10^{-8} \text{C}/\text{cm}^2\text{C}$ and increases to $3.00 \times 10^{-8} \text{C}/\text{cm}^2\text{C}$ at 50°C (Table 7). To determine the contribution from equipment noise, pyroelectric testing was performed on an electrically contacted silicon substrate without any film deposition. This test indicated that equipment noise contributed $+4$ to -2×10^{-13} amps over a temperature range of 25 to 80°C , which is two to three orders of magnitude less than the pyroelectric current resulting from the lead germanate films. Additionally, repeats of the pyroelectric test on the same lead germanate thin films indicated good reproducibility of the current versus temperature behavior. These pyroelectric data were collected for sample heating. Pyroelectric data

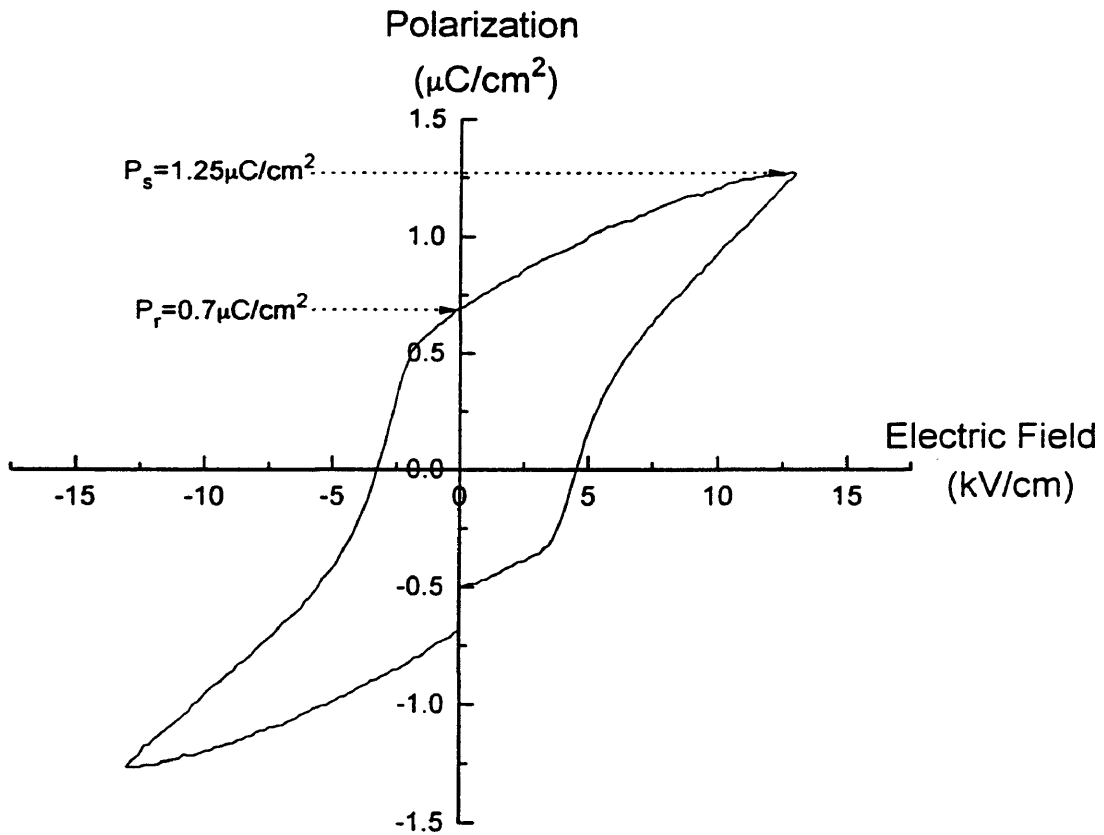


Figure 4.47. A ferroelectric hysteresis loop for a 12-layer $\text{Pb}_5\text{Ge}_3\text{O}_{11}$ film annealed at 700°C for one minute after each layer and 700°C for 10 minutes after the final layer.

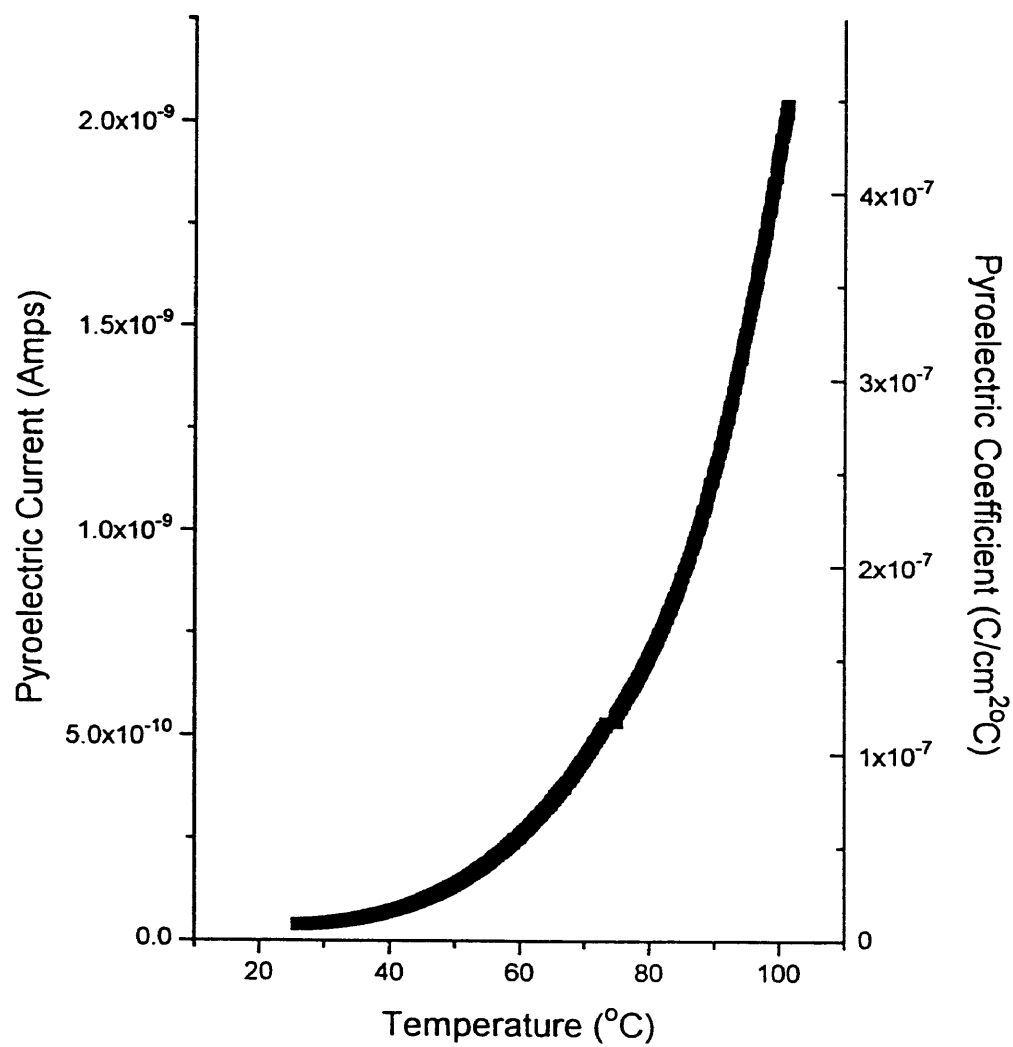


Figure 4.48. Pyroelectric current and pyroelectric coefficient versus temperature for a 10-layer $\text{Pb}_5\text{Ge}_3\text{O}_{11}$ film annealed at 700°C for one minute after each layer and 700°C for 10 minutes after the final layer.

Table 7. Pyroelectric data for a 10-layer $\text{Pb}_5\text{Ge}_3\text{O}_{11}$ film annealed at 700°C for one minute after each layer and 700°C for 10 minutes after the final layer. Electrode area was 0.137cm^2 with a temperature rate of change equal to $0.0333^\circ\text{C}/\text{sec}$.

Temperature ($^\circ\text{C}$)	Dielectric Constant	Dielectric Permittivity (F/cm)	Pyroelectric Coefficient ($\text{C}/\text{cm}^2\text{C}$)	Pyroelectric Figure of Merit ($\text{V}/\text{cm}^\circ\text{C}$)
25	27	2.39×10^{-12}	0.86×10^{-8}	3,600
30	28	2.48×10^{-12}	0.94×10^{-8}	3,800
40	30	2.66×10^{-12}	1.6×10^{-8}	5,900
50	31	2.74×10^{-12}	3.0×10^{-8}	11,000
60	32	2.83×10^{-12}	5.6×10^{-8}	20,000

collected for lead germanate thin films during the cooling cycle were significantly more erratic. This is attributed, in part, to the difficulty of maintaining a steady, smooth cooling rate.

Single crystal values for the room temperature pyroelectric coefficient of lead germanate along the c-axis have been reported in the range of 0.95 to $1.2 \times 10^{-8} \text{C}/\text{cm}^2\text{C}$ [41-43]. The similarity of the thin film results to the single crystal values indicates the significant influence of c-axis orientation in the thin films. Taking into consideration the very low dielectric constant of the films, the actual pyroelectric voltage responsivity figure of merit shows promising potential for oriented lead germanate films in pyroelectric device applications. At room temperature, this pyroelectric figure of merit is calculated to be $3,600 \text{V}/\text{cm}^\circ\text{C}$. This value is equivalent to that of highly oriented lanthanum modified lead titanate thin films ($\sim 3,000 \text{V}/\text{cm}^\circ\text{C}$) [78]. Most of the reported values for lead titanate thin films are less than

1,000V/cm°C, while those of lead zirconate titanate are even less. The value, $F_v = 3,600\text{V/cm}^\circ\text{C}$ is approximately half that of single crystal triglycine sulphate ($F_{v(\text{TGS})} = 7,100\text{V/cm}^\circ\text{C}$ at room temperature). The lead germanate thin films, however, would have the advantage of relatively simple processing methods. Single crystal pyroelectric elements require long and expensive preparations. Also, lead germanate does not show the chemical and electrical instability that is found with TGS (Section 2.3).

C-axis oriented lead germanate films annealed to develop grain sizes larger than $2\text{-}3\mu\text{m}$ showed a strong pyroelectric effect even without electrical poling. This is an unusual phenomenon, however other researchers [78] have reported pyroelectric properties for c-axis oriented La-modified lead titanate thin films without electrical poling. Figure 4.49 shows the pyroelectric current and coefficient as a function of temperature for a $\text{Pb}_5\text{Ge}_3\text{O}_{11}$ film with the lead germanate grains grown to approximately $5\mu\text{m}$ and then annealed at 760°C for one minute to promote densification of the film surface. This microstructural configuration is diagrammed in Figure 4.42B on p.119. With no electrical poling, this film showed a pyroelectric coefficient of $0.19 \times 10^{-8}\text{C/cm}^2\text{C}$ at 25°C . At 40°C , the pyroelectric coefficient had increased to $0.75 \times 10^{-8}\text{C/cm}^2\text{C}$.

Figure 4.50 shows the pyroelectric current and coefficient as a function of temperature before electrical poling for a lead germanate film with the microstructural configuration diagrammed in Figure 4.42D on p.119. This microstructural configuration was made by first growing the grains of a $1.5\mu\text{m}$ thick lead germanate layer to approximately $5\mu\text{m}$. This was followed by "capping" the large grained structure with a submicron layer of lead germanate to help fill the film voids that resulted from the grain growth (Section 4.3.2). Figure 4.51 shows the pyroelectric properties as a function

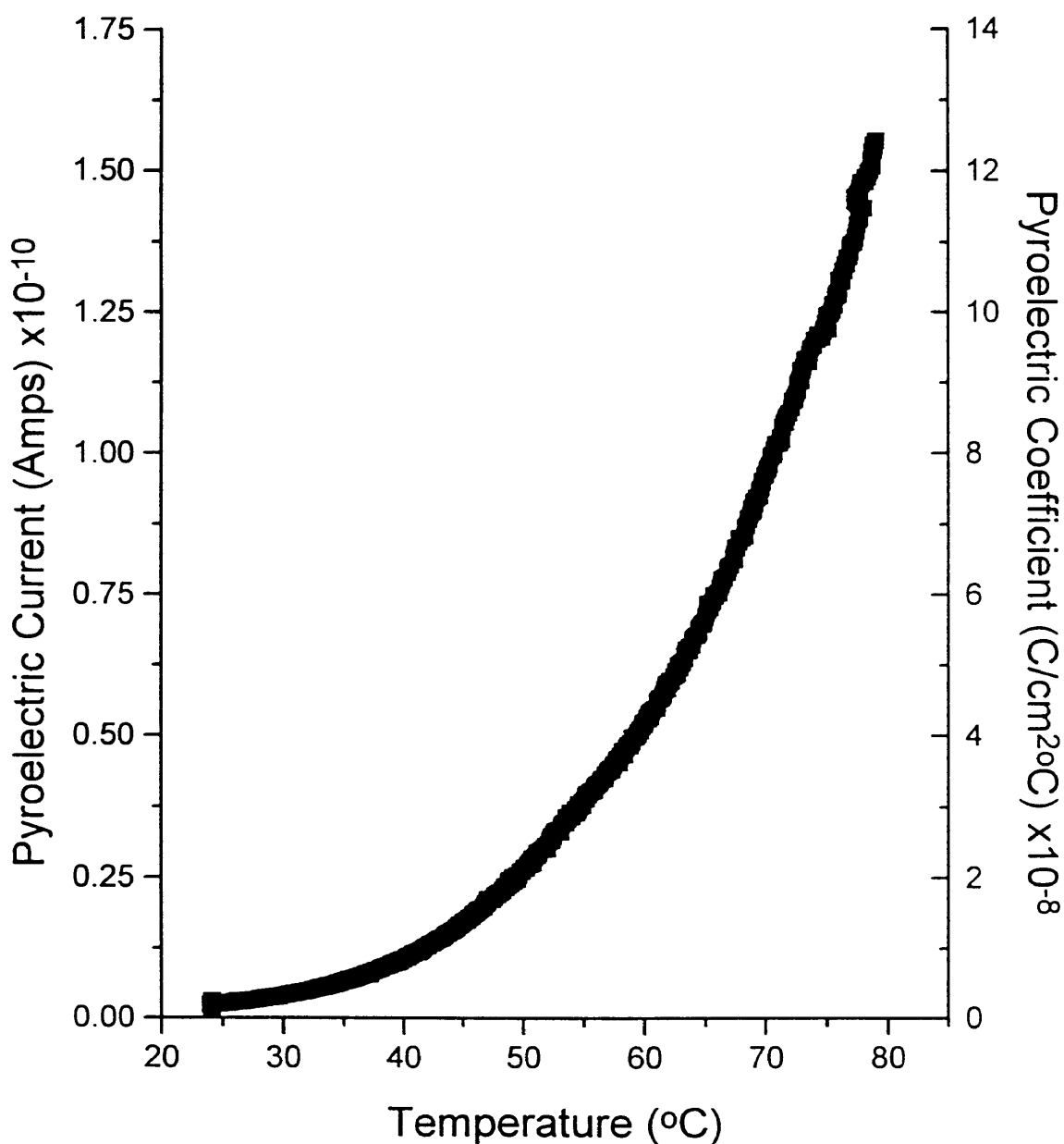


Figure 4.49. Pyroelectric current and pyroelectric coefficient versus temperature for a $\text{Pb}_5\text{Ge}_3\text{O}_{11}$ film with the configuration diagrammed in Figure 4.42B on p.119. Twelve layers were deposited with a 450°C, one minute annealing after each layer. After the final layer, the film was annealed at 730°C for 5 minutes and then 760°C for one minute. Electrical poling was not performed on this sample.

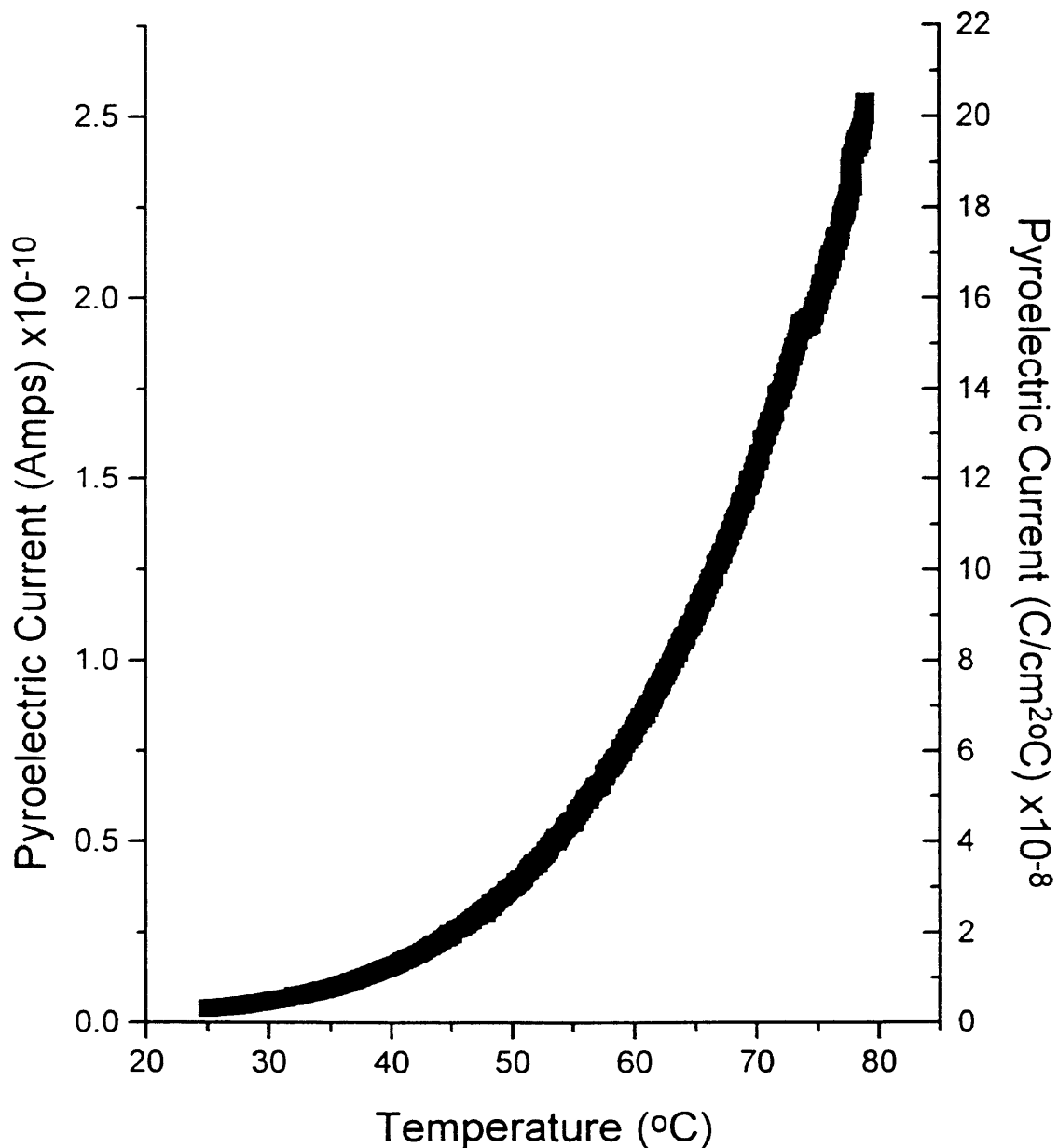


Figure 4.50. Pyroelectric current and pyroelectric coefficient versus temperature for a $\text{Pb}_5\text{Ge}_3\text{O}_{11}$ film with the configuration diagramed in Figure 4.42D on p.119. Twelve layers were deposited with a 450°C, one minute annealing after each layer. After the final layer, the film was annealed at 730°C for 5 minutes. Following this annealing step, four more layers were deposited with a 450°C, one minute annealing after each layer. Electrical poling was not performed on this sample.

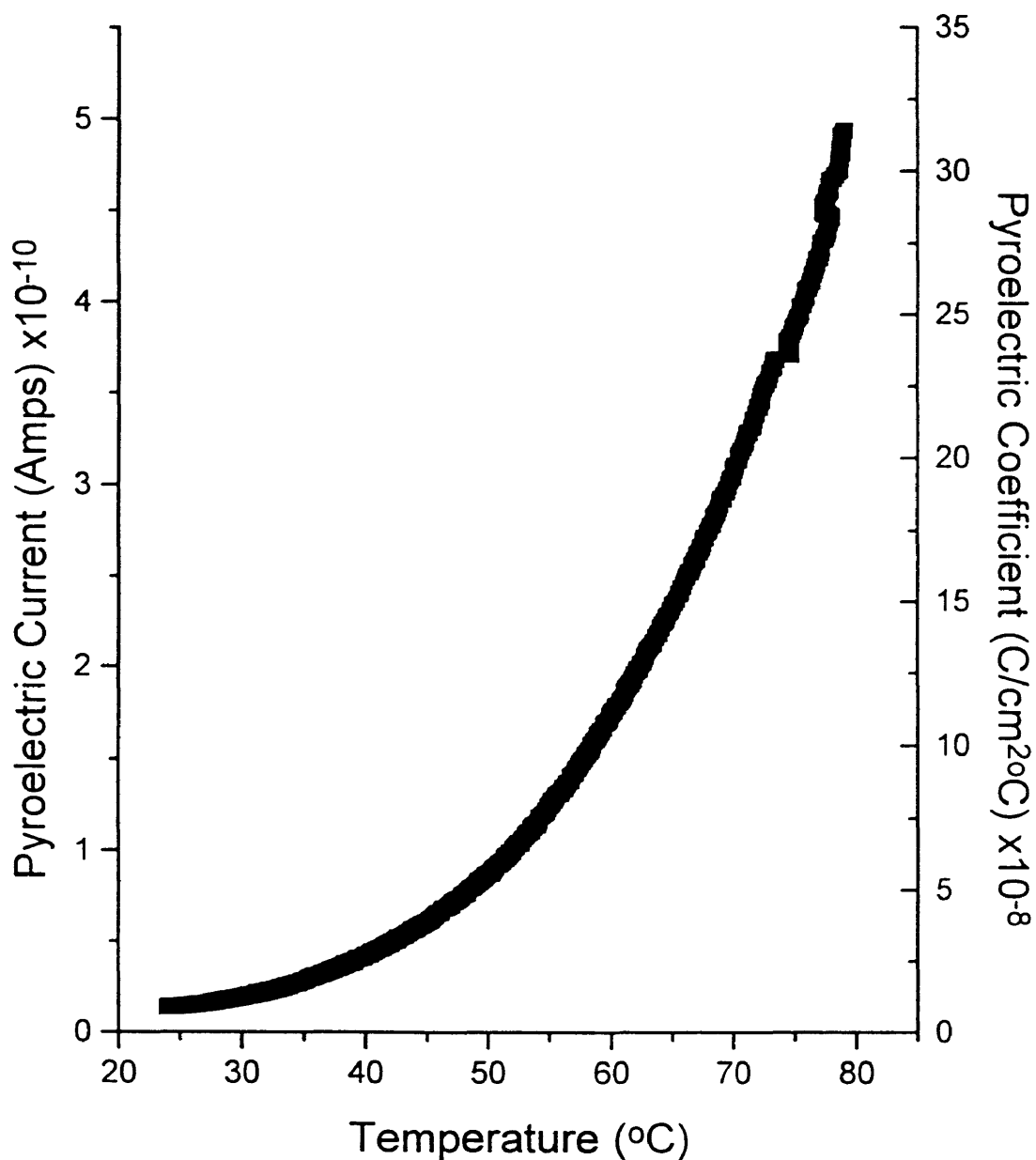


Figure 4.51. Pyroelectric current and pyroelectric coefficient versus temperature for a $\text{Pb}_5\text{Ge}_3\text{O}_{11}$ film with the configuration diagramed in Figure 4.42D on p.119. Twelve layers were deposited with a 450°C , one minute annealing after each layer. After the final layer, the film was annealed at 730°C for 5 minutes and then 760°C for one minute. This data is from the same sample as in Figure 4.50 however this is after poling with $10\text{kV}/\text{cm}$ and aging the sample for 24 hours.

Table 8. Pyroelectric coefficients for a lead germanate film before and after electrical poling. The film's microstructural configuration is diagrammed in Figure 4.42D on p.119. Electrode area was 0.048cm^2 with a temperature rate of change equal to $0.333^\circ\text{C}/\text{sec}$.

Temperature ($^\circ\text{C}$)	Pyroelectric Coefficient ($\text{C}/\text{cm}^2\text{C}$)	
	No Poling	Pole at 10kV, 24Hr. Age
25	0.25×10^{-8}	0.89×10^{-8}
30	0.38×10^{-8}	1.2×10^{-8}
40	0.99×10^{-8}	2.7×10^{-8}
50	2.4×10^{-8}	5.5×10^{-8}
60	5.1×10^{-8}	11×10^{-8}

of temperature for this film 24 hours after poling at $10\text{kV}/\text{cm}$. The effect of the poling operation was a significant increase in the pyroelectric effect (Table 8). At 25°C , the pyroelectric coefficient was $0.25 \times 10^{-8}\text{C}/\text{cm}^2\text{C}$ before poling and $0.89 \times 10^{-8}\text{C}/\text{cm}^2\text{C}$ after poling. At 60°C , the pyroelectric coefficient increased to $5.1 \times 10^{-8}\text{C}/\text{cm}^2\text{C}$ before poling and $11 \times 10^{-8}\text{C}/\text{cm}^2\text{C}$ after poling. The pyroelectric effect for the poled film described in Figure 4.51 showed a steady increase with increasing temperature up to approximately 175°C where a slight leveling off occurred. At 178°C , the pyroelectric current dropped into the range of 10^{-12} amps, indicating the switch from ferroelectric to paraelectric states (Fig.4.52). This transition temperature is in very close agreement to the reported single crystal value of 177°C and indicates that internal stresses are not significantly affecting the ferroelectric properties of these large grained films. The pyroelectric figure of merit (F_v) for the poled film described in Figure 4.51 and Table 8 was calculated to be $3,700\text{V}/\text{cm}^\circ\text{C}$ at 25°C and increased to $10,000\text{V}/\text{cm}^\circ\text{C}$ at

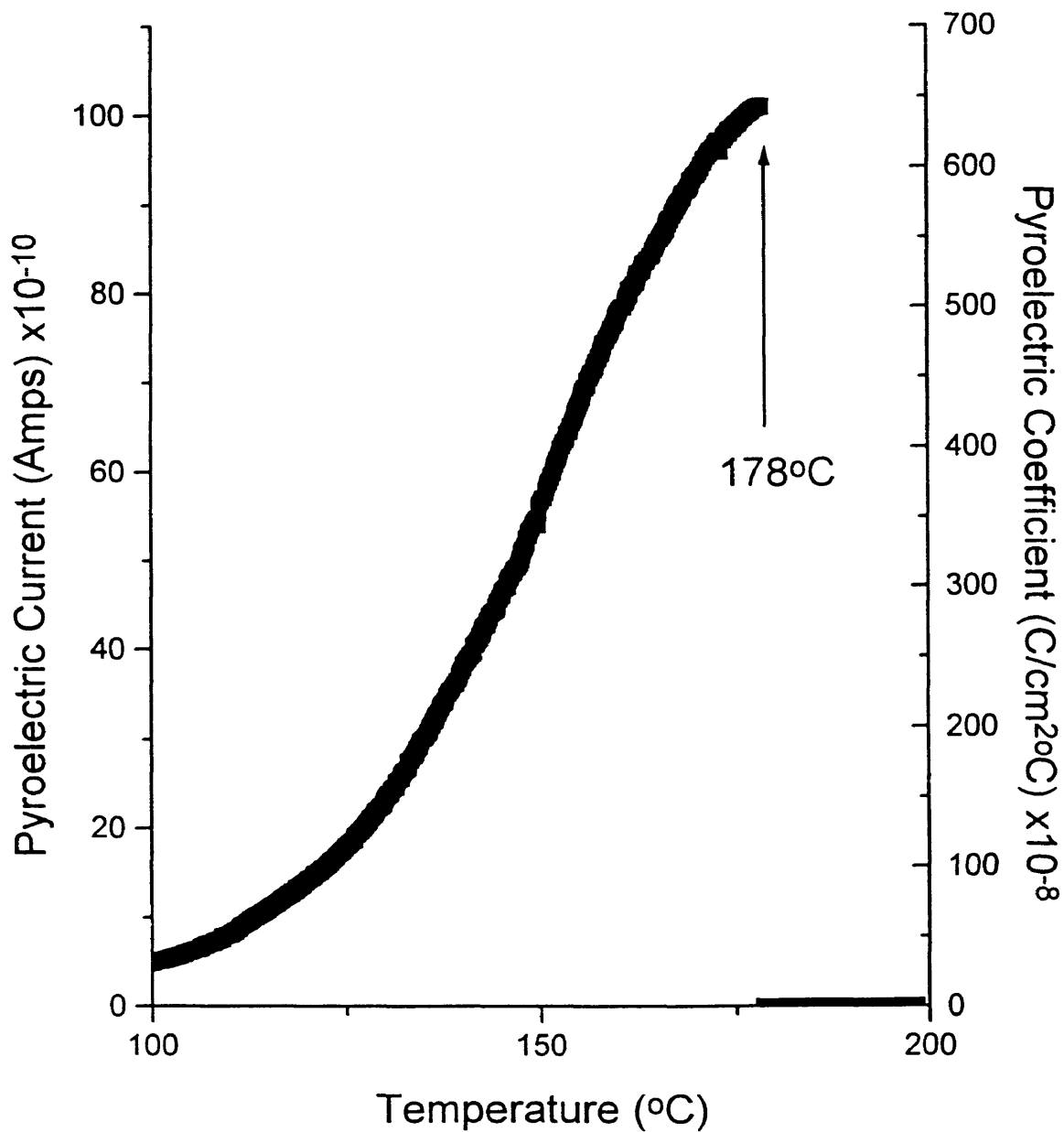


Figure 4.52. Pyroelectric current and pyroelectric coefficient versus temperature up to temperatures above the ferroelectric to paraelectric transition for the $\text{Pb}_5\text{Ge}_3\text{O}_{11}$ film described in Figure 4.51.

40°C. Therefore, at 40°C, the pyroelectric figure of merit for this lead germanate film exceeds that of single crystal TGS at room temperature. At an operating temperature of 60°C, the figure of merit for this film exceeds 35,000V/cm°C.

The dielectric constant of the "optimized" lead germanate thin films, ($\sim 5\mu\text{m}$ grain size, c-axis orientation, and no shorting) did not change significantly from the behavior observed for a film with grain sizes of approximately $1\mu\text{m}$ (Fig. 4.46 on p.125). Figure 4.53 shows the dielectric constant and dissipation factor versus temperature for the film with the pyroelectric properties and configuration described in Figure 4.51 and 4.52 on pages 134 and 136. The transition temperature is very close to 177°C with maximum dielectric constants in the range of 50 to 60 at this temperature. The room temperature dielectric constant is approximately 34. The room temperature dissipation factor is approximately 0.01. The peak in the dielectric constant for this film is, perhaps, more pronounced than for the smaller grain sized films. Given that the pyroelectric properties for this film were very close to those of single crystal $\text{Pb}_5\text{Ge}_3\text{O}_{11}$, it was expected that the dielectric properties may also be closer to those of the single crystal. The maximum dielectric constant for single crystal $\text{Pb}_5\text{Ge}_3\text{O}_{11}$ is in the range of 2000 to 3000 at the ferroelectric-paraelectric transition temperature. One possible explanation for this lowering of the maximum dielectric constant is the fact that the submicron grain sized surface layer of this film is in electrical series with the large grained material. This surface layer was annealed at 450°C. It was previously shown that films annealed at 450°C had very low dielectric constants and no distinct peak of the dielectric constant maximum (Fig. 4.44 on p.123). The data shown in Figure 4.44 have very low values of the dielectric constant that are probably not

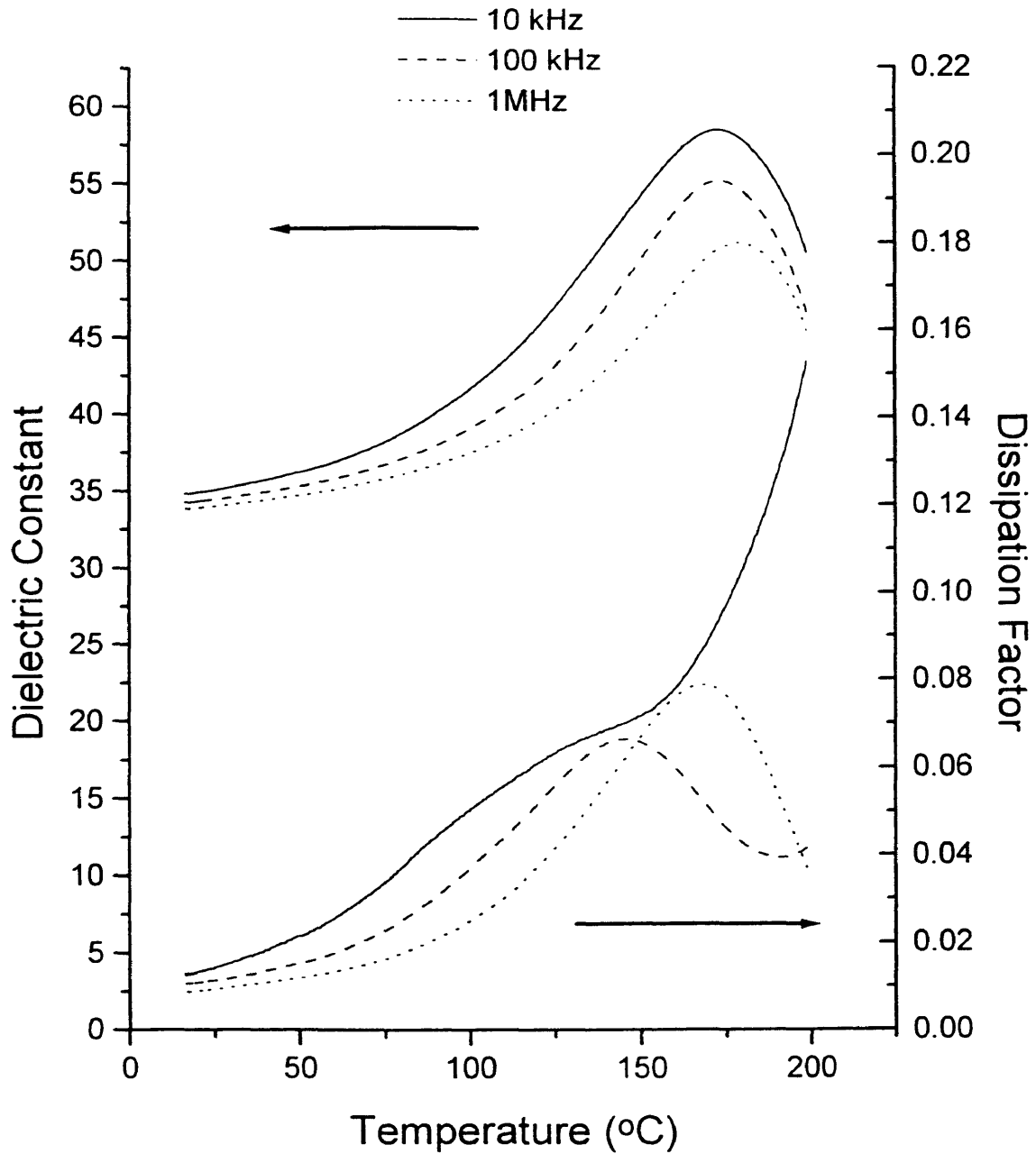


Figure 4.53. Dielectric constant and dissipation factor versus temperature for a $\text{Pb}_5\text{Ge}_3\text{O}_{11}$ film with the configuration described in Figure 4.51 on p.134.

realistic. It would be probable, however, that the dielectric constant for the films annealed at 450°C shows a relatively flat behavior with temperature. Dielectric constant values could be in the range of 16 to 20.

For a series configuration, the resulting dielectric constant can be estimated by the equation,

$$\frac{1}{K_{series}} = \frac{V_1}{K_1} + \frac{V_2}{K_2}$$

where V_1 and V_2 are the volume fractions associated with the dielectric constants, K_1 and K_2 . The "capping" layer of submicron $Pb_5Ge_3O_{11}$ consisted of four layers while the large grained $Pb_5Ge_3O_{11}$ layer underneath consisted of 12 layers. Assuming a total series dielectric constant of 60 and a surface layer dielectric constant that may range between 16 and 20, the dielectric constant of the large grained layer may range between 180 and 720 for its maximum value. These values are still significantly less than the single crystal value. A further contribution to the lowering of the dielectric constant may be from closed porosity within the large grained layer. The submicron grain sized layer is expected to close only the porosity at the surface. A volume fraction of porosity as a "third" phase would lower the dielectric constant significantly.

V. Summary and Conclusions

Solution processed thin films in the $\text{Pb}_5\text{Ge}_3\text{O}_{11}$ and $\text{Pb}_5\text{Ge}_3\text{O}_{11}$ - $\text{PbZr}_x\text{Ti}_{1-x}\text{O}_3$ systems deposited on (111) platinized silicon substrates initially formed a $\text{Pt}_{5.7}\text{Pb}$ intermetallic phase with a (111) orientation upon heating. At 450°C, this phase reoxidized after 10 seconds.

The $\text{Pb}_5\text{Ge}_3\text{O}_{11}$ phase formed first as a metastable phase and then transformed to the stable phase. The metastable phase crystallized with a strong a-axis orientation after one minute at 300°C. The stable phase initially crystallized to a very fine, sub-micron grain sized structure. The transformation from metastable to stable $\text{Pb}_5\text{Ge}_3\text{O}_{11}$ was essentially complete after one minute at 450°C and after 30 seconds at 700°C. The crystallization of the stable and metastable phases in these thin films occurred at temperatures approximately 80°C below those reported for lead germanate crystallized from glass.

The $\text{Pb}_5\text{Ge}_3\text{O}_{11}$ (003) and (006) diffraction peaks shifted and split, corresponding to an approximate 0.15Å reduction of the c-axis. Initially, the (003) and (006) peaks shifted positions, equivalent to a 0.03Å reduction of the c-axis lattice parameter. This shifting is attributed to internal stresses present in the films. A c-axis change of -0.03Å is very close to the c-axis reduction that would result from thermal strain due to thermal expansion mismatch. The splitting or "repositioning" of the (003) and (006) peaks that occurred during or immediately after the shifting constitutes an approximate 0.11Å reduction of the c-axis. This is proposed to be due to a structural change from a hexagonal $\text{Pb}_3\text{Ge}_2\text{O}_7$ phase to the hexagonal $\text{Pb}_5\text{Ge}_3\text{O}_{11}$ phase. Exact details regarding the lattice parameters of the $\text{Pb}_3\text{Ge}_2\text{O}_7$ phase have

not been previously reported, however, researchers have indicated that the c-axis lattice parameter is approximately 0.1 to 0.15Å larger than for the $\text{Pb}_5\text{Ge}_3\text{O}_{11}$ phase. The structural change of approximately -0.11Å in the c-axis reported here is in close agreement.

Earlier researchers have expressed a lot of skepticism regarding the existence of this hexagonal $\text{Pb}_3\text{Ge}_2\text{O}_7$ phase. This research proposes that hexagonal $\text{Pb}_3\text{Ge}_2\text{O}_7$ does exist and its formation in thin films with a 5Pb:3Ge composition is promoted by the Pb_{5-7} intermetallic formation at the substrate/film interface and corresponds to a reduction of Pb^{2+} in the film composition. As annealing time or temperature is increased, Pb^{2+} is made available for the $\text{Pb}_5\text{Ge}_3\text{O}_{11}$ formation due to the reoxidation of the intermetallic. At 450°C, the shifting and splitting of the (00l) peaks is complete after approximately two minutes, while at 700°C, completion is reached after 30 seconds.

The addition of $\text{PbZr}_x\text{Ti}_{1-x}\text{O}_3$ to $\text{Pb}_5\text{Ge}_3\text{O}_{11}$ caused increased splitting and shifting of the $\text{Pb}_5\text{Ge}_3\text{O}_{11}$ (00l) peaks. The (00l) peaks were actually observed to split into three distinct peaks. The increased peak shifting is considered to be a result of increased internal stresses due to the $\text{PbZr}_x\text{Ti}_{1-x}\text{O}_3$ addition. The distance between the two split peaks representing the largest two d-spacings was very similar to the magnitude of the splitting observed in the pure lead germanate films. The third split peak at the lowest d-spacing is believed to represent a different structure, possibly the non-ferroelectric Pb_3GeO_5 phase. The presence of $\text{PbZr}_x\text{Ti}_{1-x}\text{O}_3$ and the Pb^{2+} included in its composition did appear to promote the formation of the lead-rich, non-ferroelectric Pb_3GeO_5 as a more stable phase.

Lead germanate showed a very rapid orientation of the polar c-axis perpendicular to the plane of the substrate. This c-axis orientation occurred

immediately following the metastable-stable transformation. Films annealed at 450°C achieved c-axis orientations greater than 80%. At 700°C, c-axis orientations greater than 98% were observed. Lead germanate films formed on PbTiO₃ thin films still showed this (00l) orientation, indicating that this is a natural growth morphology for Pb₅Ge₃O₁₁.

PbZr_xTi_{1-x}O₃ and PbTiO₃ deposited on (111)Pt/Si substrates showed a (111) orientation as pure phases or when mixed with Pb₅Ge₃O₁₁. When pure PbZr_xTi_{1-x}O₃ was deposited on a thin film of Pb₅Ge₃O₁₁, random alignment of the PbZr_xTi_{1-x}O₃ occurred, indicating the influence of either the intermetallic (111) Pt_{5.7}Pb layer or the (111) platinum layer on the PbZr_xTi_{1-x}O₃ growth morphology.

For lead germanate films, grain growth was not significant below approximately 650°C, and was very rapid above 700°C. The grain size of c-axis oriented Pb₅Ge₃O₁₁ thin films was adjusted from less than 1μm to over 10μm by precisely controlling the thermal annealing profile. Annealing at 700°C for 10 minutes resulted in a grain size of approximately 1.0μm. After 30 minutes at 700°C, the grain size increased to 2-5μm. At 730°C, the grain size was controlled between one and 30μm by adjusting the annealing time between 3 and 20 minutes.

Lead germanate films with grain sizes greater than 1μm had very "open" or "porous" microstructures as a result of the grain growth. This resulted in electrical shorting of the films after the surface electrode was deposited. The integrity of these large grained films was significantly improved by additional processing steps. Annealing at 760°C (above the melting point) for one minute, after the annealing step for grain growth, promoted improved film density, apparently by allowing material transport through viscous flow mechanisms. The greatest success in terms of ability

to make electrical contact was for films fabricated with a "capping" layer of submicron lead germanate at the film surface. Following the annealing step for grain growth, additional layers of lead germanate were deposited and annealed at 450°C. This resulted in submicron sized lead germanate grains that served to fill the voids between the large grains, effectively "sealing" the surface.

Grain sizes in excess of 1 μ m and film thicknesses greater than 1 μ m were required for "normal" ferroelectric behavior. Similar results were reported by other researchers. Results on pyroelectric properties indicate the potential of utilizing Pb₅Ge₃O₁₁ in pyroelectric detector applications. A room temperature pyroelectric coefficient of 0.89x10⁻⁸C/cm²°C was obtained for Pb₅Ge₃O₁₁ films with a c-axis orientation and a 5 μ m grain size. This value for the pyroelectric coefficient is over 90% of the single crystal value. The pyroelectric figure of merit for the lead germanate thin films exceeded the highest reported value for oriented lead titanate thin films. The simplicity of obtaining nearly complete orientation of lead germanate could prove to be advantageous over lead titanate. The room temperature pyroelectric figure of merit for lead germanate (3,700V/cm°C) was over half that of single crystal triglycine sulphate (TGS). At higher operating temperatures, the pyroelectric figure of merit for Pb₅Ge₃O₁₁ films exceeds that of TGS. The chemical and electrical stability, as well as the ease of preparation of lead germanate compared to that of TGS would offer significant advantages for pyroelectric applications.

The final conclusion to this research is that lead germanate (Pb₅Ge₃O₁₁) thin films formed via solution processing offer a very strong potential for commercial use in pyroelectric detector applications.

- $\text{Pb}_5\text{Ge}_3\text{O}_{11}$ can be easily crystallized as a pure phase. The intermetallic phase formation does not significantly impact the $\text{Pb}_5\text{Ge}_3\text{O}_{11}$ formation.
- $\text{Pb}_5\text{Ge}_3\text{O}_{11}$ can be easily crystallized to a nearly 100% polar c-axis orientation perpendicular to the substrate. This orientation is required for obtaining the desired pyroelectric properties. This orientation is not dependent on the substrate thus permitting device fabrication on a variety of substrate materials.
- $\text{Pb}_5\text{Ge}_3\text{O}_{11}$ thin films require grain sizes greater than $1\mu\text{m}$ for normal ferroelectric properties. This research demonstrates that the grain size of solution derived films can be precisely controlled over the size range of $1\mu\text{m}$ to over $10\mu\text{m}$, allowing pyroelectric properties to be optimized.
- The combination of a relatively high pyroelectric coefficient and a low dielectric constant results in $\text{Pb}_5\text{Ge}_3\text{O}_{11}$ films having excellent pyroelectric performance characteristics. These performance characteristics exceed those of highly oriented lead titanate thin films and exceed the commercially used single crystal TGS at operating temperatures higher than room temperature.
- Large grained, c-axis oriented $\text{Pb}_5\text{Ge}_3\text{O}_{11}$ films showed a relatively strong pyroelectric effect even without electrical poling. The elimination of the poling process could be extremely significant in the viewpoint of commercial processing.
- Sol gel processing is a relatively inexpensive, high volume manufacturing method for the production of thin films. Total thermal processing time for $\text{Pb}_5\text{Ge}_3\text{O}_{11}$ films of suitable thickness and microstructure for applications is less than 20 minutes.

- Lead germanate polycrystalline thin films offer significant advantages over the currently used single crystal detectors. These include simple inexpensive fabrication methods, increased design possibilities, and greatly enhanced chemical and electrical stability.

The major difficulty observed in this research was the development of an "open" or "porous" microstructure when films were annealed to develop a suitably large grain size. Two "novel" processing methods were developed to address this problem. The most promising method consisted of forming a "microstructural gradient" through the thickness of the film. The preliminary results presented here show this technique to be highly successful with no detrimental effects to the film properties. This processing method would also be easily integrated and controlled in a commercial processing operation.

VI. Suggestions for Future Work

This research is viewed as laying the groundwork for future investigations that can more fully develop and enhance the processing methods and properties of thin films based on $\text{Pb}_5\text{Ge}_3\text{O}_{11}$. A few possibilities for future work are discussed here.

$\text{Pb}_5\text{Ge}_3\text{O}_{11}$

- Adjustments to the solution chemistry were not made in this investigation. Other researchers have shown the significant impact of the sol gel composition and processing parameters on final film qualities in other compositional systems.
- Better control of the thermal annealing profile for the lead germanate films will probably lead to an improved method for producing dense, defect free microstructures with the desired grain sizes.
- A more detailed investigation needs to be performed in regards to the electrical properties of these thin films.

$\text{Pb}_5\text{Ge}_3\text{O}_{11}$ - $\text{PbZr}_x\text{Ti}_{1-x}\text{O}_3$

- Research needs to be performed in regards to understanding the phase development and interactions in this system.
- The microstructural optimization and characterization for this system needs to be investigated.

- Research needs to be performed to characterize the electrical properties of thin films in this diphasic system as a means of determining if the phase ratio can be used to adjust electrical properties for specific applications.
- Investigations focusing on compositions with high and low ratios of PG:PZT would help to determine if a small lead germanate addition to PZT would improve piezoelectric device possibilities, or if a small addition of PZT to lead germanate will improve pyroelectric properties.

Substitutions in $\text{Pb}_5\text{Ge}_3\text{O}_{11}$

In consideration of the results for pure lead germanate thin films reported in this research, incorporation of either silicon or barium substitutions into the composition could conceivably result in polycrystalline pyroelectric thin films with pyroelectric performance characteristics that exceed any of the currently used single crystal detector elements.

- Silicon substitutions for germanium have been shown to improve the room temperature pyroelectric performance of lead germanate by lowering the transition temperature. This effectively shifts the pyroelectric current versus temperature curve to lower temperatures. Single crystals with a $\text{Pb}_5\text{Ge}_2\text{SiO}_{11}$ composition have been reported to have room temperature pyroelectric coefficients more than double that of pure $\text{Pb}_5\text{Ge}_3\text{O}_{11}$ single crystals. It would also be very interesting to examine the effect of the silicon substitution on the microstructural development.
- Barium substitutions for lead have also been shown to increase the room temperature pyroelectric response as well as the DC resistivity of lead germanate. Single crystals with a composition of $\text{Pb}_{4.7}\text{Ba}_{0.3}\text{Ge}_3\text{O}_{11}$ were

reported to have room temperature pyroelectric coefficients more than double that of pure $\text{Pb}_5\text{Ge}_3\text{O}_{11}$ single crystals.

References

- [1] J. Valasek, "Piezoelectric and Allied Phenomena in Rochelle Salt," *Phys. Rev.*, Vol.15, (1920): 537-538.
- [2] M. Lines and A. Glass, Principles and Applications of Ferroelectrics and Related Materials, Oxford University Press, Oxford, 1977.
- [3] J. Slater, "Theory of the Transition in KH_2PO_4 ," *J. Chem. Phys.*, Vol.9, (1941): 16-33.
- [4] W. Cochran, "Crystal Stability and the Theory of Ferroelectricity," *Adv. Phys.*, Vol.9, (1960): 387-423.
- [5] W. Kingery, H. Bowen and D. Uhlman, Introduction to Ceramics, 2nd. Edition, John Wiley and Sons, New York, 1976.
- [6] C. Kittel, Introduction to Solid State Physics, 5th. Edition, John Wiley and Sons, New York, 1976.
- [7] G. Burns, Solid State Physics, Academic Press, Orlando, 1985.
- [8] Z. Surowiak, M. Łoposzko, I. Zakharchenko, A. Bakirov, E. Marchenko, E. Sviridov, Y. Mukhortov and V. Dudkevich, "Thin Ferroelectric Films of the Lead Zirconate-Titanate Type Obtained by R.F. Sputtering," *Thin Solid Films*, 205, 76, 76-84 (1991).
- [9] J. Burfoot, "Pyroelectric and Ferroelectric Thin Film Devices," Ch. 12 in Active and Passive Thin Film Devices, Edited by T. Coutts, Academic Press, New York, 1978.
- [10] J. Scott and C. Paz de Araujo, "Ferroelectric Memories," *Science*, 246, 1400-1405, (1989).
- [11] J.M. Herbert, Ferroelectric Transducers and Sensors, Gordon and Breach, New York, 1982.

- [12] A. Halliyal, A.S. Bhalla, R.E. Newnham and L.E. Cross, "Glass-Ceramics for Piezoelectric and Pyroelectric Devices," Ch. 8 in Glasses and Glass-Ceramics, Edited by M.H. Lewis, Chapman and Hill, 1989.
- [13] R.W. Whatmore, J.M. Herbert and F.W. Ainger, "Recent Developments in Ferroelectrics," *Phys. Stat. Sol.(a)*, Vol.61, (1980): 73-80.
- [14] E.I. Speranskaya, "System PbO-GeO₂," [in Russian] *Izvest. Akad. Nauk. SSSR*, (1959): 162-163.
- [15] H. Iwasaki, K. Sugii, T. Yamada, and N. Niizeki, "5PbO·3GeO₂ Crystal; A New Ferroelectric," *App. Phys. Lett.*, Vol.18, No.10, (1971): 444-445.
- [16] S. Nanamatsu, H. Sugiyama, K. Dor, and Y. Kondo, "Ferroelectricity in Pb₅Ge₃O₁₁," *J. Phys. Soc. Jpn.*, Vol.31, (1971): 616.
- [17] K. Hisano and J.F. Ryan, "Raman Scattering from the Ferroelectric Mode in 5PbO·3GeO₂," *Solid State Comm.*, Vol.11, No.1, (1972): 119-121.
- [18] H. Iwasaki, S. Miyazawa, H. Koizumi, K. Sugii, and N. Niizeki, "Ferroelectric and Optical Properties of Pb₅Ge₃O₁₁ and Its Isomorphous Compound Pb₅Ge₂SiO₁₁," *J. Appl. Phys.*, Vol.43, No.12, (1972): 4907-4915.
- [19] H. Iwasaki and K. Sugii, "Optical Activity of Ferroelectric 5PbO·3GeO₂ Single Crystals," *Appl. Phys. Lett.*, Vol.19, No.4, (1971): 92-93.
- [20] H. Iwasaki, K. Sugii, N. Niizeki, and H. Toyoda, "Switching of Optical Rotatory Power in Ferroelectric 5PbO·3GeO₂ Single Crystal," *Ferroelectrics*, Vol.3, (1972): 157-161.
- [21] A.M. Glass, K. Nassau, and J.W. Shiever, "Evolution of Ferroelectricity in Ultrafine-Grained Pb₅Ge₃O₁₁ Crystallized from the Glass," *J. Appl. Phys.*, Vol.48, No.12, (1977): 5213-5216.
- [22] H. Hasegawa, M. Shimada, and M. Koizumi, "Phase Relations and Crystallization of Glass in the System PbO-GeO₂," *J. Mater. Sci.*, Vol.8, No.12, (1973): 1725-1730.

- [23] K. Nassau, J.W. Shiever, D.C. Joy, and A.M. Glass, "The Crystallization of Vitreous and Metastable $\text{Pb}_5\text{Ge}_3\text{O}_{11}$," *J. Cryst. Growth*, Vol.42, (1977): 574-578.
- [24] O.Yu. Malevanaya, V.V. Mikhnevich, S.R. Syrtsov, and V.N. Shut, "Influence of the Microstructure on Electrophysical Properties of $\text{Pb}_5\text{Ge}_3\text{O}_{11}$ Prepared by the Glass-Ceramic Technology," *Sov. Phys. Solid State*, Vol.32, No.2, (1990): 244-247.
- [25] V.D. Sal'nikov, M.V. Pentegova, Yu.Ya. Tomashpol'skii, and Yu.N. Venevtsev, "Preparation and Properties of Single Crystals of Ferroelectric Solid Solutions $\text{Pb}_3(\text{Ge,Si})_2\text{O}_7$," *Izv. Akad. Nauk SSSR, Neorg. Mater.*, Vol.11, No.10, (1975): 1897-1898.
- [26] Y. Iwata, N. Koyano, and I. Shibuya, "Neutron Diffraction Studies of Crystal Structure of Ferroelectric $5\text{PbO}\cdot 3\text{GeO}_2$," *Annu. Rep. Res. Reactor Inst. Kyoto Univ.*, Vol.6, (1973): 86-90.
- [27] R.E. Newnham, R.W. Wolfe, and C.N. Darlington, "Prototype Structure of $\text{Pb}_5\text{Ge}_3\text{O}_{11}$," *J. Solid State Chem.*, Vol.6, (1973): 378-383.
- [28] Y. Iwata, N. Koyano, and I. Shibuya, "Neutron Diffraction Studies of Ferroelectric $5\text{PbO}\cdot 3\text{GeO}_2$ Above the Curie Point," *J. Phys. Soc. Jpn.*, Vol.35, (1973): 1269.
- [29] J.L. Kirk, L.E. Cross, and J.P. Dougherty, "Pressure and Temperature Dependence of the Dielectric Properties and Phase Transitions of the Ferroelectric $\text{Pb}_5\text{Ge}_3\text{O}_{11}$," *Ferroelectrics*, Vol.11, (1976): 439-443.
- [30] Y. Iwata, "Neutron Diffraction Study of the Structure of Paraelectric Phase of $\text{Pb}_5\text{Ge}_3\text{O}_{11}$," *J. Phys. Soc. Jpn.*, Vol.43, No.3, (1977): 961-967.
- [31] V.N. Gavrilov, A.G. Zakharyants, É.V. Zolotoyabko, E.M. Iolin, A.G. Maloyan, and A.V. Muromtsev, "Investigation of the Lattice Dynamics of Lead Germanate in the Vicinity of its Ferroelectric Phase Transition," *Sov. Phys. Solid State*, Vol.25, No.1, (1983): 4-7. [*Fiz. Tverd. Tela*, Vol.25, (1983): 10-15]

- [32] A.A. Bush and Yu.N. Venevtsev, New Data from an Investigation of Ferroelectric Crystals of Solid Solutions $Pb_5(Ge_{1-x}Si_x)_3O_{11}$, "Sov. Phys. Crystallogr., Vol.26, No.2, (1981): 198-202.
- [33] V.D. Sal'nikov, S.Yu. Stefanovich, V.V. Chechkin, M.V. Pentegova, Yu.Ya. Tomashpol'skii, and Yu.N. Venevtsev, "Ferroelectric Crystals in the System $PbO-GeO_2-SiO_2$," *Ferroelectrics*, Vol.8, (1974): 491-493.
- [34] M. Malinowski, A. Pietraszko, and M. Polomska, "Thermal Expansion and Dielectric Permittivity in the Vicinity of Transition Points of Lead Germanate," *Phys. Stat. Sol. (a)*, Vol.41, (1977): K55-K58.
- [35] K.H. Germann, W. Müller-Lierheim, H.H. Otto, and T. Suski, "High Temperature Phase Transition in $Pb_5Ge_3O_{11}$," *Phys. Stat. Sol. (a)*, Vol.35, (1976): K165-K167.
- [36] A. Mansingh, K.N. Srivastava, and B. Singh, "Dielectric Behavior of Polycrystalline Lead Germanate," *J. Phys. Chem. Solids*, Vol.40, (1979): 9-15.
- [37] A. Mansingh, K.N. Srivastava, and B. Singh, "Effect of Surface Capacitance on the Dielectric Behavior of Ferroelectric Lead Germanate," *J. Appl. Phys.*, Vol.50, No.6, (1979): 4319-4323.
- [38] K. Gesi and K. Ozawa, "Effect of Hydrostatic Pressure on the Ferroelectric Curie Temperature of $Pb_5Ge_3O_{11}$," *Jpn. J. Appl. Phys.*, Vol.13, No.5, (1974): 897-898.
- [39] W. Gebhardt and W. Müller-Lierheim, "The Ferroelectric Soft Mode in $Pb_5Ge_3O_{11}$ and in the $Pb_5Ge_{3-x}Si_xO_{11}$ Mixed Crystal System," in Lattice Dynamics; Proc. Int. Conf., ed. M. Balkanski, Flammarion Med-Sci., Paris, France, (1977): 689-692.
- [40] T. Suski, W. Müller-Lierheim, W. Dultz, H.H. Otto, and W. Gebhardt, "Raman Spectroscopic Investigation of the Ferroelectric Soft Mode in $Pb_5Ge_3O_{11}$ under High Hydrostatic Pressure," in High-Pressure Science and Technology; Sixth AIRAPT Conf., Vol.1, ed. K.D. Timmerhaus and M.S. Barber, Univ. of Colorado, Boulder, CO, (1977): 447-452.

- [41] G.R. Jones, N. Shaw, and A.W. Vere, "Pyroelectric Properties of Lead Germanate," *Electronics Lett.*, Vol.8, No.14, (1972): 345-346.
- [42] K. Takahashi, "Pyroelectric Sensors of Lead Germanate Thick Films," Chap.14 in *Advanced Ceramics*, ed. S. Saito, Oxford Univ. Press, (1988).
- [43] R. Watton, C. Smith, and G.R. Jones, "Pyroelectric Materials: Operation and Performance in the Pyroelectric camera Tube," *Ferroelectrics*, Vol.14, (1976): 719-721.
- [44] D. Luff, R. Lane, K. Brown and H. Marshallsay, "Ferroelectric Ceramics with High Pyroelectric Properties," *Trans. J. Brit. Ceram. Soc.*, Vol.73, (1974): 251-264.
- [45] K. Takamatsu, N. Kobayashi, T. Tsujimura, K. Matsumoto, K. Takada, and H. Ichimura, "Ceramic Films of $\text{Pb}_{4.95}\text{Ba}_{0.05}\text{Ge}_3\text{O}_{11}$ by Printing Technique and Their Pyroelectric Characteristics," *Jpn. J. Appl. Phys.*, Vol.24, Suppl.24-3, (1985): 175-177.
- [46] K. Takahashi, S.I. Shirasaki, K. Takamatsu, N. Kobayashi, Y. Mitarai, and K. Kakegawa, "Pyroelectricity of Preferably-Oriented $\text{Pb}_5\text{Ge}_{3-x}\text{Si}_x\text{O}_{11}$ Thick Films Prepared by the Printing Technique," *Jpn. J. Appl. Phys.*, Vol.22, Suppl.22-2, (1983): 73-76.
- [47] Yu.Ya. Tomashpol'skii and M.V. Pentegova, "Ferroelectric Behavior of Vacuum Condensates of Lead Germanate," *Sov. Phys. Solid State*, Vol.15, No.6, (1973): 1304.
- [48] G. Kleer, H. Schmitt, H.E. Müser, and K.H. Ehses, "Sputtered Ferroelectric Thin Films of Lead Germanate," *Ferroelectrics*, Vol.26, (1980): 757-760.
- [49] H. Schmitt and G. Kleer, "Reactive Sputtering of Ferroelectric Lead Germanate $\text{Pb}_5\text{Ge}_3\text{O}_{11}$," *Proc. 4th Coll. Internat. S. 1, Plasmas e. 1, Pulverisation Cath., Nice*, (1982): 137-141.
- [50] H. Schmitt, H.E. Müser, R. Karthein, and G. Kleer, "Properties of Undoped and Doped Ferroelectric Lead Germanate Thin Films," *Ferroelectrics*, Vol.56, (1984): 141-144.

[51] H. Schmitt and G. Kleer, "Transformation from the Glassy State in Sputtered Amorphous Films of the Ferroelectric Lead Germanate $Pb_5Ge_3O_{11}$," *Mat. Res. Bull.*, Vol.20, (1985): 829-833.

[52] H. Schmitt, R. Karthein, and G. Kleer, "Production and Properties of Undoped and Doped Lead Germanate Thin Films," *Ferroelectrics*, Vol.51, (1983): 35-39.

[53] H. Maiwa, N. Ichinose, and K. Okazaki, "Preparation of $Pb_5Ge_3O_{11}$ Thin Films by Multiple Cathode Sputtering," *Proceedings of the 8th International Meeting on Ferroelectricity*, August 8-13, 1993, Gaithersburg, MD.

[54] A. Mansingh and S.B. Krupanidhi, "Preparation and Properties of Thermally Evaporated Lead Germanate Films," *J. Appl. Phys.*, Vol.51, No.10, (1980): 5408-5412.

[55] A. Mansingh and S.B. Krupanidhi, "Electrical and Structural Properties of Flash-Evaporated Ferroelectric Lead Germanate Films on Silicon," *Thin Solid Films*, Vol.80, (1981):359-371.

[56] S.B. Krupanidhi, A. Mansingh, and M. Sayer, "I-V & C-V Characteristics of Ferroelectric Lead Germanate on Silicon," *Ferroelectrics*, Vol.50, (1983):117-122.

[57] S.B. Krupanidhi, D. Roy, N. Maffei, and C.J. Peng, "Pulsed Excimer Laser Deposition of Ferroelectric Thin Films," Proceedings of the 3rd International Symposium on Integrated Ferroelectrics, Colorado Springs, CO, April 3-5, 1991, pp.100-115.

[58] C.J. Peng, D. Roy, and S.B. Krupanidhi, "Oriented Lead Germanate Thin Films by Excimer Laser Ablation," *App. Phys. Lett.*, Vol.60, No.7, (1992): 827-829.

[59] J.J. Lee and S.K. Dey, "Processing of the Uniaxial Ferroelectric $Pb_5Ge_3O_{11}$ Thin Film at 450°C with C-Axis Orientation," *App. Phys. Lett.*, Vol.60, No.20, (1992): 2487-2488.

[60] S.M. Landin and M.J. Haun, "Solution-Derived Ferroelectrics in the $Pb_5Ge_3O_{11}$ - $PbTiO_3$ - $PbZrO_3$ System," *Ferroelectrics*, Vol.152, (1994): 91-96.

- [61] S.M. Landin and M.J. Haun, "Processing and Characterization of Ferroelectric Thin Films in the $\text{Pb}_5\text{Ge}_3\text{O}_{11}$ - $\text{PbZr}_x\text{Ti}_{1-x}\text{O}_3$ System," Proceedings of the Ninth International Symposium on the Applications of Ferroelectrics, Penn. State Univ., University Park, PA, Aug. 7-10, 1994.
- [62] V.V. Mikhnevich, V.N. Shut, and S.R. Syrtsov, "Preparation and Investigation of Glass-Ceramic Lead Germanate Having Oriented Surface Layers," *Sov. Phys. Solid State*, Vol.33, No.3, (1991): 456-459.
- [63] V.V. Mikhnevich and V.N. Shut, "Microstructure and Pyroelectric Properties of a Lead Germanate Textured Glass-Ceramic," *Neorg. Mater.*, Vol.28, No.3, (1992): 563-566.
- [64] K. Takahashi, S.I. Shirasaki, K. Takamatsu, N. Kobayashi, Y. Mitarai, and K. Kakegawa, "Oriented $\text{Pb}_5\text{Ge}_{3-x}\text{Si}_x\text{O}_{11}$ Thick Films Prepared by the Printing Technique," *J. Mat. Sci. Lett.*, Vol.3, (1984): 239-241.
- [65] I.A. Cornejo, J. Collier, and M.J. Haun, "Ferroelectric and Crystallization Behavior in the $\text{Pb}_5\text{Ge}_3\text{O}_{11}$ - PbTiO_3 - PbZrO_3 Glass-Ceramic System," *Ferroelectrics*, Vol.154, (1994): 53-58.
- [66] S. Swartz, "Topics in Electronic Ceramics," *IEEE Trans. Elec. Insul.*, Vol.25, No.5, (1990): 935-987.
- [67] B. Jaffe, W.R. Cook Jr., and H. Jaffe, Piezoelectric Ceramics, Academic Press, New York, NY, (1971).
- [68] S. Mabud, "The Morphotropic Phase Boundary in PZT Solid Solution," *J. Appl. Cryst.*, Vol.13, No.3, (1980): 211-216.
- [69] M. Sayer, C.V.R. Vasant Kumar, D. Barrow, L. Zou and D.T. Amm, "Integrated Piezoelectric and Pyroelectric Devices from Thin Film Ferroelectrics," *Mat. Res. Symp. Proc.*, Vol.243, (1992): 39-48.
- [70] A.H. Carim, B.A. Tuttle, D.H. Doughty, and S.L. Martinez, "Microstructure of Solution-Processed Lead Zirconate Titanate (PZT) Thin Films," *J. Am. Ceram. Soc.*, Vol. 74, No. 6, (1991): 1455-1458.

[71] B.A. Tuttle, T.J. Headley, B.C. Bunker, R.W. Schwartz, T.J. Zender, C.L. Hernandez, D.C. Goodnow, R.J. Tissot, and J. Michael, "Microstructural Evolution of $\text{Pb}(\text{Zr},\text{Ti})\text{O}_3$ Thin Films Prepared by Hybrid Metallo-Organic Decomposition," *J. Mater. Res.*, Vol. 7, No. 7, (1992): 1876-1882.

[72] L.N. Chapin and S.A. Myers, "Microstructure Characterization of Ferroelectric Thin Films Used in Non-Volatile Memories - Optical and Scanning Electron Microscopy," *Mat. Res. Soc. Symp. Proc.*, Vol.200, (1990): 153-158.

[73] S. Chen and I. Chen, "Temperature-Time Texture Transition of $\text{Pb}(\text{Zr}_{1-x}\text{Ti}_x)\text{O}_3$ Thin Films: I, Role of Pb-rich Intermediate Phases," *J. Am. Cer. Soc.*, Vol.77, No.9, (1994): 2332-2336.

[74] K.G. Brooks, I.M. Reaney, R. Klissurska, Y. Huang, L. Bursill and N. Setter, "Orientation of Rapid Thermally Annealed Lead Zirconate Titanate Thin Films on (111) Pt Substrates," *J. Mat. Res.*, Vol.9, No.10, (1994):

[75] B.A. Tuttle, R.W. Schwartz, D.H. Doughty, and J.A. Voigt, "Characterization of Chemically Prepared PZT Thin Films," *Mat. Res. Soc. Symp. Proc.*, Vol. 200, (1990): 159-165.

[76] A. Patel, D.A. Tossell, N.M. Shorrocks, R.W. Whatmore and R. Watton, "Pyroelectric Properties of Lead Based Ferroelectric Thin Films," *Mat. Res. Soc. Symp. Proc.*, Vol.310, (1993):

[77] A. Bell, Y. Huang, M. Kohli, O. Paul, P. Ryser and M. Forster, " PbTiO_3 Thin Films for Pyroelectric Detection," Proceedings of the Ninth International Symposium on the Applications of Ferroelectrics, Penn. State Univ., August 7-10, 1994.

[78] R. Takayama, Y. Tomita, K. Iijima and I. Ueda, "Preparation and Characteristics of Pyroelectric Infrared Sensors Made of C-Axis Oriented La-Modified PbTiO_3 Thin Films," *J. Appl. Phys.*, Vol.61, No.1, (1986): 411-415.

[79] S. Hirano, T. Yogo, K. Kikuta, Y. Araki, M. Saitoh, and S. Ogasahara, "Synthesis of Highly Oriented Lead Zirconate-Lead Titanate Film Using Metallo-Organics," *J. Am. Ceram. Soc.*, Vol. 75, No. 10, (1992): 2785-2789.

- [80] S.J. Lockwood, R.W. Schwartz, B.A. Tuttle, and E.V. Thomas, "Solution Chemistry Optimization of Sol-Gel Processed PZT Thin Films," *Mat. Res. Soc. Symp. Proc.*, Vol. 310, (1993): 275-280.
- [81] S. Merklein, D. Sporn and A. Schonecker, "Crystallization Behavior and Electrical Properties of Wet-Chemically Deposited Lead Zirconate Titanate Thin Films," *Mat. Res. Soc. Symp. Proc.*, Vol.310, (1993): 263-268.
- [82] B.A. Tuttle, J.A. Voigt, D.C.Goodnow, D.L. Lamppa, T.J. Headley, M.O. Eatough, G. Zender, R.D. Nasby, and S.M. Rodgers, "Highly Oriented, Chemically Prepared $\text{Pb}(\text{Zr},\text{Ti})\text{O}_3$ Thin Films," *J. Am. Ceram. Soc.*, Vol. 76, No. 6, (1993): 1537-1544.
- [83] W. Eysel, R.W. Wolfe, and R.E. Newnham, " $\text{Pb}_5(\text{Ge},\text{Si})_3\text{O}_{11}$ Ferroelectrics," *J. Am. Ceram. Soc.*, Vol.56, No.4, (1973): 185-188.
- [84] W.A. Schulze and J.V. Biggers, "Piezoelectric Properties of $\text{Pb}_5\text{Ge}_3\text{O}_{11}$ Bonded PZT Composites," *Mat. Res. Bull.*, Vol.14, (1979): 721-730.
- [85] I.A. Cornejo and M.J. Haun, "Crystallization Behavior of Glass-Ceramics with Multiple Ferroelectric Phases, Part I: The $\text{Pb}_5\text{Ge}_3\text{O}_{11}$ - PbTiO_3 System," Submitted to *J. Mat. Res.* (1994).
- [86] I.A. Cornejo and M.J. Haun, "Crystallization Behavior of Glass-Ceramics with Multiple Ferroelectric Phases, Part II: The $\text{Pb}_5\text{Ge}_3\text{O}_{11}$ - $\text{Pb}(\text{Zr}_{1/2}\text{Ti}_{1/2})\text{O}_3$ System," Submitted to *J. Mat. Res.* (1994).
- [87] I.A. Cornejo, "Low Temperature Crystallization of $\text{Pb}_5\text{Ge}_3\text{O}_{11}$ - PbTiO_3 and $\text{Pb}_5\text{Ge}_3\text{O}_{11}$ - $\text{Pb}(\text{Zr}_{1/2}\text{Ti}_{1/2})\text{O}_3$ Glass-Ceramic Systems with Multiple Ferroelectric Phases for Pyroelectric Applications," Ph.D. Thesis, T-5631, Colorado School of Mines, Golden, CO, (1994).
- [88] J. Collier, I.A. Cornejo, and M.J. Haun, "Ferroelectric Thick-Films for Piezoelectric Applications," *Ferroelectrics*, Vol.154, (1994): 47-52.
- [89] J. Collier, "Ferroelectric Thick-Films for Piezoelectric Applications Produced by Amorphous $\text{Pb}_5\text{Ge}_2\text{SiO}_{11}$ and Crystalline $\text{Pb}(\text{Zr},\text{Ti})\text{O}_3$," M.Sc. Thesis, T-4479, Colorado School of Mines, Golden, Co, (1994).

[90] F.K. Lotgering, "Topotactical Reactions with Ferrimagnetic Oxides Having Hexagonal Crystal Structures - I," *J. Inorg. Nucl. Chem.*, Vol.59, (1959): 113-123.

[91] T.W. Cline, "Domain Contributions to the Dielectric Response in Ferroelectric Crystals," Ph.D. Thesis, The Pennsylvania State University, 1977.

[92] G.R. Barsch, L.J. Bonczar, and R.E. Newnham, "Elastic Constants of $\text{Pb}_5\text{Ge}_3\text{O}_{11}$ from 25 to 240°C," *Phys. Stat. Sol. (a)*, Vol.29, (1975): 241-250.

[93] C.K. Kwok and S.B. Desu, "A Novel Method for Determining the Curie Temperature of Ferroelectric Films," *Mat. Res. Soc. Symp. Proc.*, Vol.310, (1993): 429-433.

[94] S.Yu. Stefanovich, V.V. Chechkin, V.D. Sal'nikov, T.O. Sokolova, N.S. Sarkis'yan, and Yu.N. Venevtsev, "Generation of the Second Optical Harmonic and the Pyroeffect in $\text{Pb}_3(\text{Ge}_{1-x}\text{Si}_x)_2\text{O}_7$ Single Crystals," *Sov. Phys. Crystallogr.*, Vol.21, No.3, (1976): 300-302.